TRANSCEND

Transformative Science and Engineering for Nuclear Decommissioning

Drying of Spent AGR Fuel

Thomas Bainbridge, University of Leeds

pmtoba@leeds.ac.uk

Theme Meeting 3

18/05/2021
Online

Energy
For a Low Carbon Future

Background

- With Sellafield ceasing reprocessing focus now shifts to storage of spent fuel pending disposal to a GDF.
- This is expected for 2075.
- Current plan is to wet store remaining spent AGR fuel in the THORP R&S Pond.
- Potential for water to enter the fuel pin while in storage.
- If the water is not removed then during dry storage or disposal it presents a corrosion risk.
- Radiolysis can also cause the production of H_2 and H_2O_2.

AGR Fuel element [1].

[1] https://collection.sciencemuseumgroup.org.uk/objects/co5473/agr-fuel-element-c-1982-nuclear-fuel-fuel-rods

Stress Corrosion Cracking

- Produced when the material is subject to a tensile stress while in a corrosive environment.
- The cladding will become irradiated while in the reactor and this, combined with the high temperature results in precipitation of carbides such as chromium.
- Leaves material more susceptible to SCC as chromium has been depleted from the grain boundaries.
- These cracks are often highly tortuous and branched.

Example of SCC [2].

[2] https://www.nace.org/resources/general-resources/corrosion-basics/group-3/stress-corrosion-cracking#:~:text=Stress%20corrosion%20cracking%20(SCC)%20is,fatigue%20threshold%20of%20that%20material.

Cracking Methods

- **Huey Test** [3]
  Sample held in boiling 65% nitric acid for 240 hours.

  Can be reduced to 30 minutes with addition of oxidising ions such as Cr(VI).

  Issues with the use of concentrated nitric acid – if an alternative, safer method can be found that would be preferable.

- **Immersion Test** [4]
  Sample submerged in electrolyte containing Na^+, Ca^{2+}, K^+, Mg^{2+}, Cl^- and SO_4^- and air bubbled through.

  Placed in autoclave and heated in oil bath.

  Pressurised to 0.5 bar above pure water vapour pressure for test temperature.

  Took 1300+ hours to crack samples.

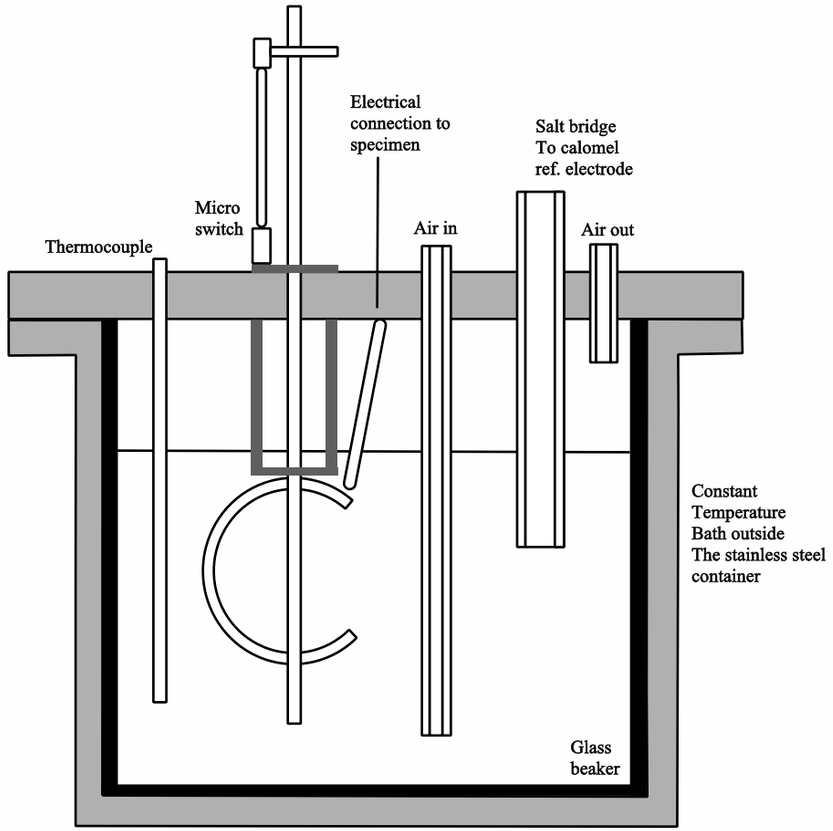

Immersion test set up

[3] Goode, J. *Transitioning of Spent Advanced Gas Reactor Fuel from Wet to Dry Storage*. thesis, University of Leeds, 2017.
[4] Drugli, J.M. and Steinsmo, U. Assessment Of Susceptibility To Chloride Stress Corrosion Cracking Of Highly Alloyed Stainless Steels. Part Ii: A New Immersion Test Method. In: Corrosion97: OnePetro, 1997.

Drop Evaporation Test

- Work done previously using this method to test stainless steels used in offshore oil rigs.
- Focuses on 10mm thick samples.
- Salt deposit causing anodic reaction leading to preferential nucleation site for SCC.
- Pereira et al found solution with a pH of 11 in dripping zone arising from the use of a pH 8.2 synthetic seawater.
- SCC produced was highly branched.

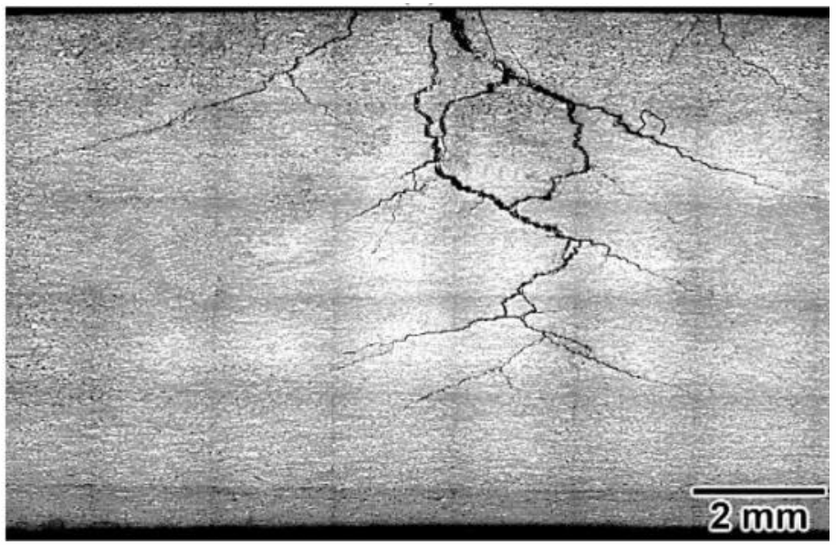

Macrograph of SSC produced at 110°C

[5] Pereira, H.B. and Azevedo, C.R.F., 2019. Can the drop evaporation test evaluate the stress corrosion cracking susceptibility of the welded joints of duplex and super duplex stainless steels?. *Engineering Failure Analysis*, *99*, pp.235-247.

Drop Evaporation Test

Method:

- Sample is stressed by lowering the top jaws.
- Sample heated to ≈120°C.
- Saline solution dripped onto the centre of the sample.
- 1 drop of solution falls every 10 seconds – the previous drop will ideally have evaporated.
- The cracked area of the sample will then be cut out and examined.

Features:

- Hole in the crew for a DTI and solution delivery.
- Springs to prevent weight of the jaw deflecting the sample.
- Dowels to guide the top jaw.

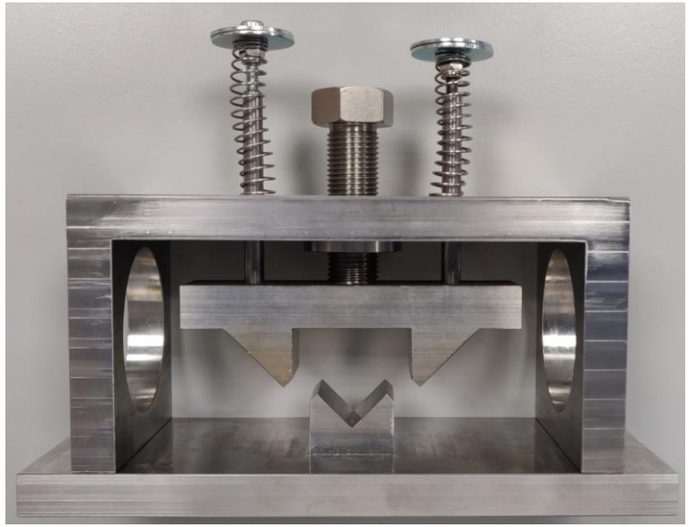

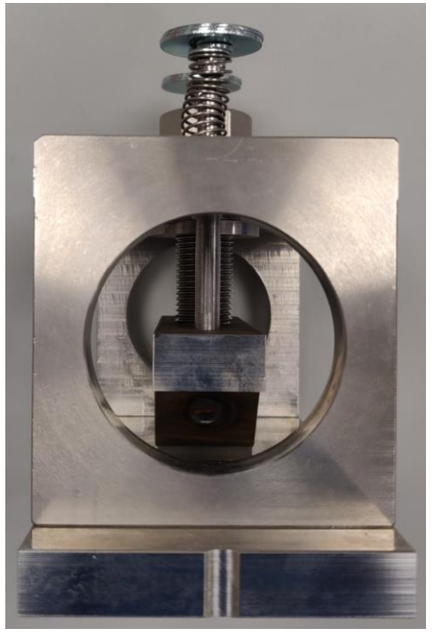

Permeability Test

Proposed Method:

- A disc with a pinhole in will be placed into the rig.
- The chamber will be evacuated.
- Once evacuated one side will be opened to atmospheric pressure.
- Pressure on other side of the disc will be recorded.
- This should allow for the leak rate through the pinhole to be found.
- It will be repeated for water leak rate with one side being pressurised.
- Once samples of stainless steel have been cracked then they will be subject to the same experiments

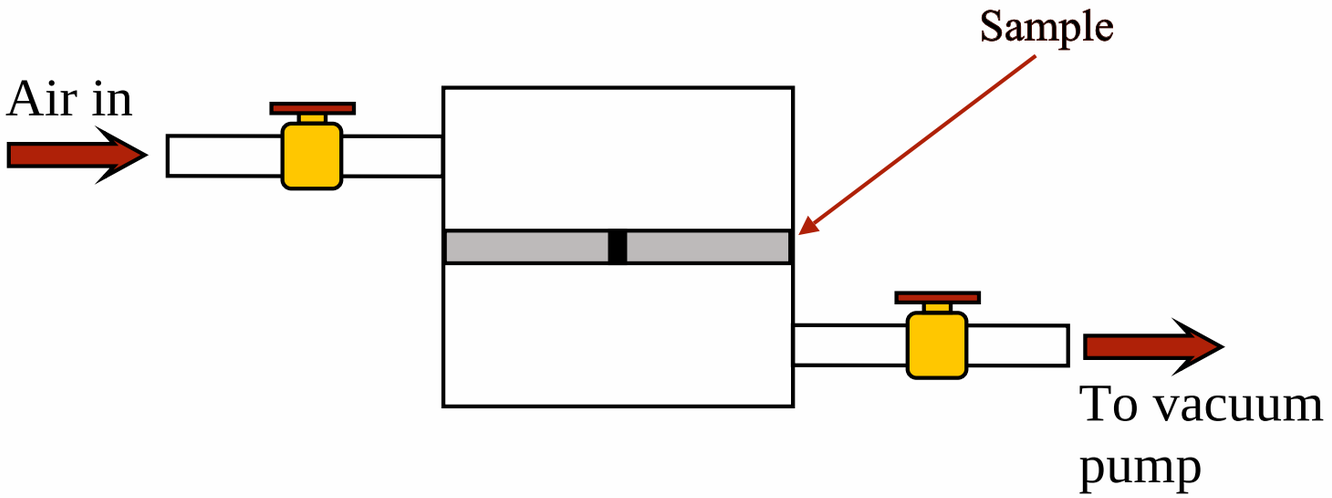

A simplified schematic of the proposed permeability leak rig.

Image Analysis

- Image “cleaned” in software such as MS Paint or Serif DrawPlus
- Image is converted from RGB to black and white.
- Image then skeletonised to find the centre line.
- Code then counts the number of pixels on the centre line
- The triangles are then delt with to find the straight line distance from the vertex to edge of the image.
- The average width is found by counting the number of pixels for the full length and also counting the number of black pixels. The number of black pixels divided by the length gives the average width.

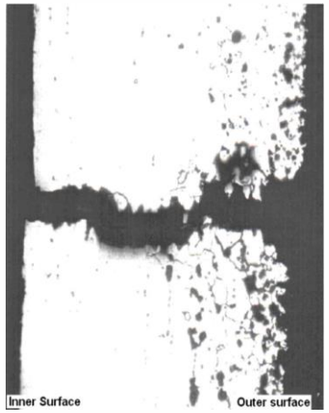

Original image [2]


“Cleaned” image


Binarised image

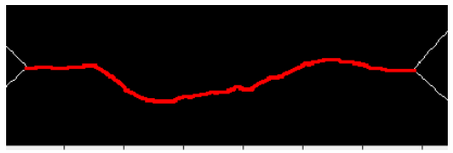
Skeleton and output

[6] John Kyffin. Technological Development to Support a Change in the United Kingdom’s Strategy for Management of Spent AGR Oxide Fuel. In Proceedings of the International Conference on Management of Spent Fuel from Nuclear Power Reactors, Vienna, June 2015. IAEA

Image Analysis

- The code must be ran twice.
- The first time the image on the right is generated and the coordinates of A, B, C and D are found by the user.
- These coordinates are then input to the code and then ran a second time to obtain the length and average width of the crack.

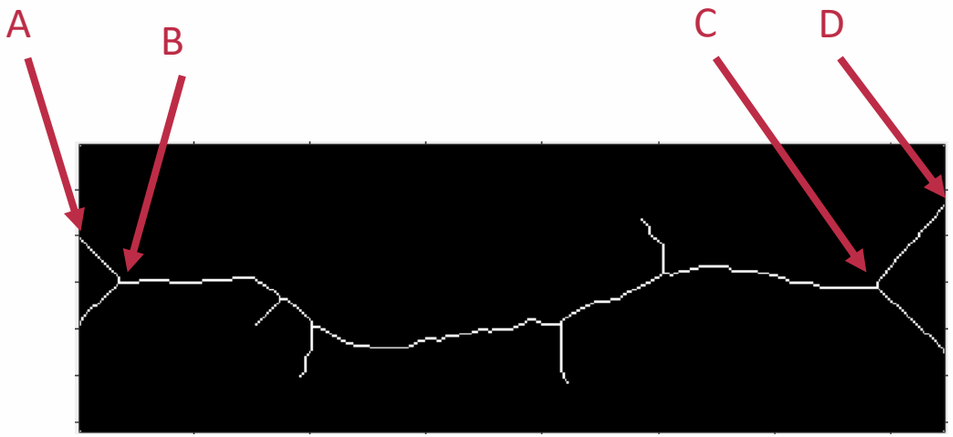

Skeleton

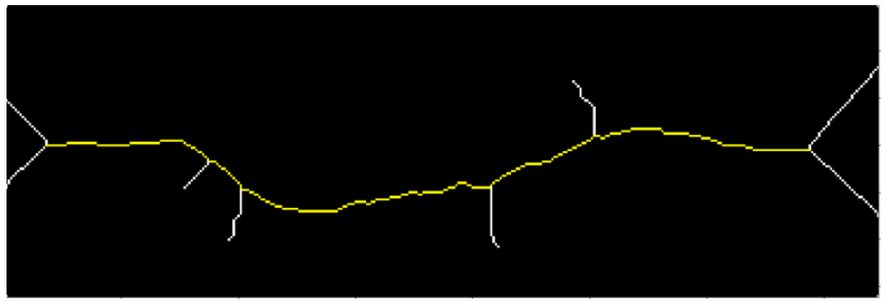
Path on skeleton


Overlay

Simple “Cracks”

Sample	Measured		Calculated		% Variation	
	Length	Width	Length	Width	**Length**	**Width**
1	16.12	0.63	15.45	0.71	**13.39**	**4.13**
2	58.10	0.63	60.69	0.62	**1.45**	**4.45**
3	24.92	0.63	25.63	0.65	**2.81**	**2.86**
4	32.58	0.63	33.85	0.61	**2.96**	**3.89**
5	65.16	0.63	67.72	0.64	**1.14**	**3.92**
6	99.95	2.33	102.09	2.28	**1.97**	**2.14**

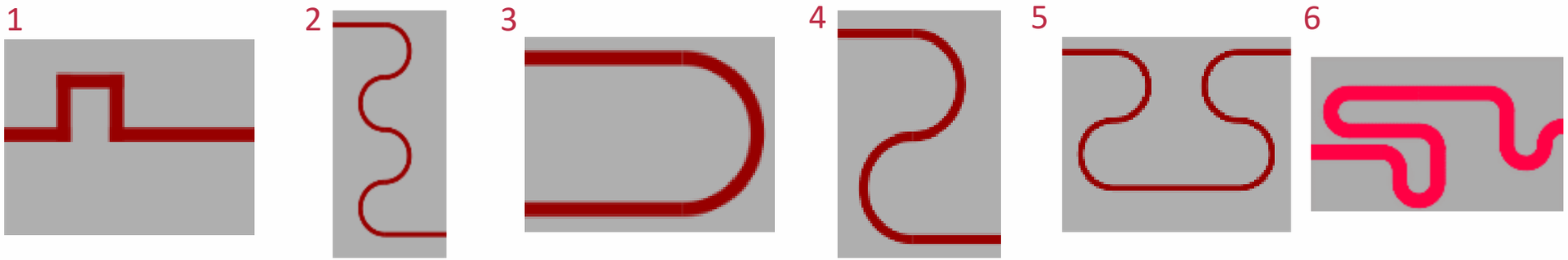

Literature Cracks

Sample	Measured		Calculated		% Variation	
	Length	Width	Length	Width	**Length**	**Width**
F1	2021.25	317	2247.74	311.28	**11.21**	**1.80**
F2	2197.13	275	2109.06	261.58	**4.01**	**4.88**
F3	1646.50	322	1772.35	311.90	**7.64**	**3.14**
F4	2310.88	288	2602.13	250.25	**12.60**	**13.11**
F5	1994.13	298	2302.59	290.68	**15.47**	**2.46**
F6	2085.75	311	2210.25	319.86	**5.97**	**2.85**

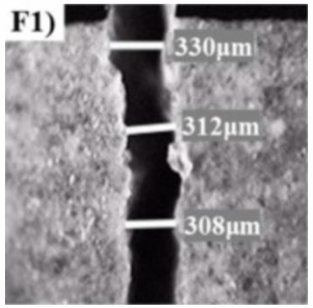

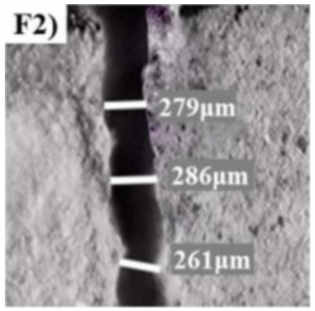

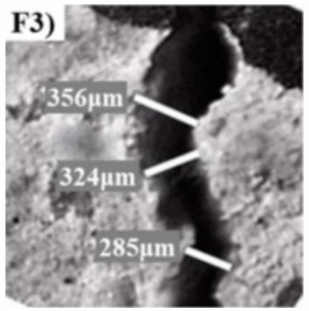

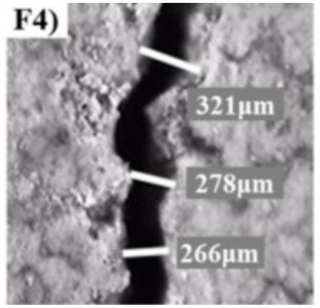

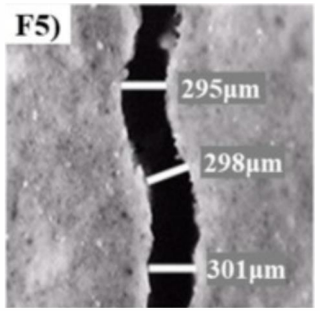

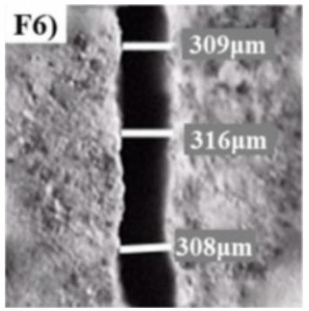

[3] Yuan L, Chen S, Wang S, Huang Y, Yang Q, Liu S, Wang J, Du P, Cheng X and Zhou Z 2019 Research on the Improvement of Concrete Autogenous Self-healing Based on the Regulation of Cement Particle Size Distribution (PSD) Materials 12 2818

Orifice Computational Flow Rate

- Initially orifice flow and idealised cracks were considered
- 3 methods trailed to see if any produced a curve similar to the experimental results
- Bomelburg – most simplistic model for orifice flow
- Beck – for idealised cracks
- Gill – a leak before break approach for single phase flow.
- An ODE method developed by Gill was investigated however it was not possible to isolate a flow rate equation.

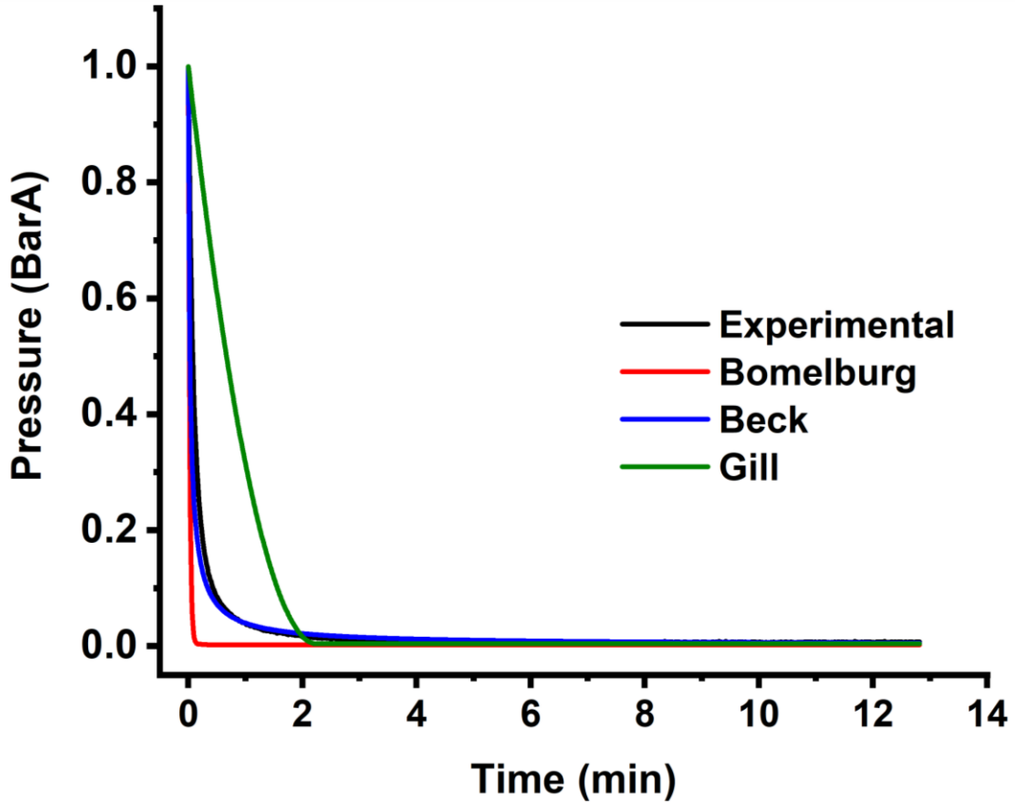

The pressure change for several different equations and the experimental trace.

Capillary Computational Flow Rate

$$Q = 54.8\, m\, \frac{d^4 \pi}{256\, \mu l} \left(p_u^2 - p_d^2\right)$$

Q – mass flow (g/s)
m – molecular weight (g)
d – diameter (cm)
μ – viscosity (centipoise)
L – length (cm)
p_u – upstream pressure (atm)
p_d - downstream pressure (atm)

- This code takes into account thermal expansion of the metal as heating occurs.
- Does not include provision for roughness of the capillary / crack.

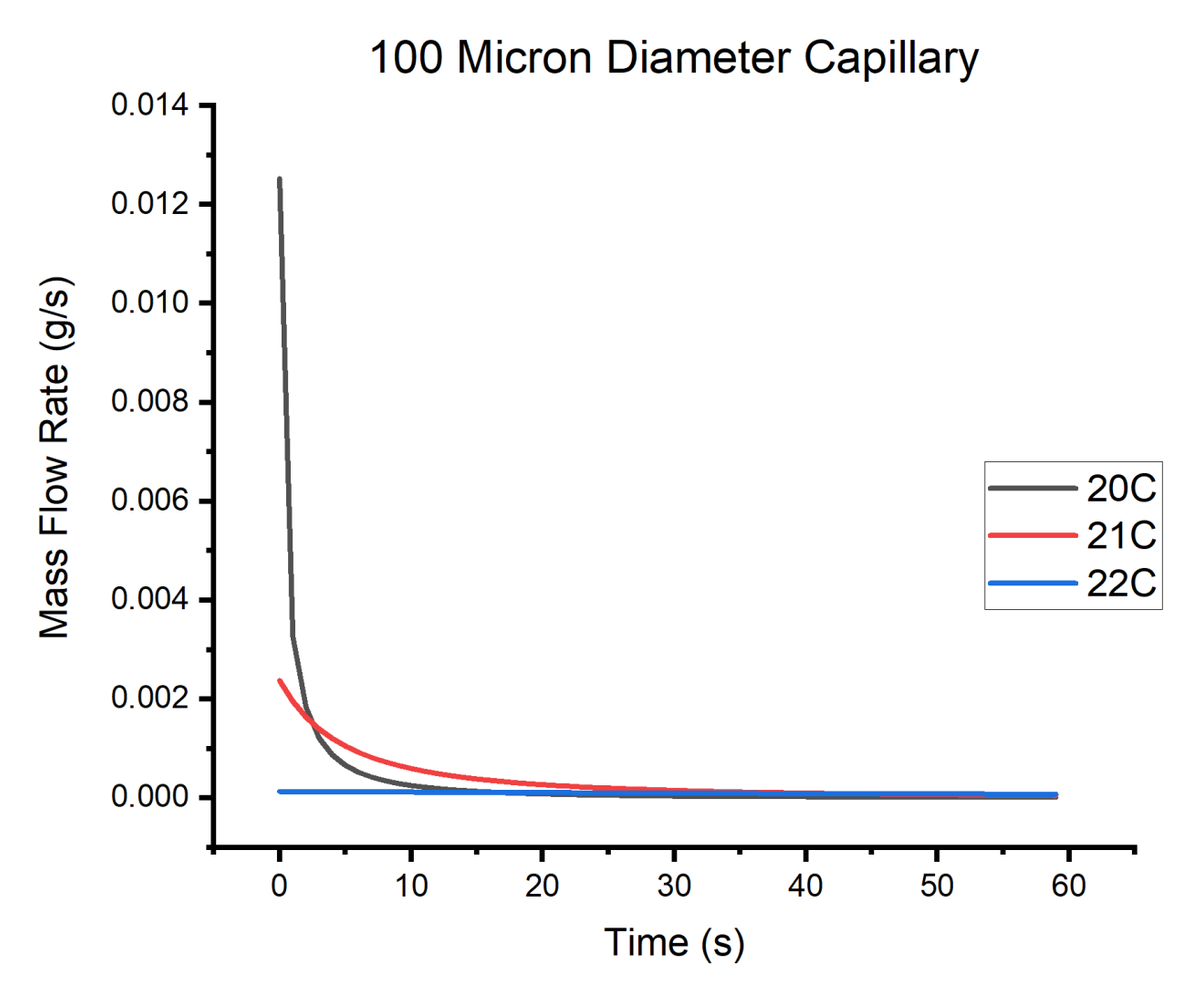

The flow rate for different temperatures using the Bomelburg capillary equation.

[7] Bomelburg, H.J. 1977. *Estimation of gas leak rates through very small orifices and channels.* Battelle Pacific Northwest Labs.

Capillary Computational Flow Rate

- Crack diameter could be under 10 microns.
- These graphs assume constant external vacuum.
- Does not include evaporation of any water present in the pin.

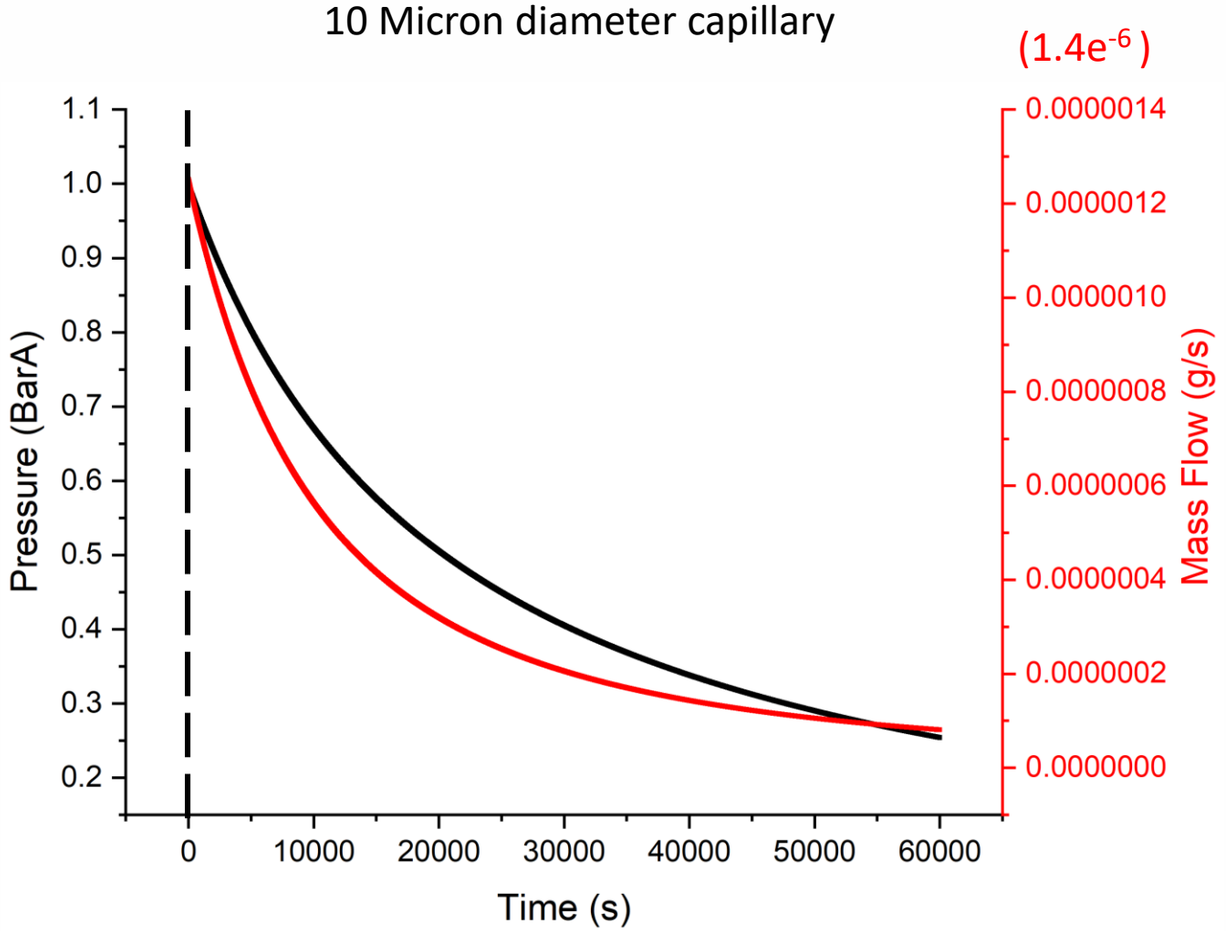

The mass flow and pressure change for a 10 micron diameter capillary.

Acknowledgements

Academic Supervisor: Prof. Bruce Hanson

Industrial Supervisor: Dr Carlos de la Fontaine

TRANSCEND

Transformative Science and Engineering for Nuclear Decommissioning

Thank you

pmtoba@leeds.ac.uk

TRANSCEND

Transformative Science and Engineering for Nuclear Decommissioning

Feasibility of using Stand-off Laser Techniques for SNF Characterisation During Storage

Victoria L. Frankland, Antoni E. Milodowski and David Read

University of Surrey, Guildford, UK

18th May 2021
Theme 3

Energy
For a Low Carbon Future

Spent Nuclear Fuel Characterisation

Alteration of U metal and UO_2 can follow several pathways

Environment	Potential SNF Species
Oxidising/fresh	*Uranyl (per)oxides* (e.g. schoepite, studtite, ianthinite)
Cementitious	*Ca uranyl oxides* (e.g. becquerelite, calcium uranates) *Ca uranyl silicates* (e.g. uranophane, haiweeite)
Groundwater	*Uranyl silicates* (e.g. uranophane, soddyite, boltwoodite) *Uranyl phosphates* (autunites), *carbonates* (rutherfordine) *etc.*
Seawater	*(Metal) uranyl oxides*

Harsh radioactive environment - traditional analysis impracticable

Aim:
Remote identification/characterisation technique(s) for SNF storage environments

Stand-off Laser Techniques

Benefits:

- **Remotely operated; no sample preparation required**
- **Independent of physical form (e.g. crystalline and amorphous solids, thin films, solutions)**
- **Small sampling area - µm**
- **Multiple, complementary techniques:**
  - **Laser-induced breakdown spectroscopy (LIBS)**
  - **Raman spectroscopy**
  - **Time-resolved laser fluorescence spectroscopy (TRLFS)**

Disadvantages:

- **Sensitivity (LOD, resolution, interferences)**
- **Incomplete spectroscopic database**

Laser-induced Breakdown Spectroscopy (LIBS)

Compositional information

Elemental abundance

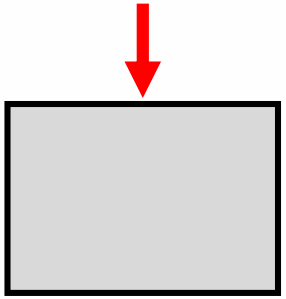

Surface mapping

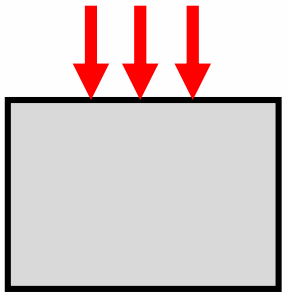

Depth mapping

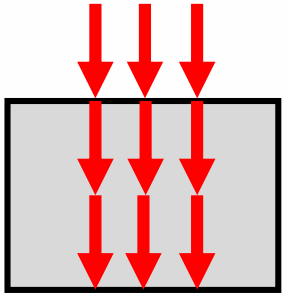

Raman Spectroscopy

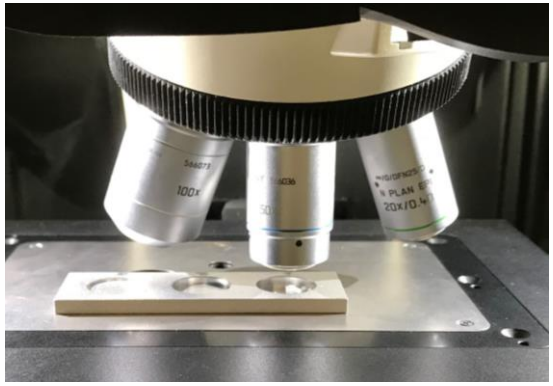

Structural information

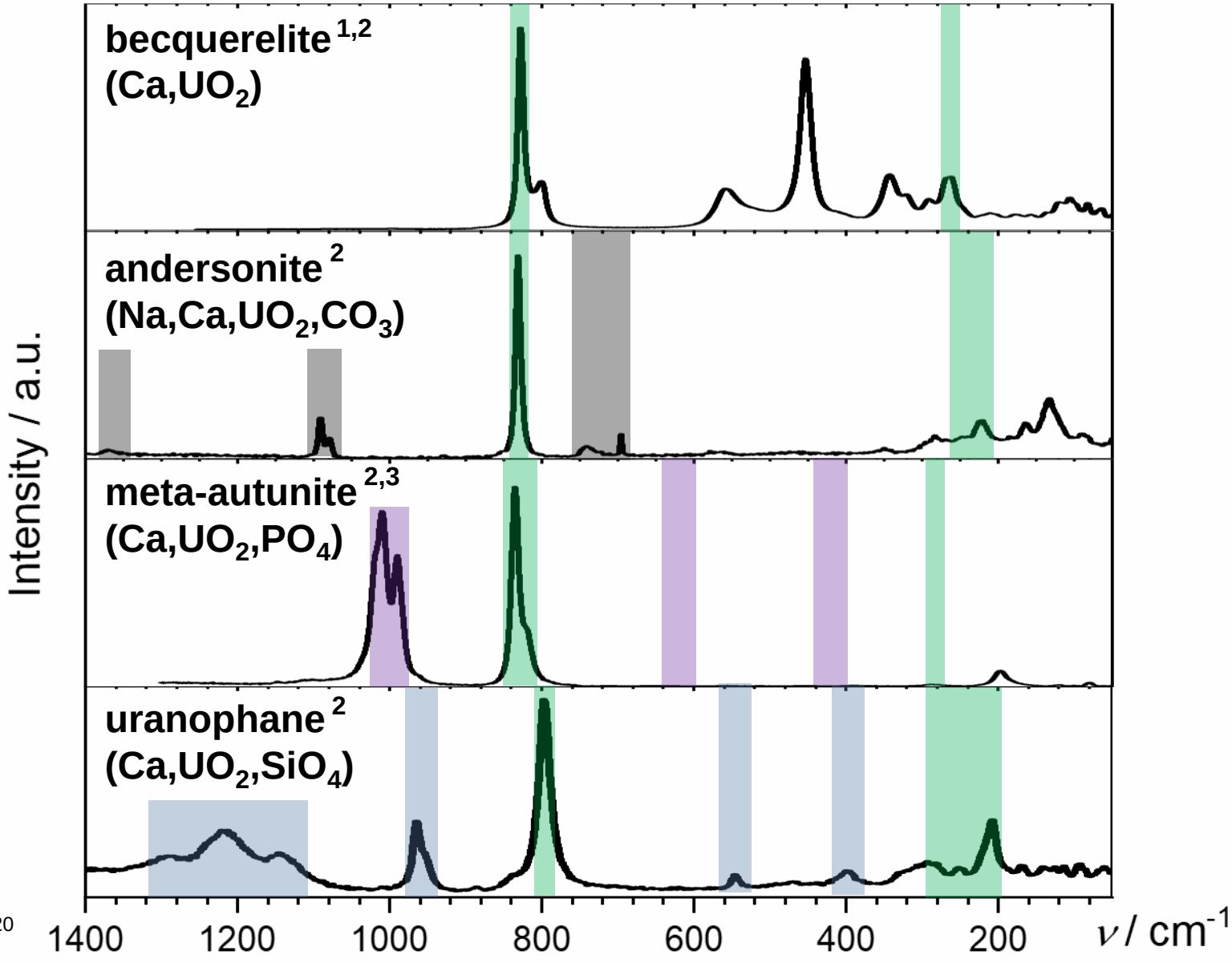

1) Frankland et al., 2021
2) Lit. comparison: e.g.) Driscoll et al., 2014
3) Frankland et al., 2020

Luminescence Emission Spectroscopy

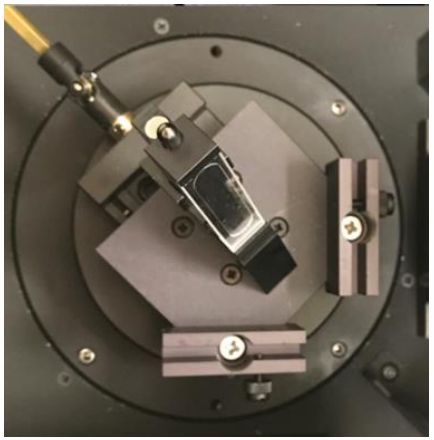

Phase and polymorph identification

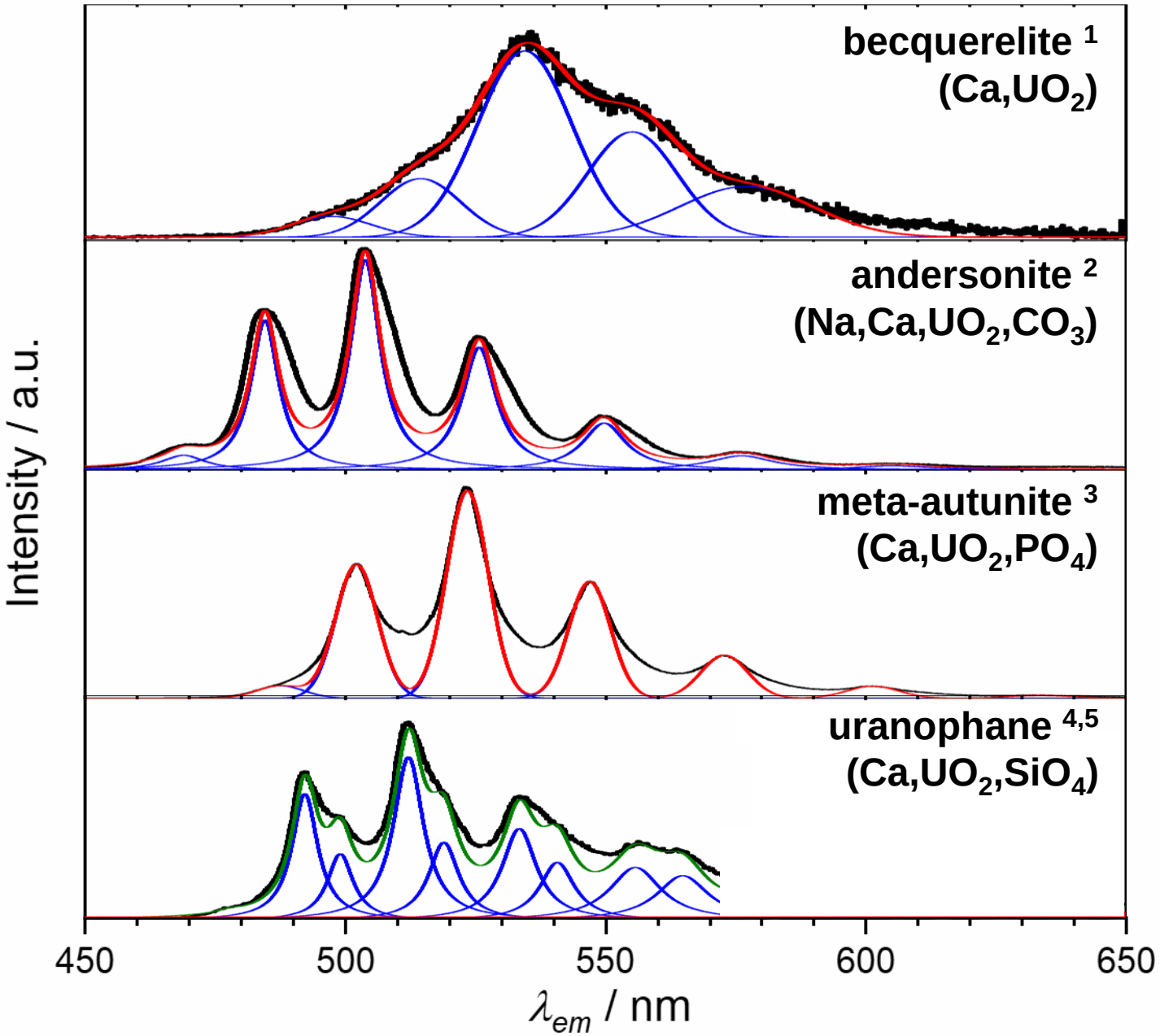

1) Frankland et al., 2021
2) Amayri et al., 2004
3) Frankland et al., 2020
4) Lehmann et al., 2008
5) Wang et al., 2005

Time-Resolved Luminescence Spectroscopy (TRLFS)

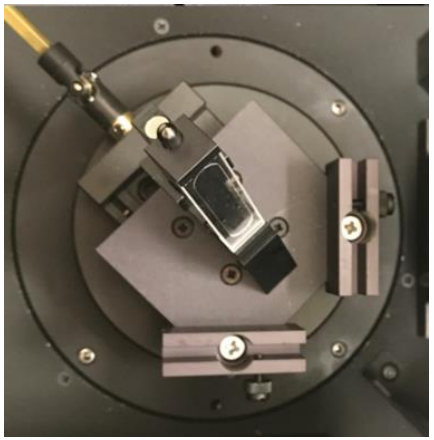

Meta-phase identification

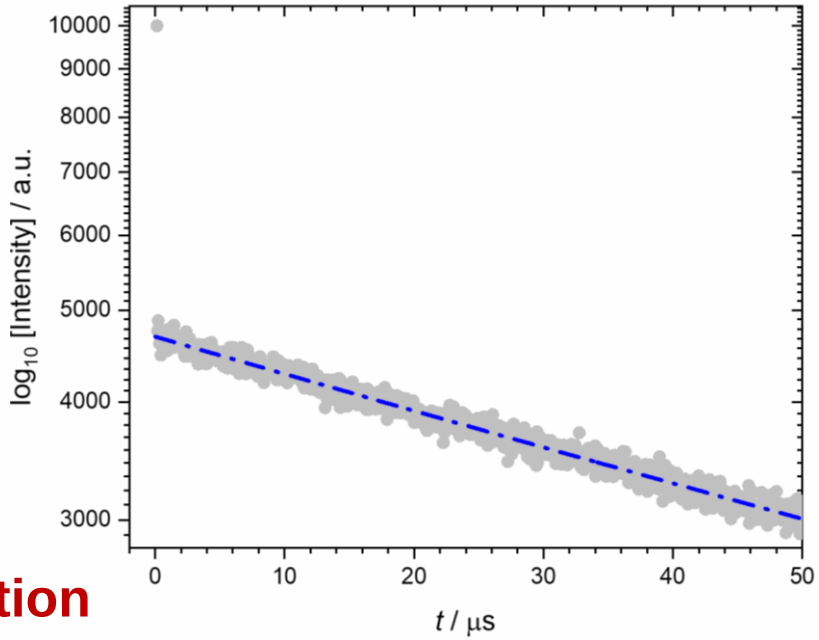

andersonite, τ = 97 ± 8 µs

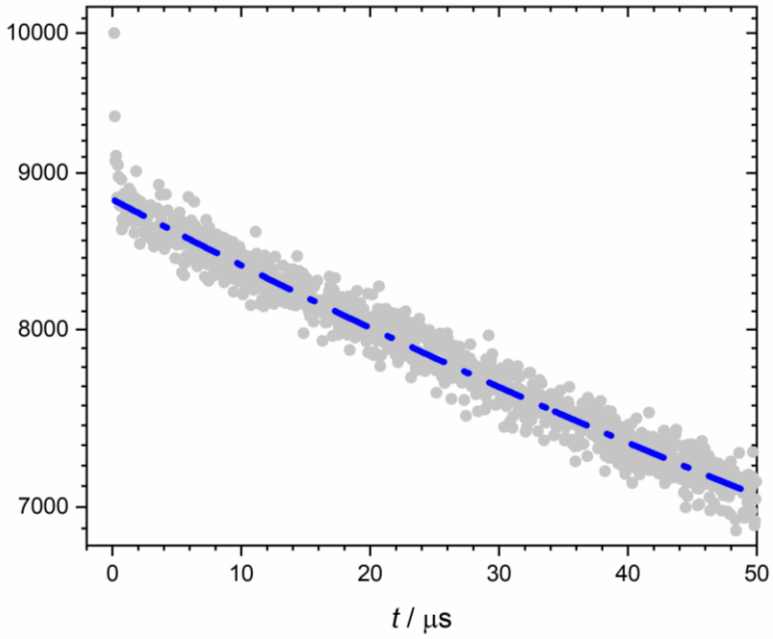

meta-autunite I, τ = 100 ± 9 µs
meta-autunite II, τ = 148 ± 15 µs

Modelling

Vandenbrandeite ($CuUO_2(OH)_4$)

- Simulate Raman spectrum
- Projected density of states (PDOS)
- Thermodynamic variables

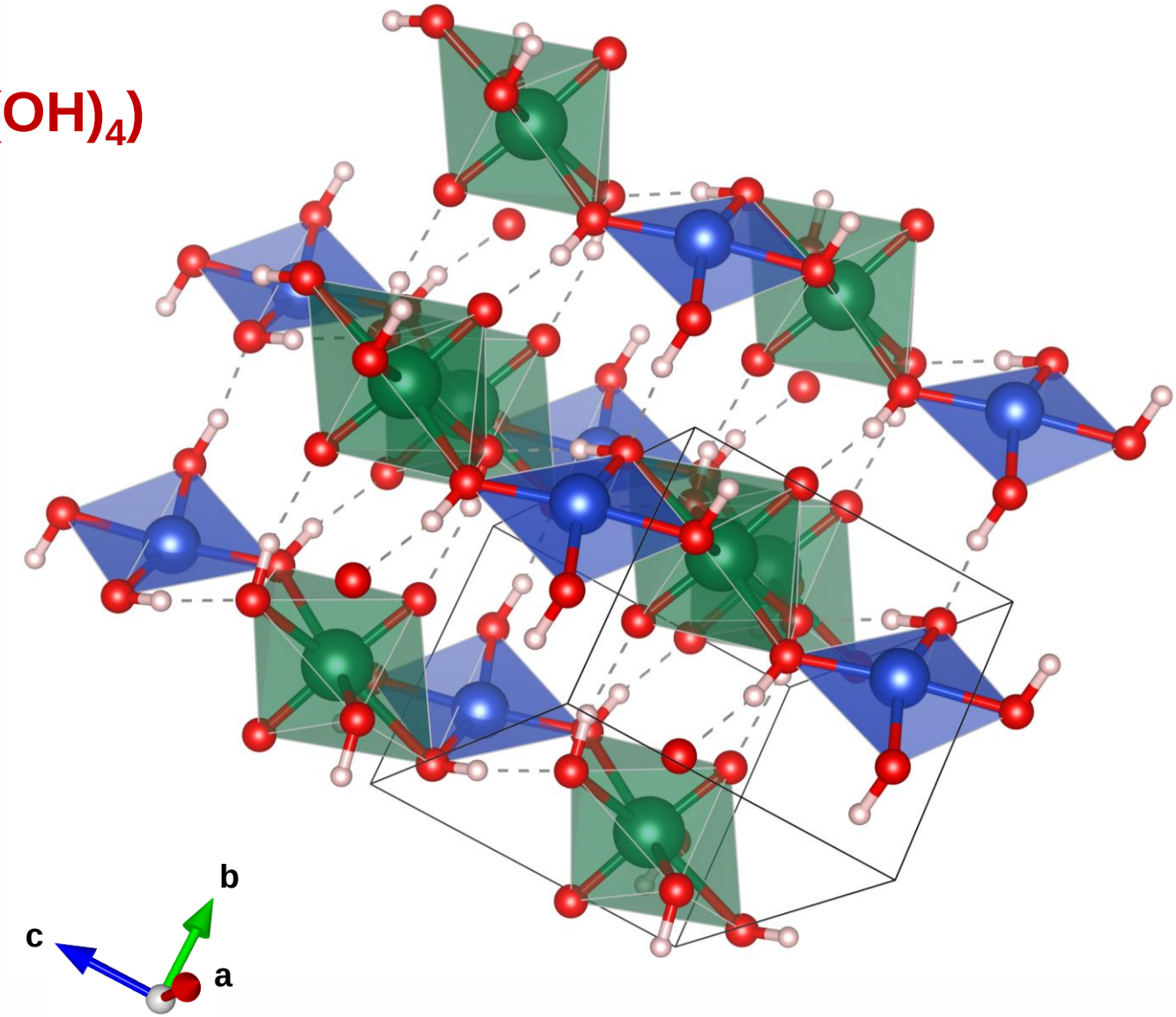

Method validation (Raman) – planned 2021

Blind testing on selection of ‘unknown’ U phases using remotely-controlled apparatus at University of Bristol

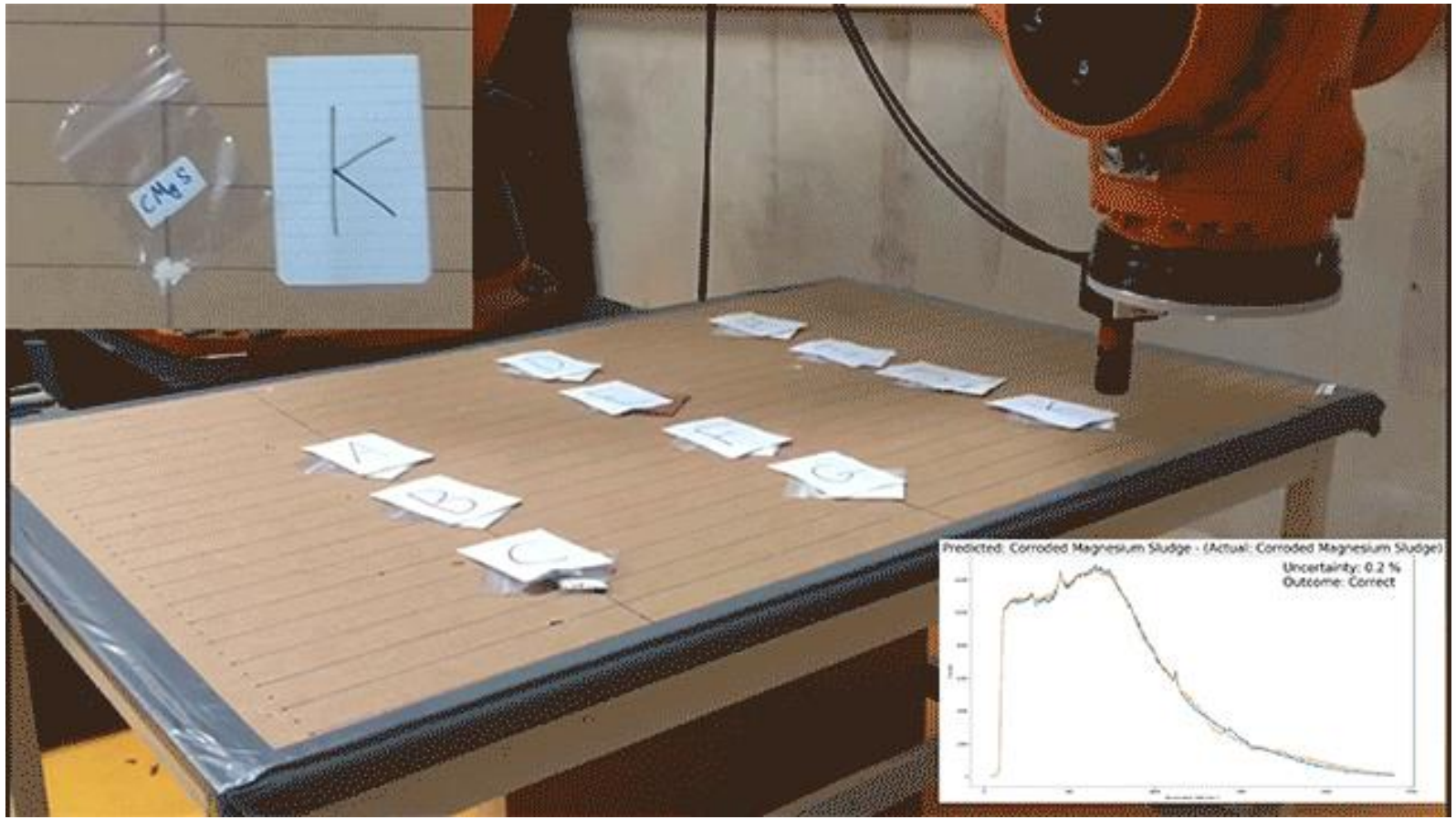

Validation Testing on UO_2 Fuels (ARF proposal)

NNL using unirradiated & irradiated AGR fuel pellets

Raman spectra:
785, 633, 514 nm

Identify products from *in situ* alteration expts.

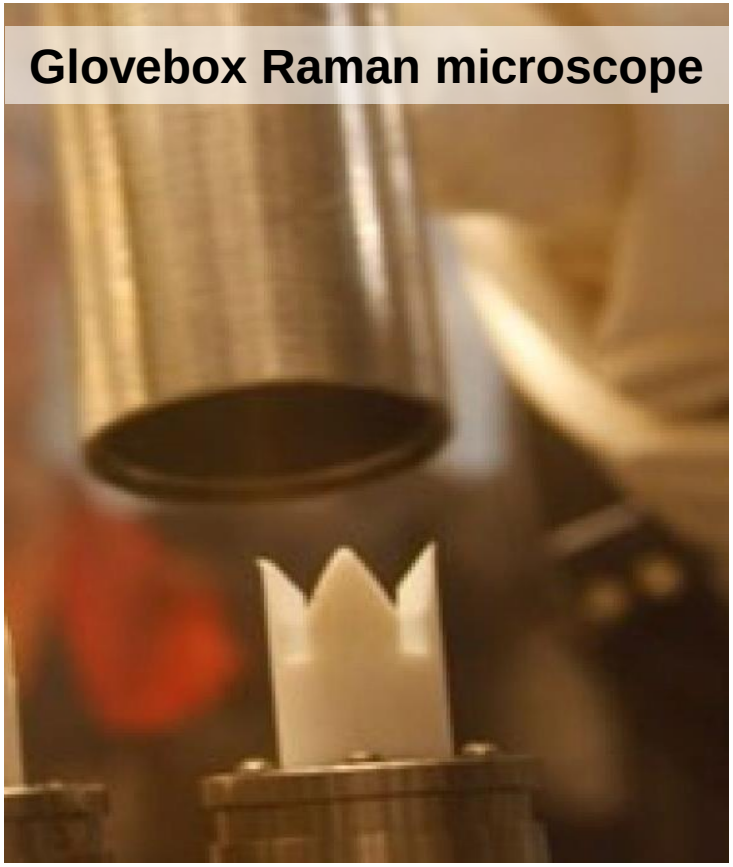

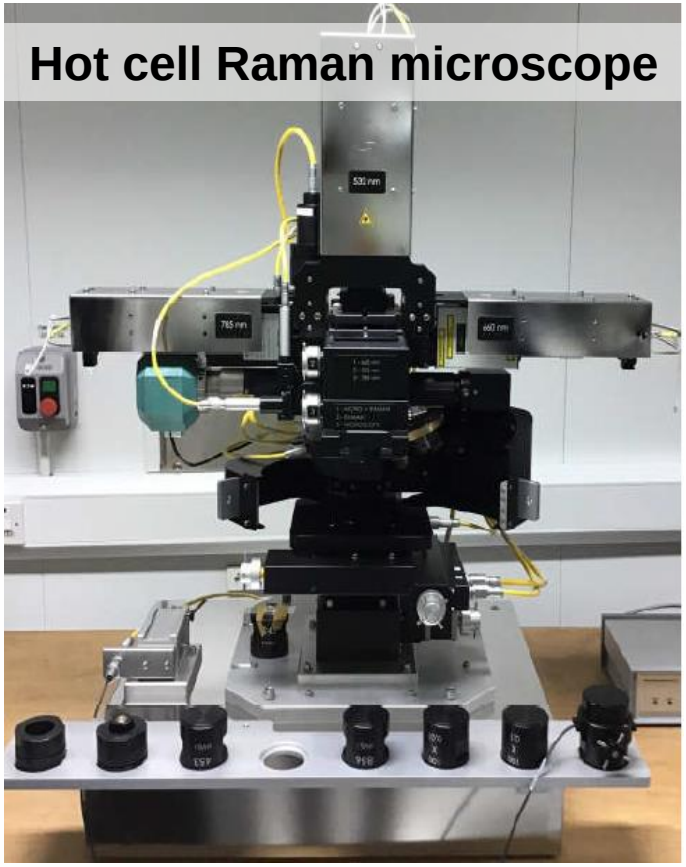

Conclusions & Future Work

- **Promising results from Transcend development work:**
  - **Raman and TRLFS ➡ phase identification, structure**
  - **LIBS (LA-ICPMS) system ➡ elemental composition**
  - **Expanding database of potential SNF alteration products**
- **Remotely-operated Raman validation with UoB – planned 2021**
- **Validation on 'real' SNF – ARF proposal**

Publications

- V.L. Frankland, A.E. Milodowski, J.W.G. Bright and D. Read. The use of Raman and TRLF spectroscopy for differentiating early stage alteration products of spent nuclear fuel. Appl. Geochem., 104934, Online April 2021
- N.B.A. Thompson, V.L. Frankland, J.W.G. Bright, D. Read, M.R. Gibert, M.C. Stennett and N.C. Hyatt. The thermal decomposition of studtite: analysis of the amorphous phase. J. Radioanal. Nucl. Chem., 327, 1335-1347 (2021)
- V.L. Frankland, A.E. Milodowski and D. Read. Characterisation of meta-autunite: towards identifying potential alteration products of spent nuclear fuel. Appl. Geochem., 123, 104792 (2020)
- V.L. Frankland, R. Bance-Souhali and D. Read. Raman analysis of meta-autunite. Environmental Radiochemical Analysis VI: 79-88 (2019). RSC Spec. Pub 354. IBSN:978-1-78801-735-0.

TRANSCEND

Transformative Science and Engineering for Nuclear Decommissioning

Radiation Laboratories: John-William Brown, Sarah Heisig and Michelle Willows
Raman: Dr Carol Crean and Dr Rachida Bance-Soualhi
SEM-EDX: David Jones
XRD: Dr Dan Driscoll

Loan of minerals: Kay Green,
Tom Cotterell, Mike Rumsey

Modelling: Dr Marco Sacchi and
Robert Lawrence

Funding:

Thank you

TRANSCEND

Transformative Science and Engineering for Nuclear Decommissioning

Investigating Uranium Corrosion in different environments Using X-ray Tomography

Dr Haris Paraskevoulakos, University of Bristol

TRANSCEND Virtual Meeting

Energy
For a Low Carbon Future

TRANSCEND

Transformative Science and Engineering for Nuclear Decommissioning

INDUSTRIAL CASE

- As of March 2015, the FGMSP has processed 27,000 tonnes of nuclear fuel (14,000 m^3 of contaminated water)
- Content: **Magnox** (Mg-Al alloy) cladding and **uranium** swarf
- Over the storage period Corrosion of Magnox cladding
- Formation of Magnox and uranic sludges

NOWADAYS

- ❑ Pond decommissioning (Uranium and CMS)
- ❑ *What is the uranium state? Corrosion products?*
- ❑ *How is the system affected with reducing sludge water content (sludge drying)?*

- ***Sellafield Ltd**: (FGMSP) The storage pond has processed 27,000 tonnes of nuclear fuel*

THEORY

$$Mg + 2H_2O \rightarrow \boldsymbol{Mg(OH)_2} + H_2$$

$$U + 2H_2O \rightarrow \boldsymbol{UO_2} + H_2$$

$$2U + 3H_2 \rightarrow 2UH_3$$

HAZARDS

- ❑ *Radioactivity/Toxicity*
- ❑ *Hydrogen Flammability*
- ❑ *UH_3 Pyrophoricity*

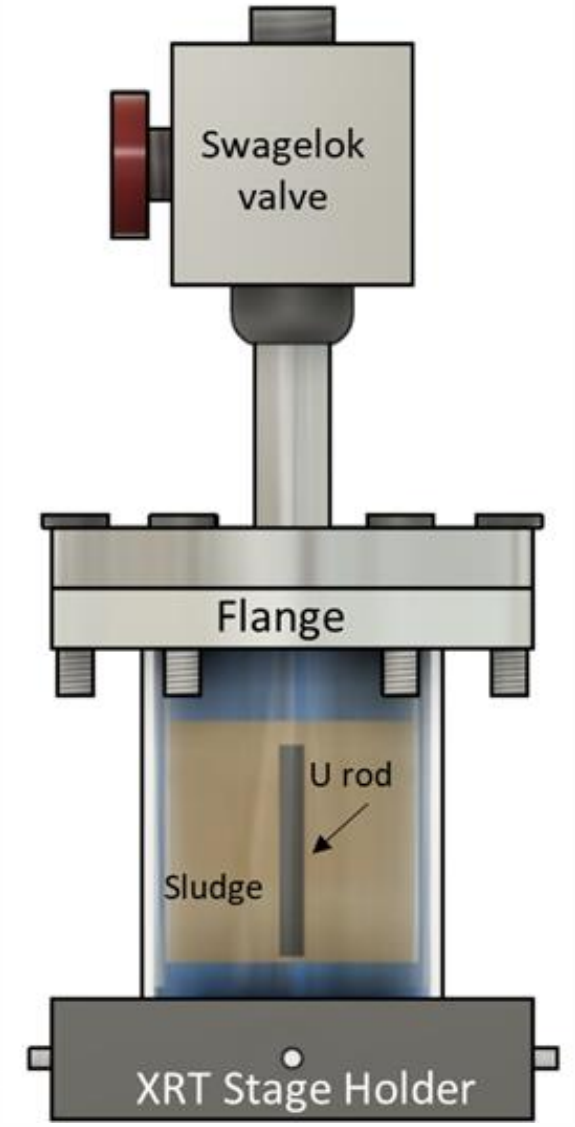

Scans

- Low-resolution, high FOV
  (~30µm/pixel, ~1 h 30 mins per scan)
- High-resolution, low FOV
  (~2.8µm/pixel, ~20 hours per scan)

Data Collection

- 20 days after preparation
- 50 days after preparation
- 360 days after preparation
- 540 days after preparation

TRANSCEND

Transformative Science and Engineering for Nuclear Decommissioning

50 Days Post Preparation

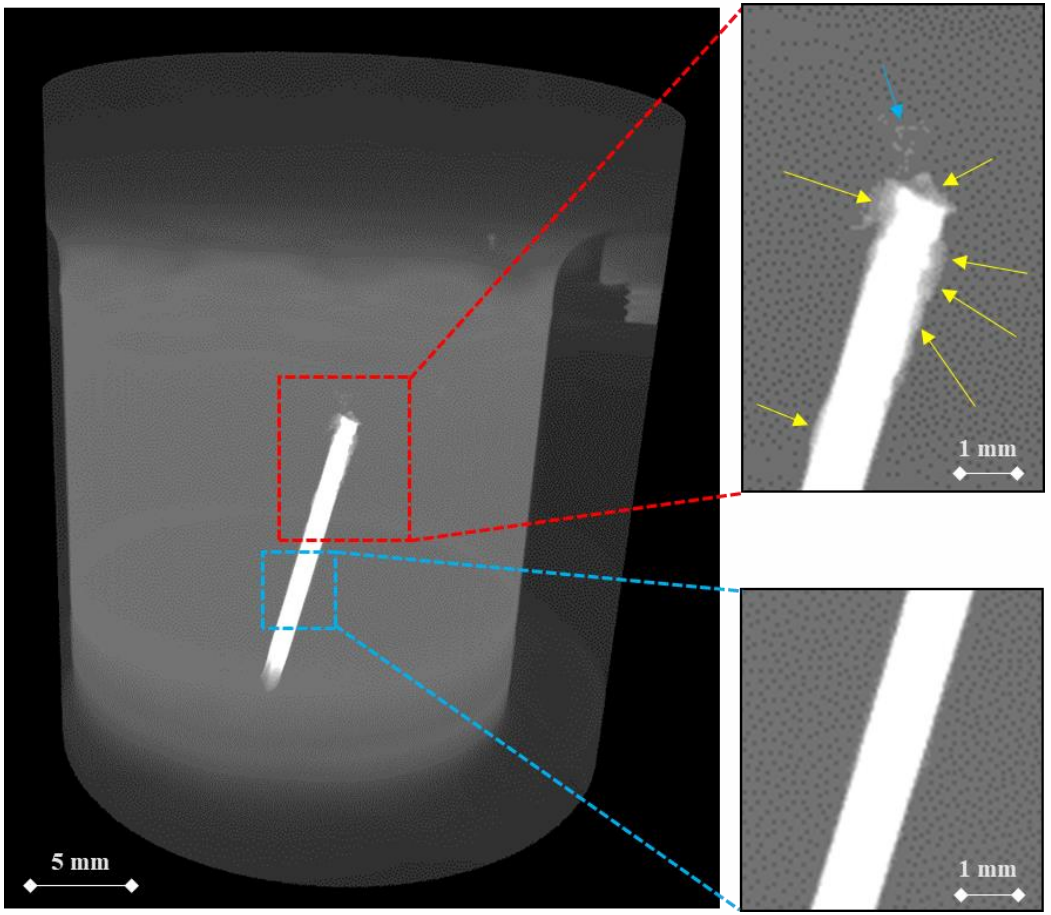

Key findings

- *Corrosion Product Volume Growth*
- *Signs of Coalescence*
- *Migration away from the Corroding Front*
- *Intact Low Surfaces*

TRANSCEND

Transformative Science and Engineering for Nuclear Decommissioning

540 Days Post Preparation

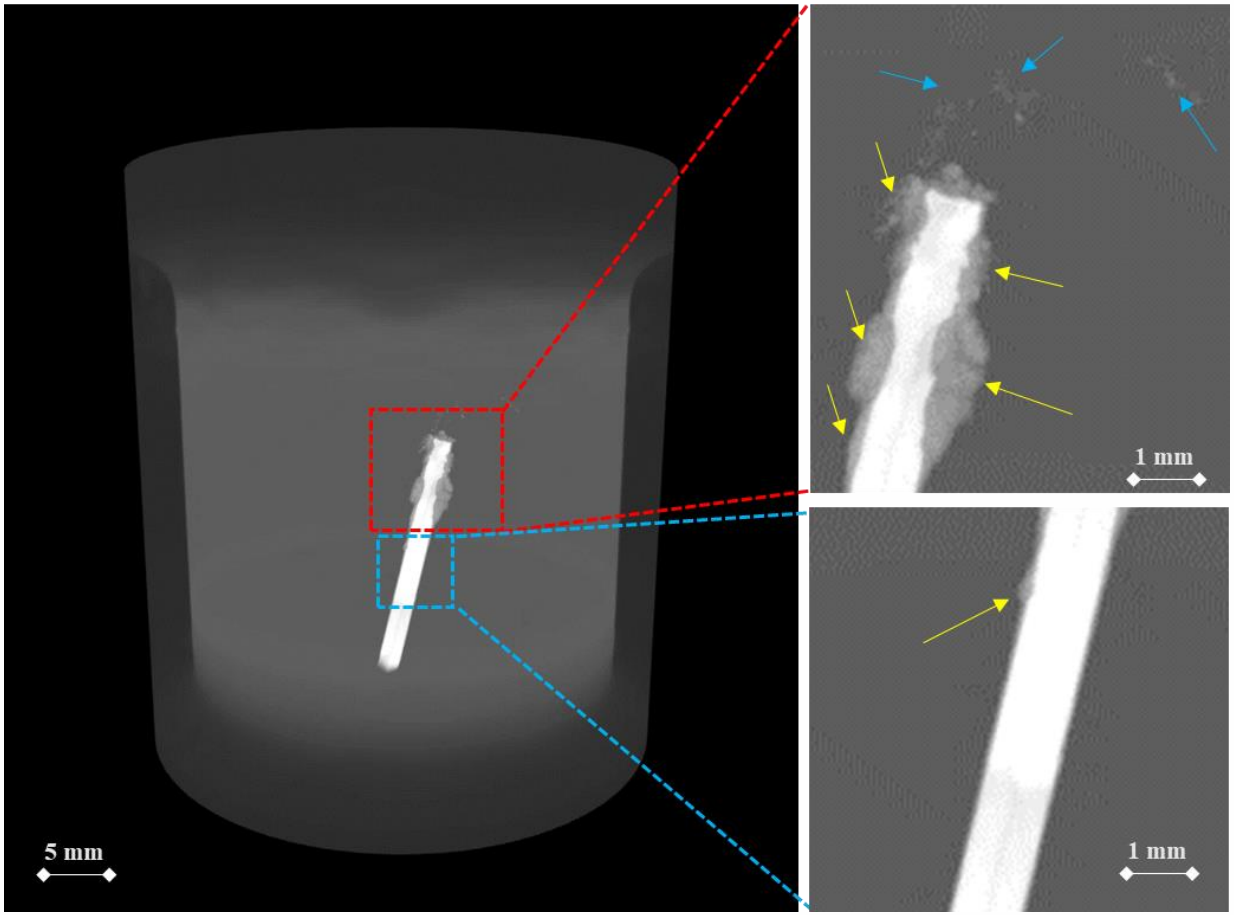

Key findings

- *Corrosion product volume remained constant*
- *Intact low surfaces*
- *Further migration of particles away from the uranium*

Quantitative Analysis

- Image processing software Avizo®
- Material segmentation (Uranium, Corrosion products)
- Determination of relevant volumes
- ***Calculation of corrosion percentage***
- ***Calculation of corrosion rate***

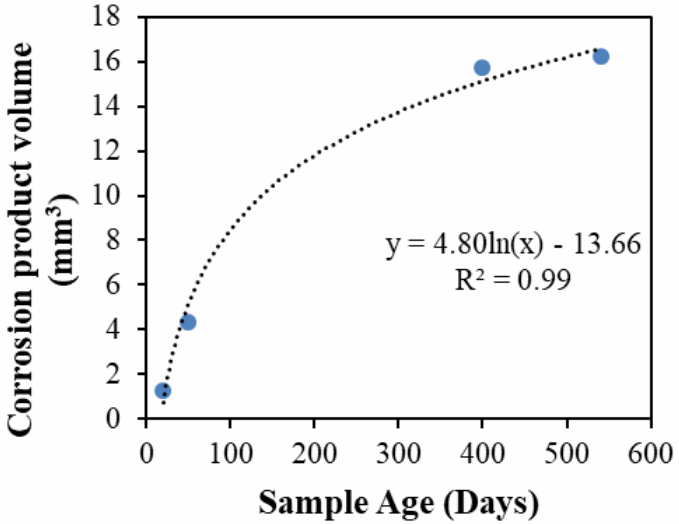

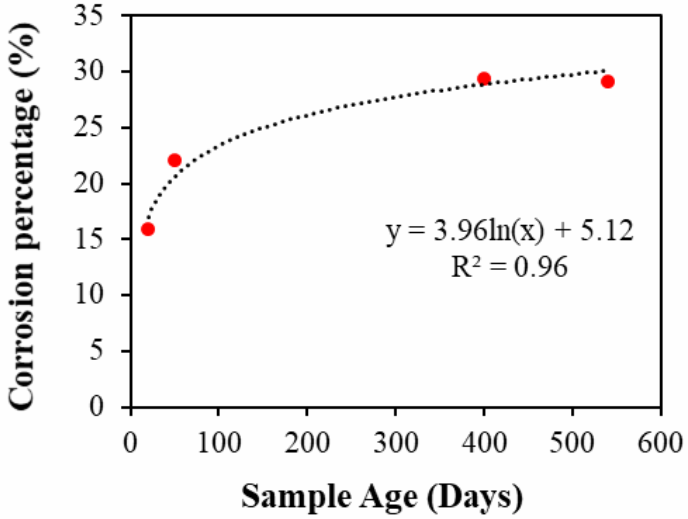

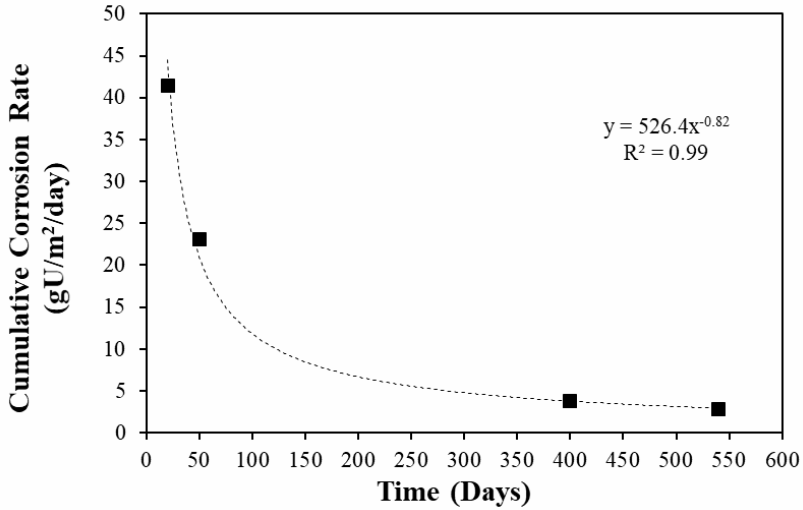

Weaknesses

- Hydrogen pressure was not recorded for this particular system
- Gas analysis was not performed
- Sludge was not probed
- Sealed system – Sludge drying behaviour could not be evaluated

Uranium Corrosion in Mixed Grout Systems – Large Scale

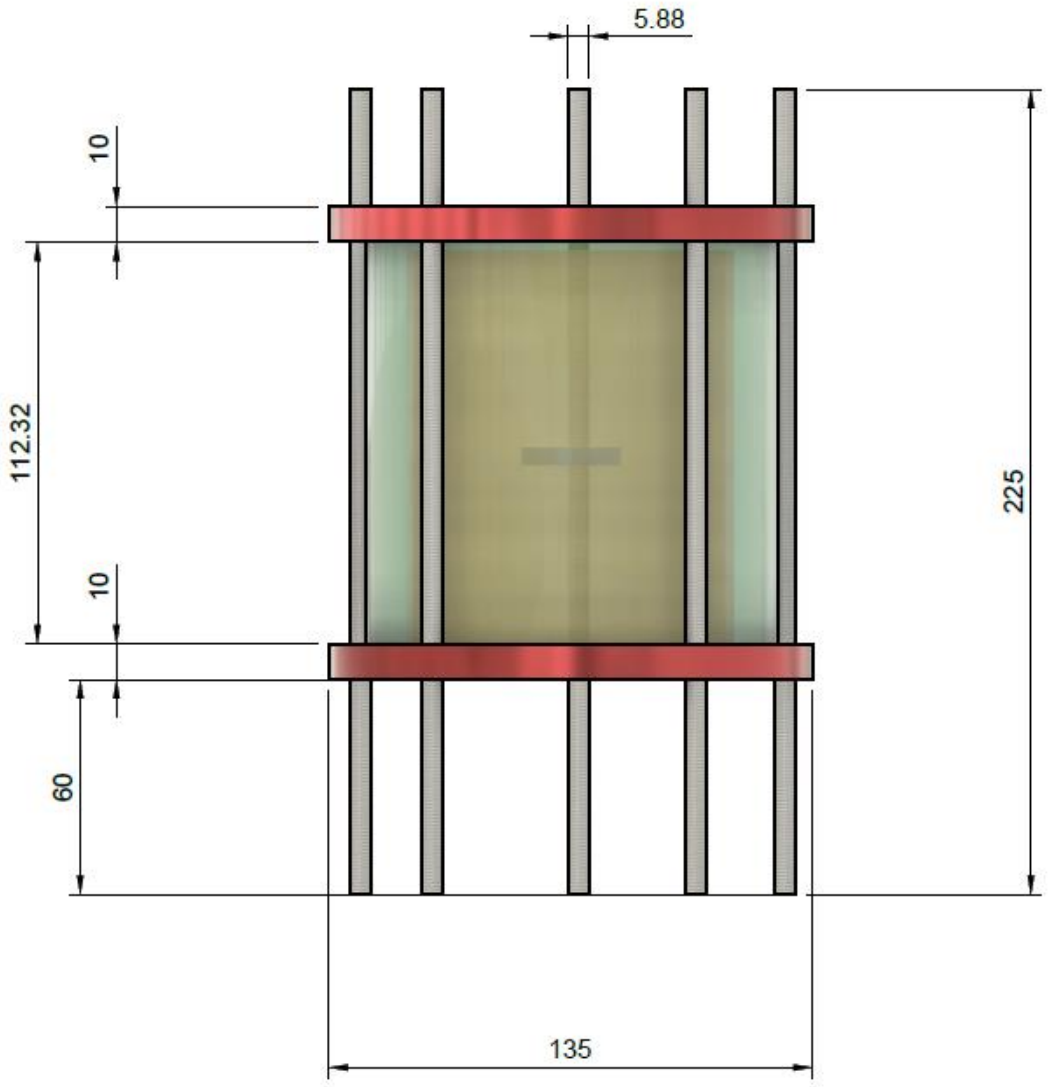

TRANSCEND

Transformative Science and Engineering for Nuclear Decommissioning

Uranium Corrosion in Mixed Grout Systems – Large Scale

- Custodians of 14 samples originally produced by NNL

- 6 trials U + Grout
- 4 trials U + Grout + Magnox Sludge
- 2 trials U + $Mg(OH)_2$
- 1 trial U + NaOH
- 1 trial U + Polymer

- Uranium long term (~15 years) metallic corrosion in mixed grout and sludge) formulations

- Corrosion under ambient conditions

Experimental Goals

- What is the state of uranium?
- What is the state of corrosion products?
- What is the identity of corrosion products?
- What is the state of the encapsulants?

1	STT 2	U metal + Grout	-
2	STT 9	U metal + Grout	3:1 PFA/OPC, 0.40 w/s
3	STT 11	U metal + Grout	3:1 PFA/OPC, 0.45 w/s
4	STT 20	U metal + Grout	3:1 BFS/OPC, 0.20 w/s, s'plasticised
5	STT 25	U metal + pH13 NaOH	Water at pH 13
6	STT 40	U metal + Vinyl Ester polymer	Vinyl ester polymer 0.30 w/p
7	SDP 1	U metal + Grout + CMS	1:1 PFA/OPC + sludge, 0.6 w/s
8	SDP 2	U metal + Grout + CMS	1:1 PFA/OPC + sludge, 0.6 w/s
9	CT 10	U metal + Grout	5:1 GGBS/CEM I
10	CT 11	U metal + Grout	5:1 GGBS/CEM I
11	SDP LET 8	U metal + Grout + CMS	-
12	SDP LET 11	U metal + Grout + CMS	1:1 GGBS/CEM I + sludge, 0.48 w/s
13	PCT 6	U metal + sat. $Mg(OH)_2$	-
14	PCT7	U metal + sat. $Mg(OH)_2$	-

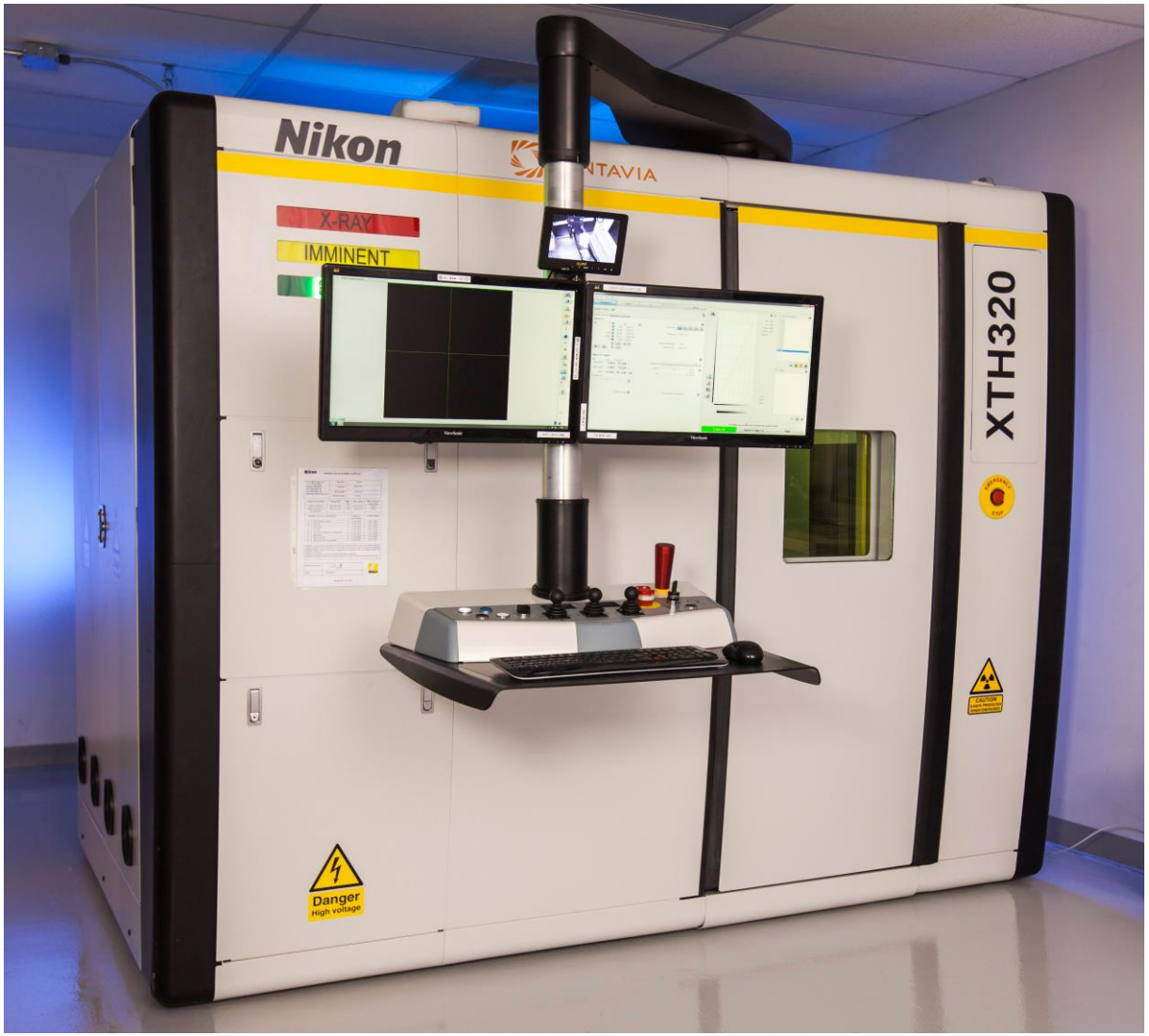

Primary Research Activities

- X – Ray Tomography
- National Composite Centre (NCC)
- High Energy X-Ray beam (~320 kV)
- 7 samples scanned
- Voxel resolution 83.5 µm
- FOV: Entire Sample

Excellent Opportunity

- *Sample size impossible to be probed using **synchrotron X-ray imaging** (Lower energies available)*
- ***Neutron Imaging** suitable based on the sample size*

- **CT 10**

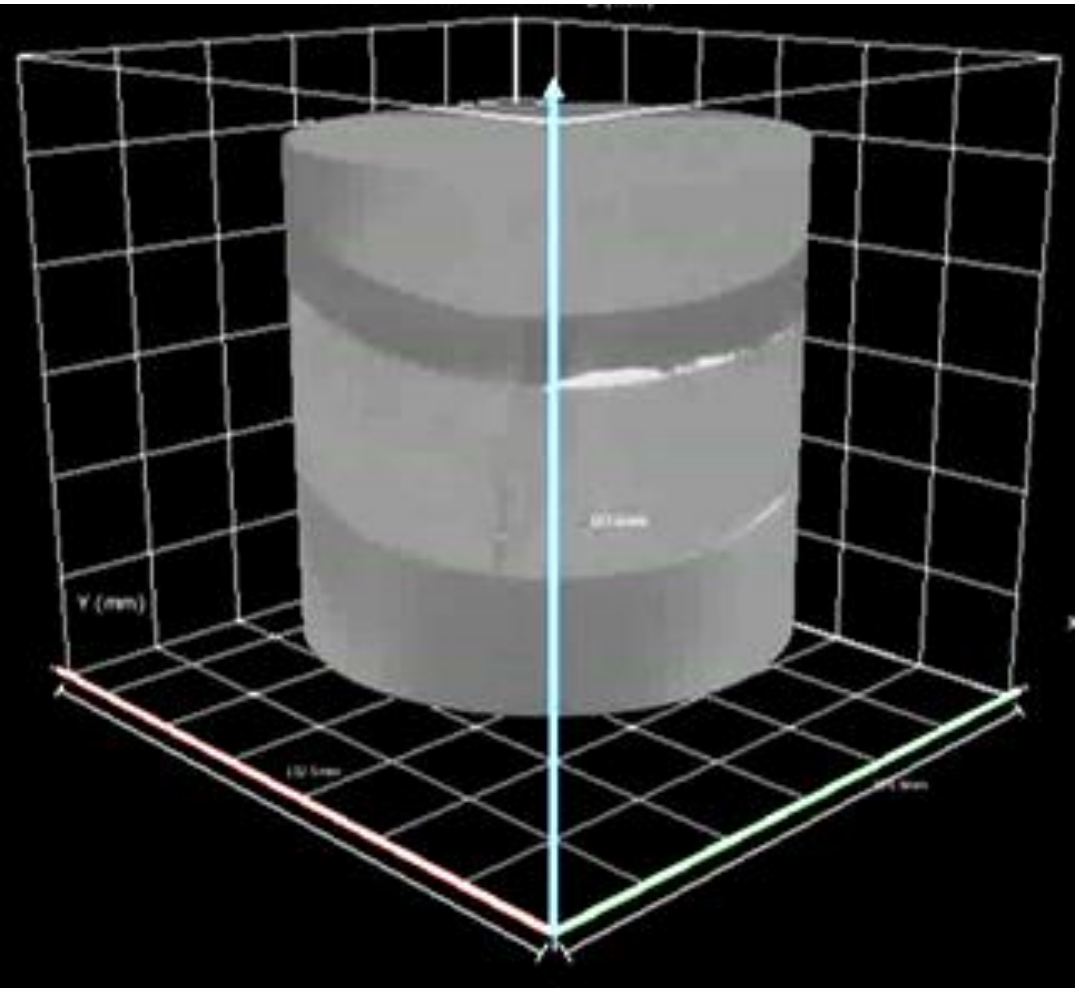

- **CT 11**

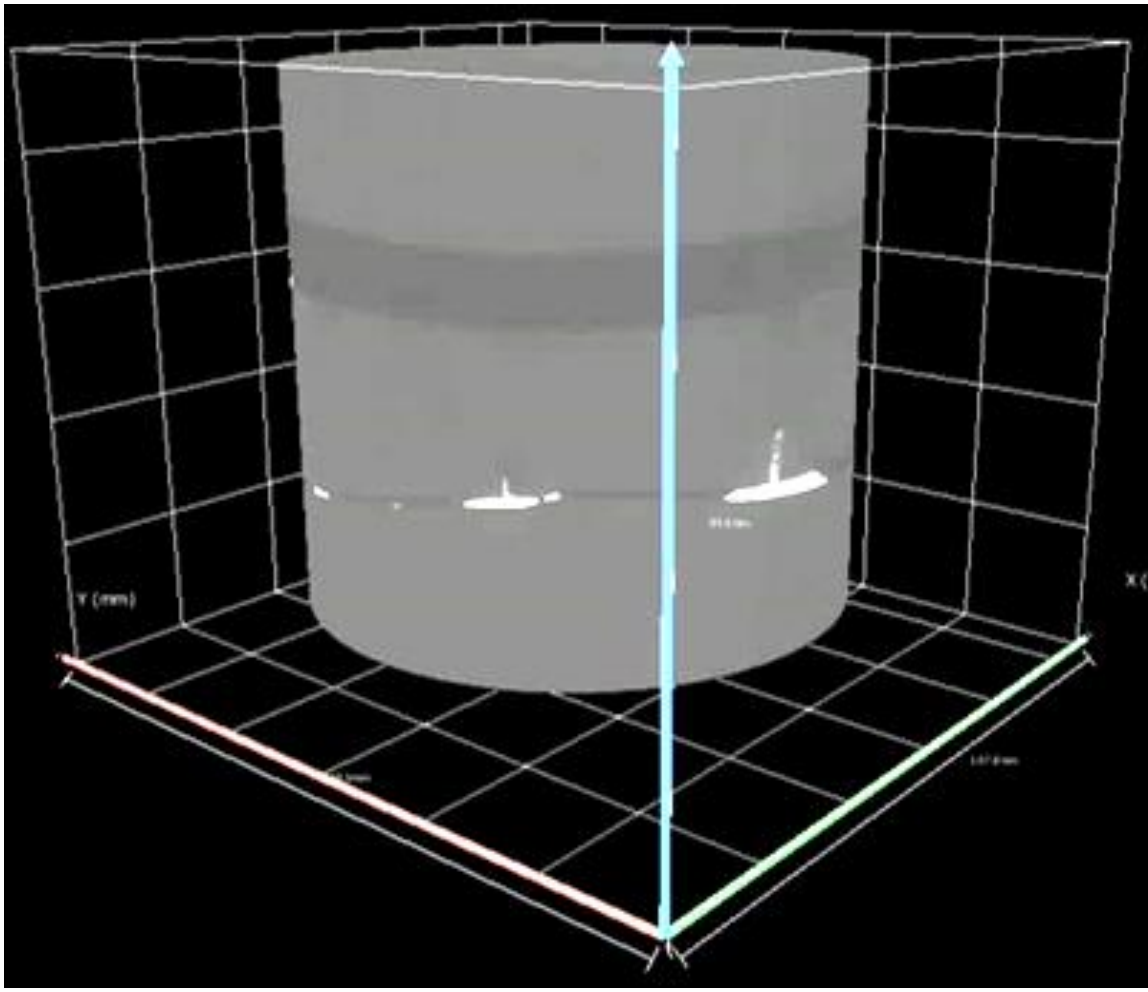

- **STT 9**

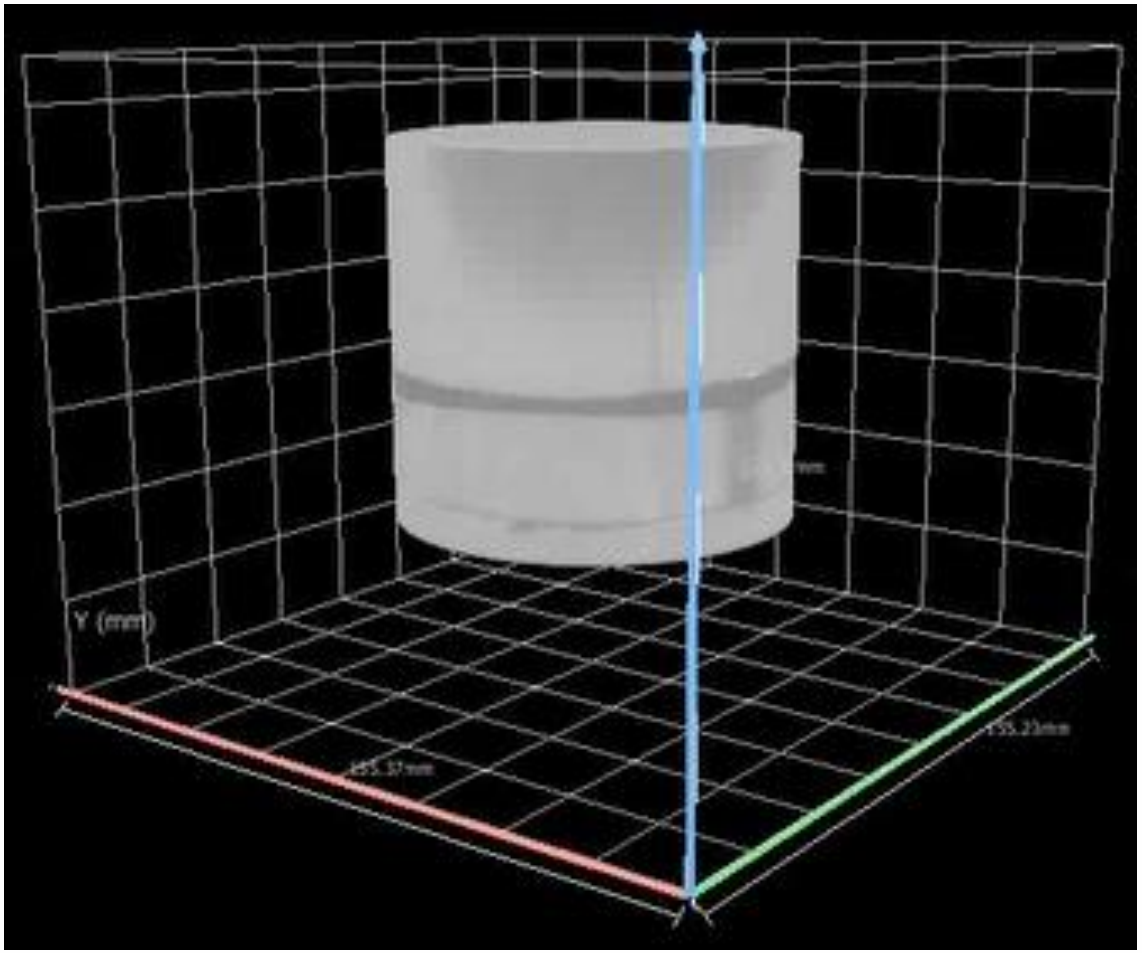

- **STT 11**

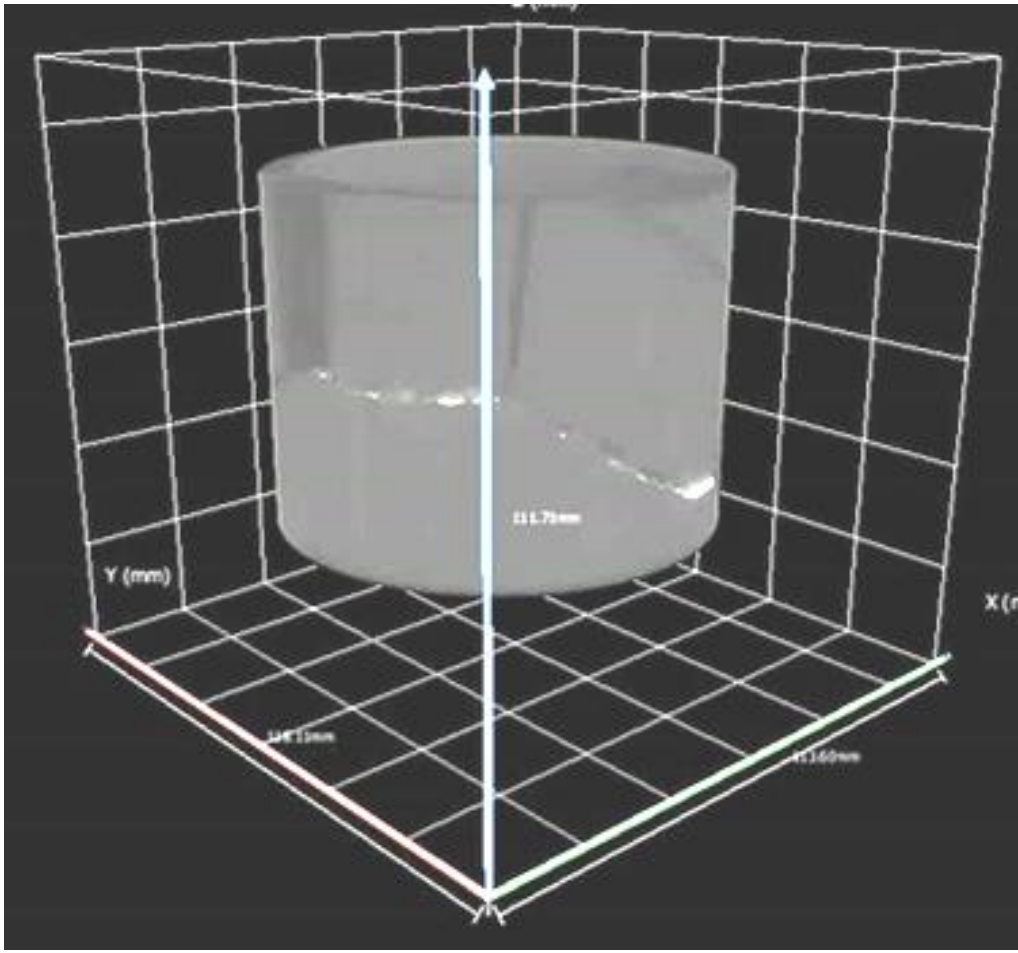

- **STT 20**

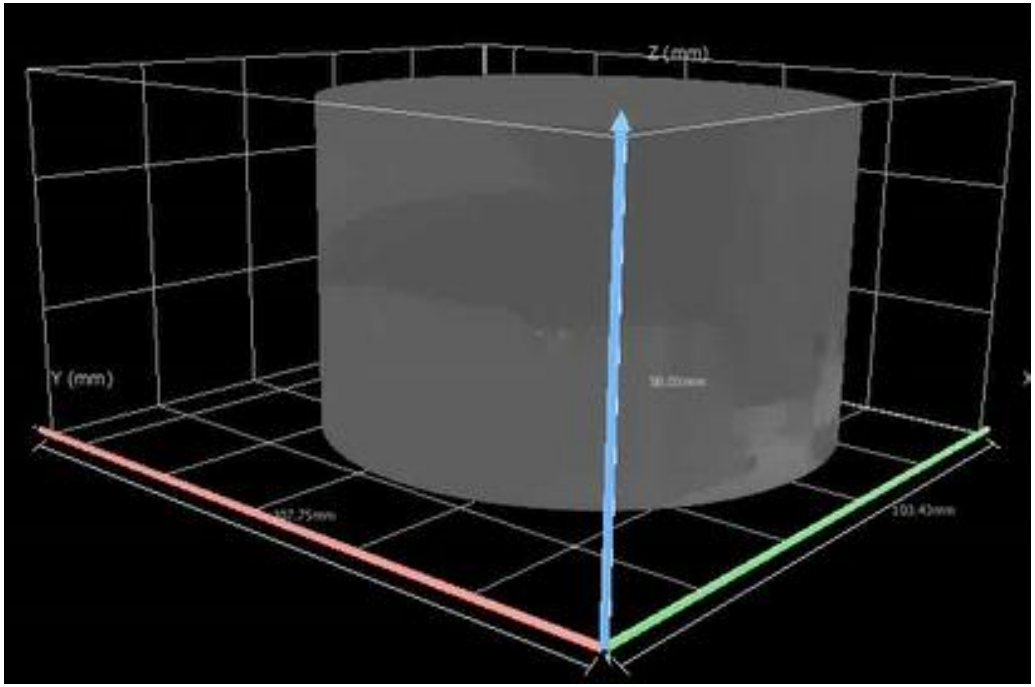

- **STT 40**

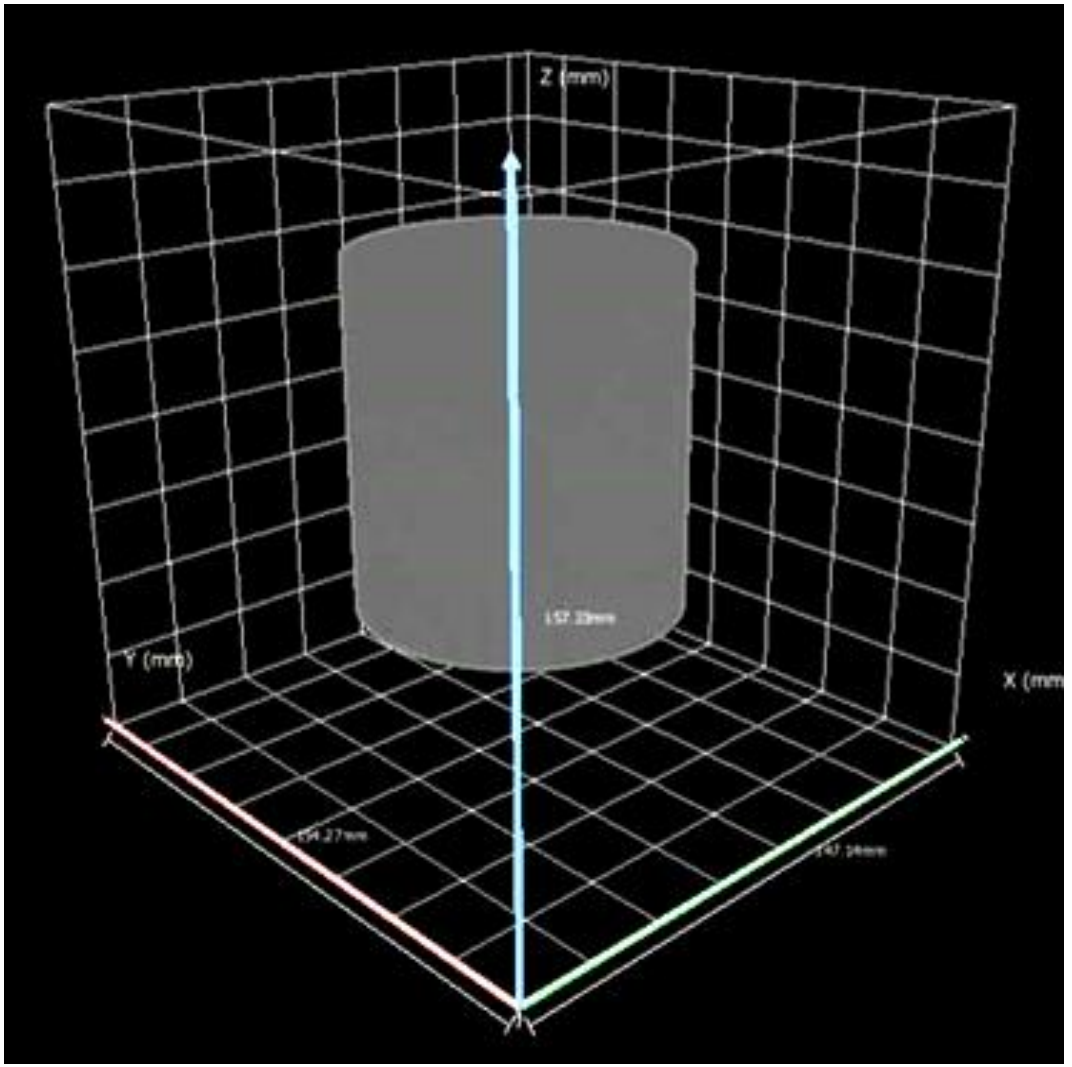

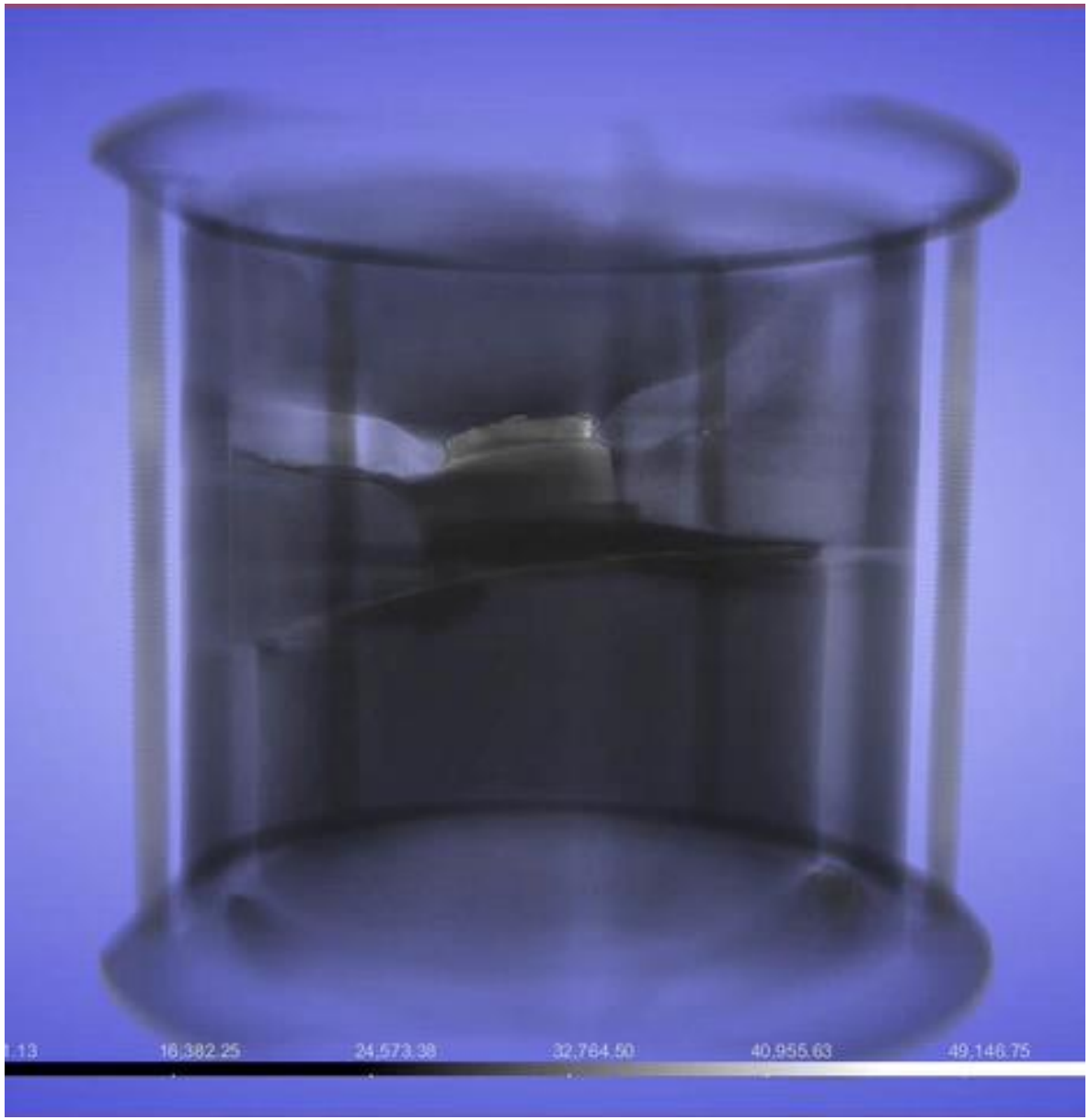

Targets

- *Uranium corrosion magnitude*
- *Uranium corrosion product identity*
- *3D mapping of uranium corrosion products diffusion/migration*
- *Grout damage magnitude (crack volume)*
- *Corrosion-Degradation quantitative correlation*

➢ STT 40
Material Segmentation

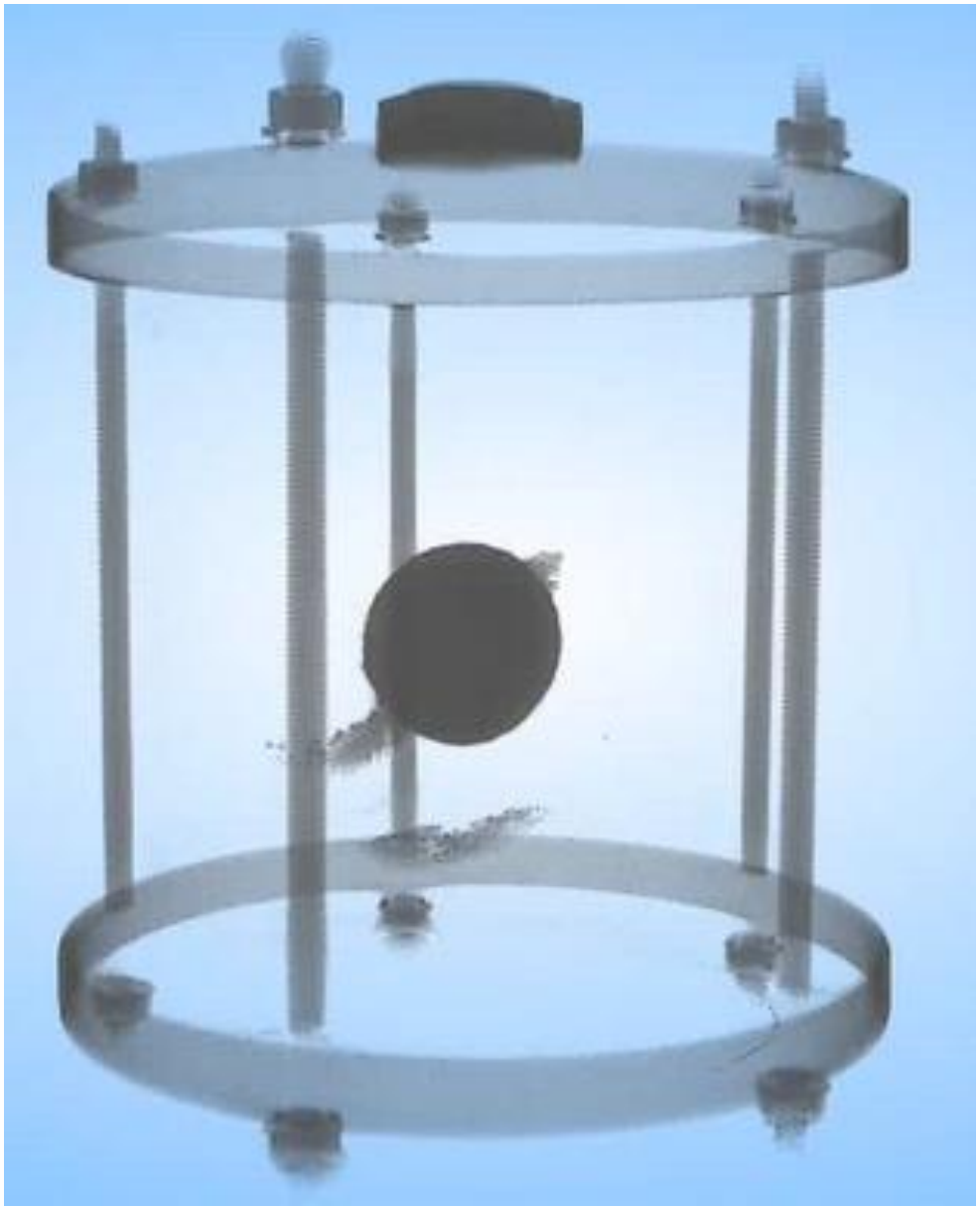

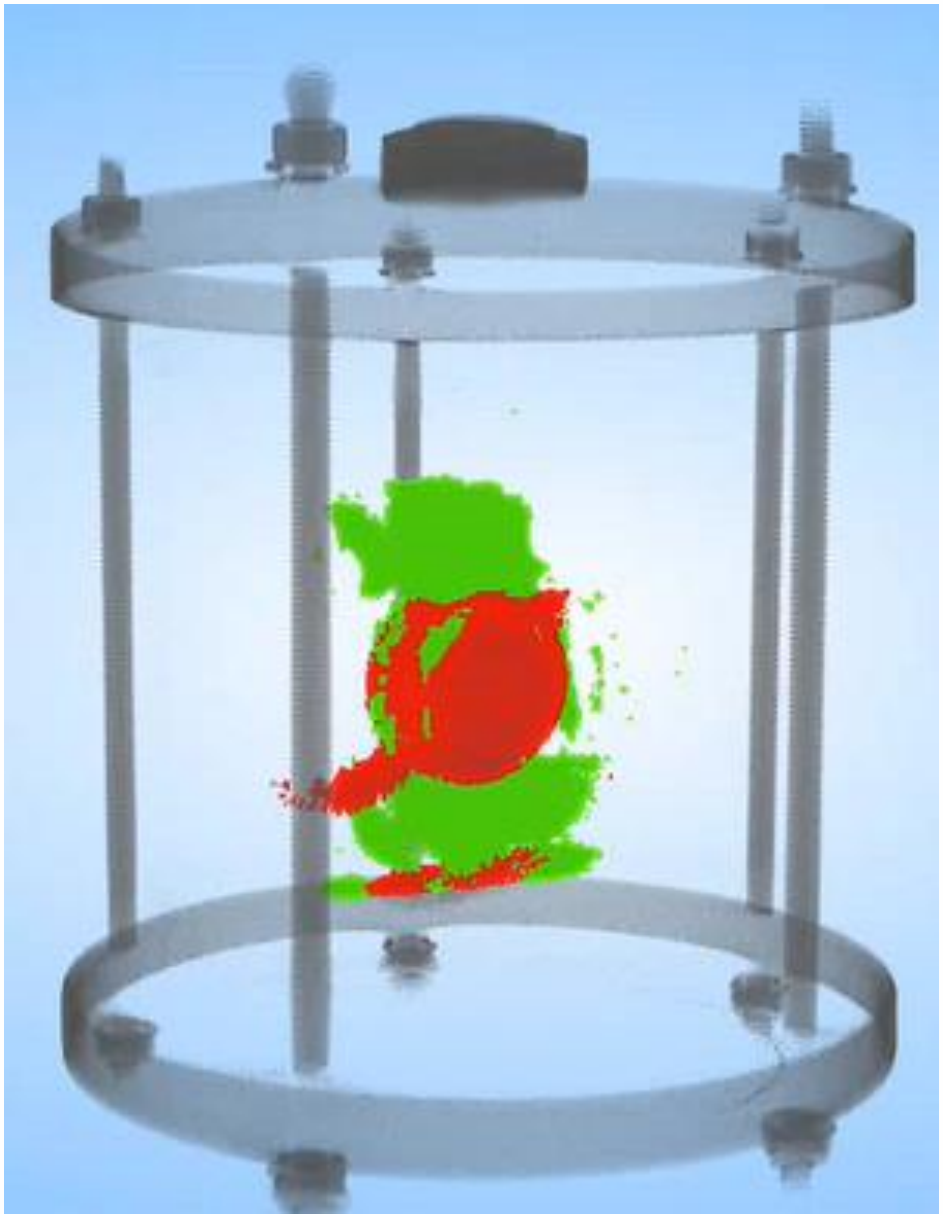

➢ CT 10 – Visual Material Segmentation

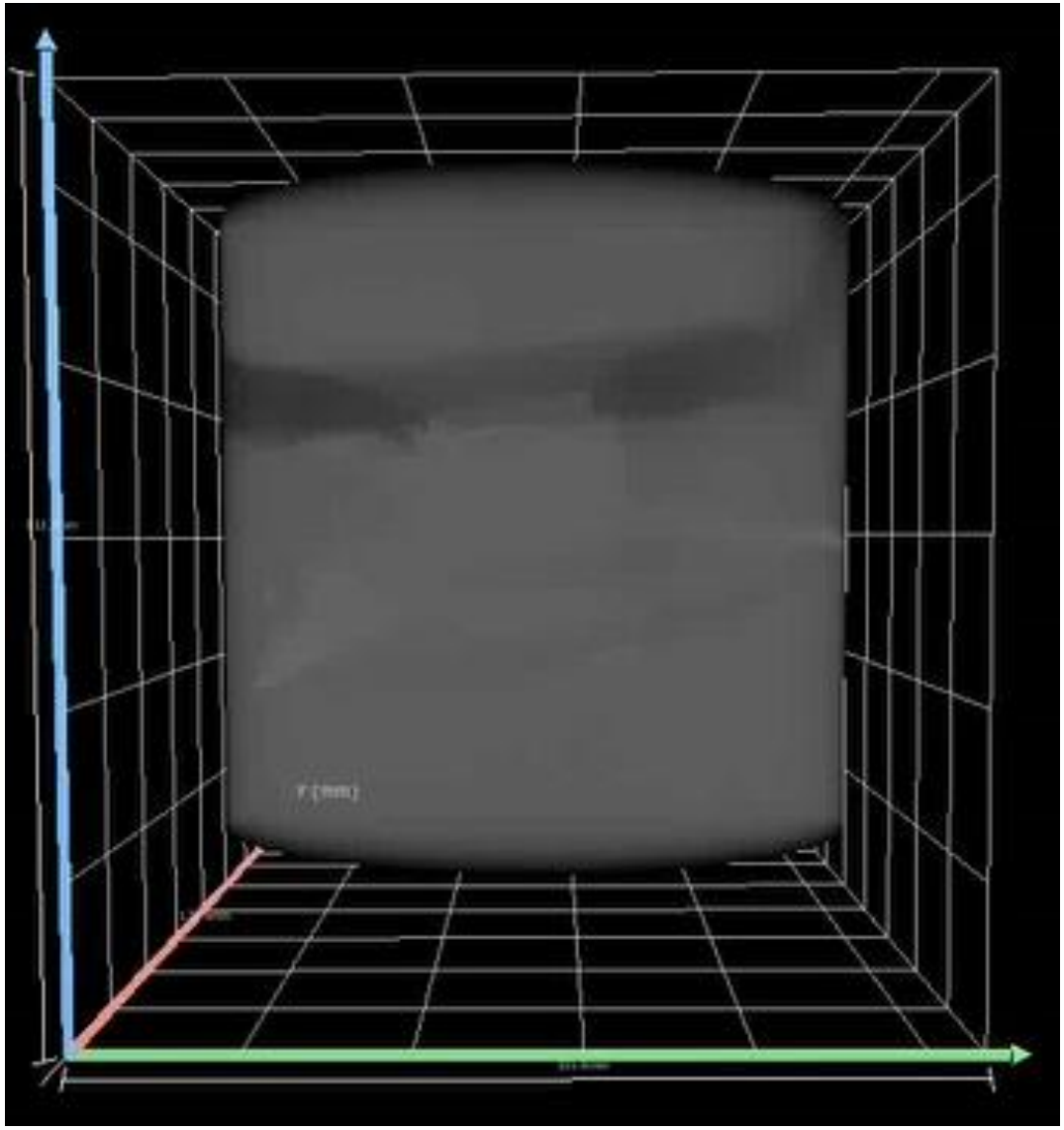

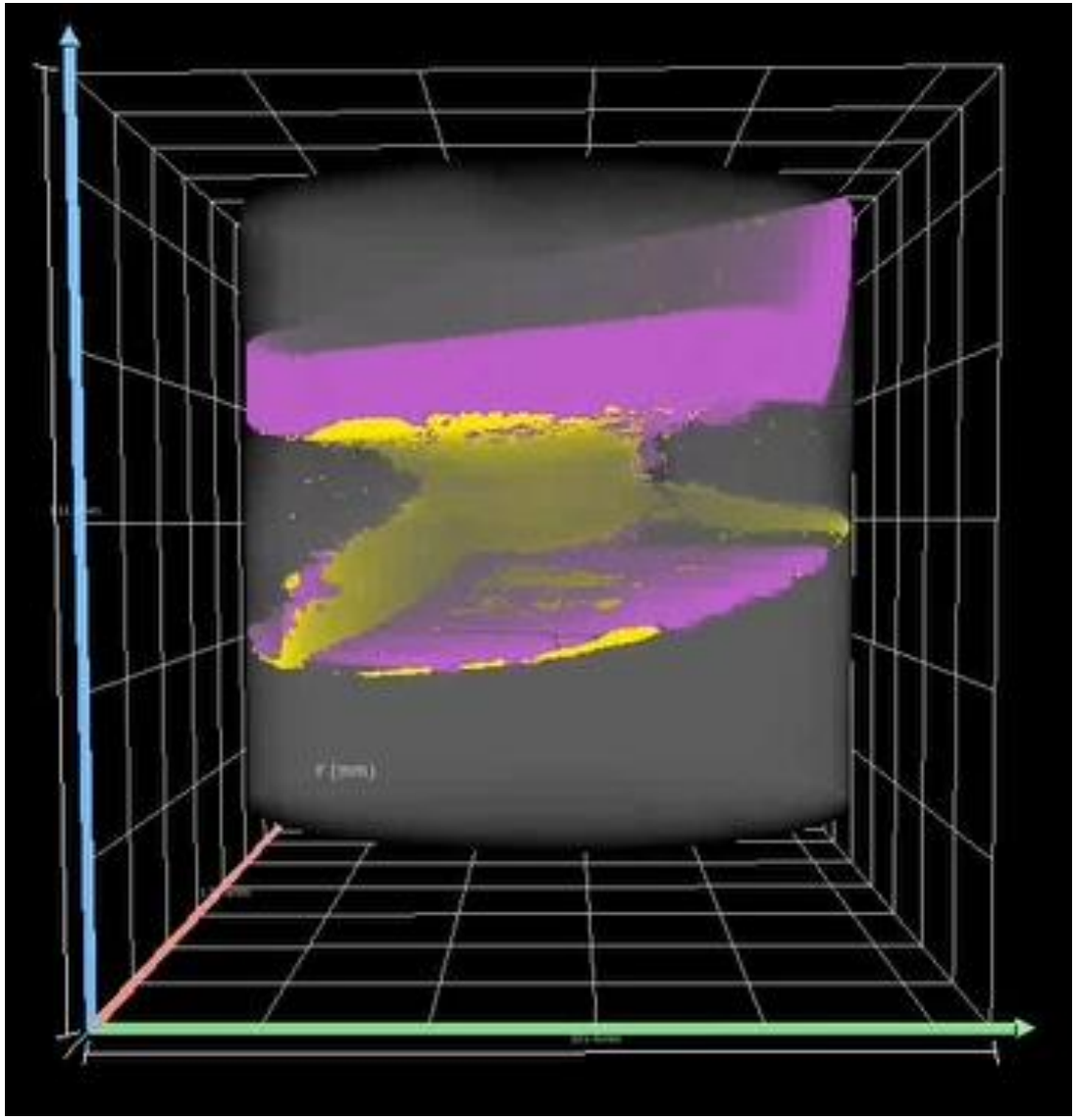

➢ CT 11 – Visual Material Segmentation

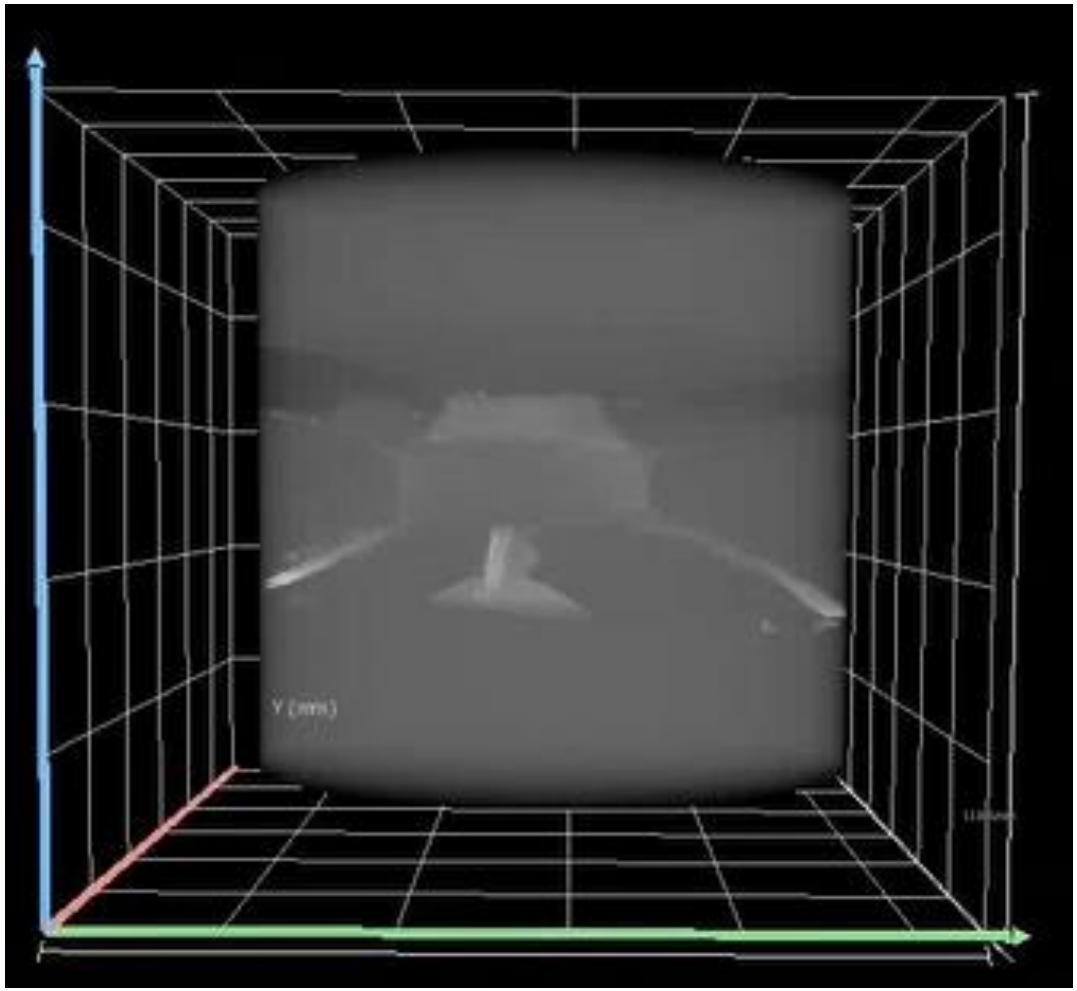

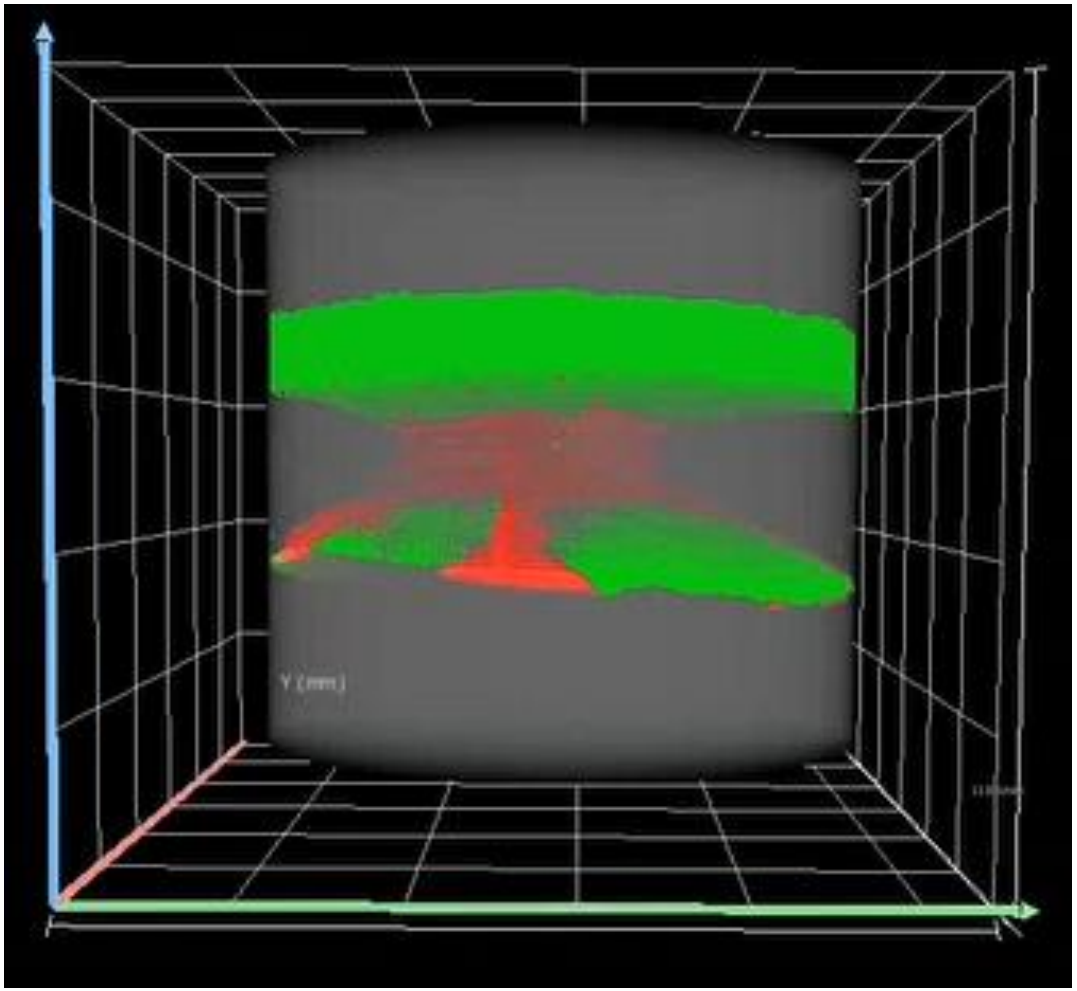

Quantitative Segmentation

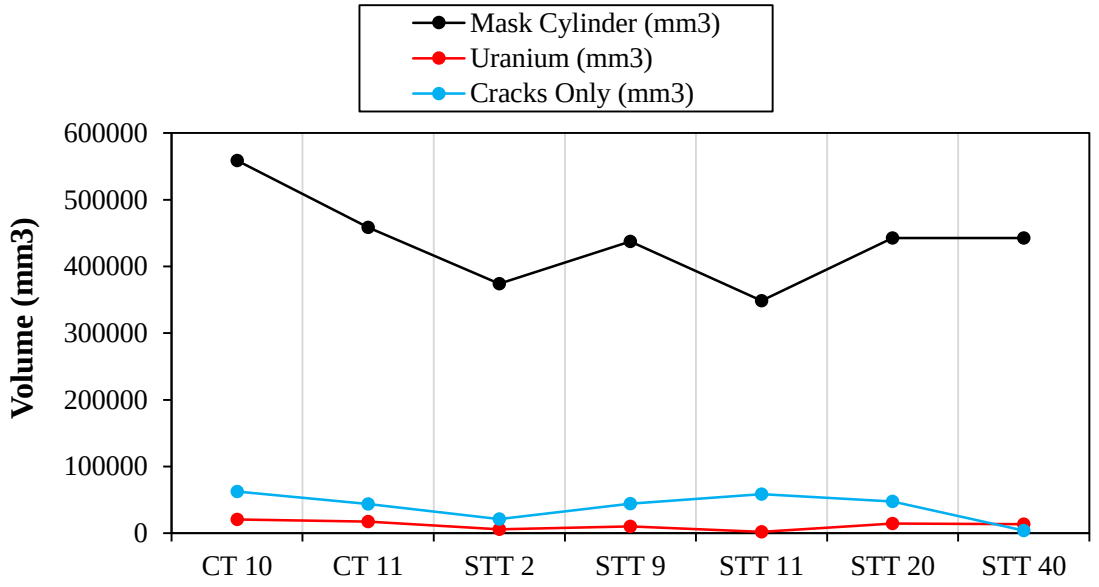

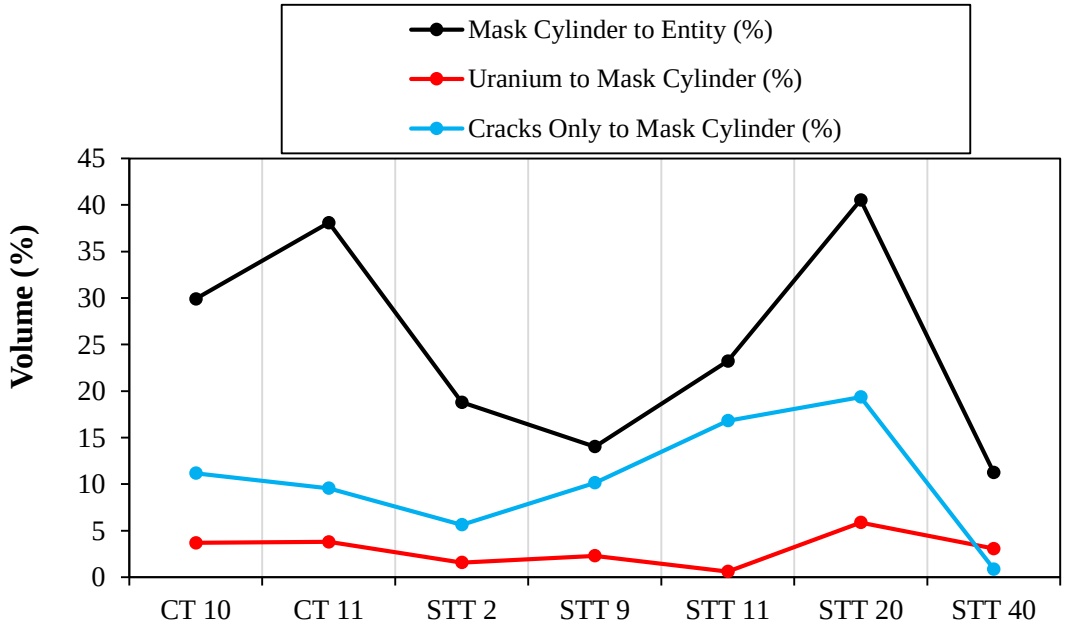

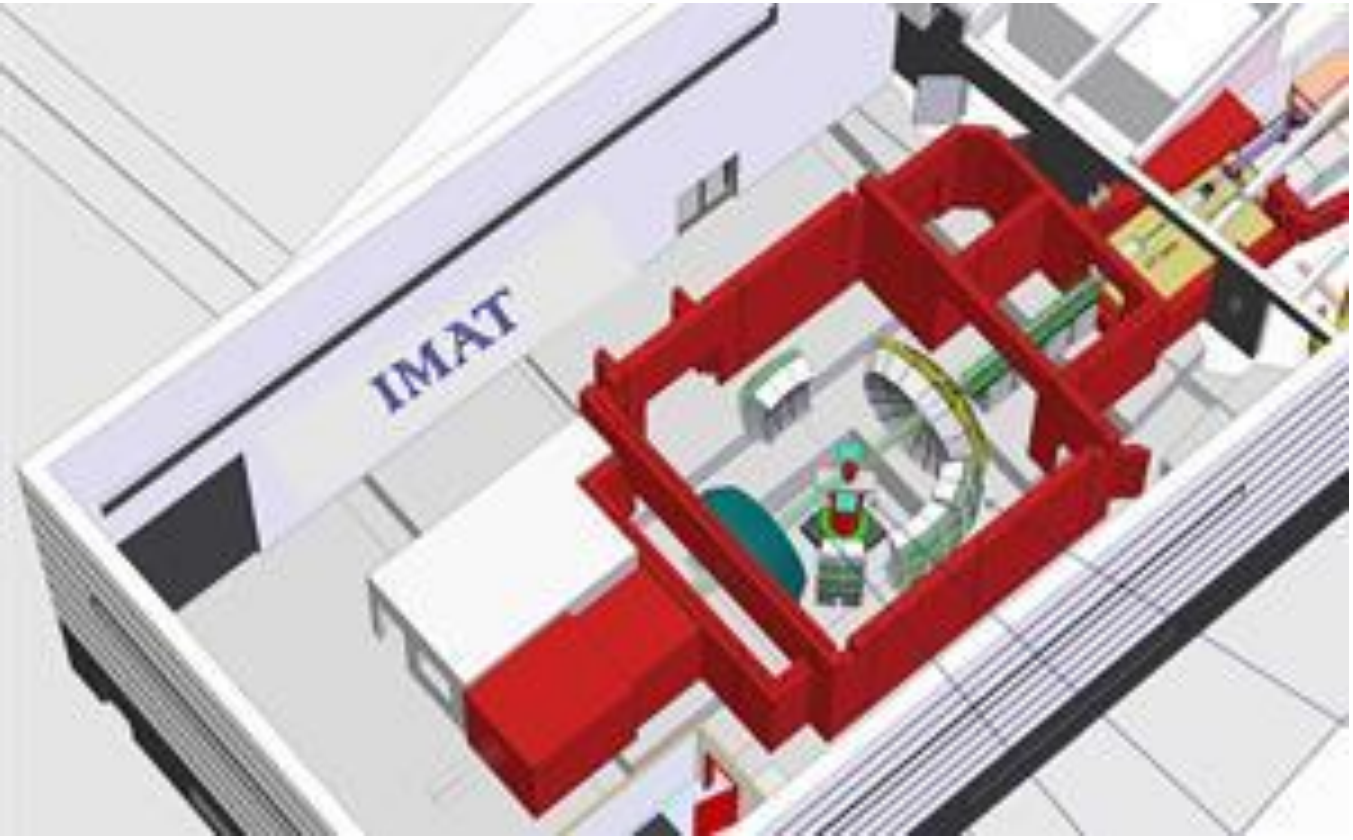

Future Research Activities

- XRT at higher energy (Full Power at 320 kV
- Higher geometric magnification
- Scanning of all samples
- ISIS Neutron Imaging
- ISIS Neutron Diffraction

Acknowledgments

- Dr Chris Jones
- Dr Yusuf Mahadik
- Prof Tom Scott
- Dr Genoveva Burca

TRANSCEND

Transformative Science and Engineering for Nuclear Decommissioning

TRANSCEND

Transformative Science and Engineering for Nuclear Decommissioning

Lancaster University

UTGARD LABORATORY

Radioactive Waste Management

MOX SIMfuels: Preparatory Studies
Preparation of Europium doped Cerium Oxide Surrogates

18th May 2021

Presenter: Ian Robertson

Authors: Ian Robertson, Colin Boxall, Richard Wilbraham

Supervisor: Professor Colin Boxall, Dr Samuel Murphy

Energy

Background

- The UK possesses small amounts of both Unirradiated and Irradiated Mixed Oxide (MOX) fuel formed of a blend of plutonium oxide and uranium oxide.
- In line with current government policy, this MOX would not be reprocessed; rather, it would be sent to disposal within a geologic disposal facility (GDF).
- MOX simulant fuel (SIMFUEL) pellets will be produced as a safer alternative to actual plutonium MOX.

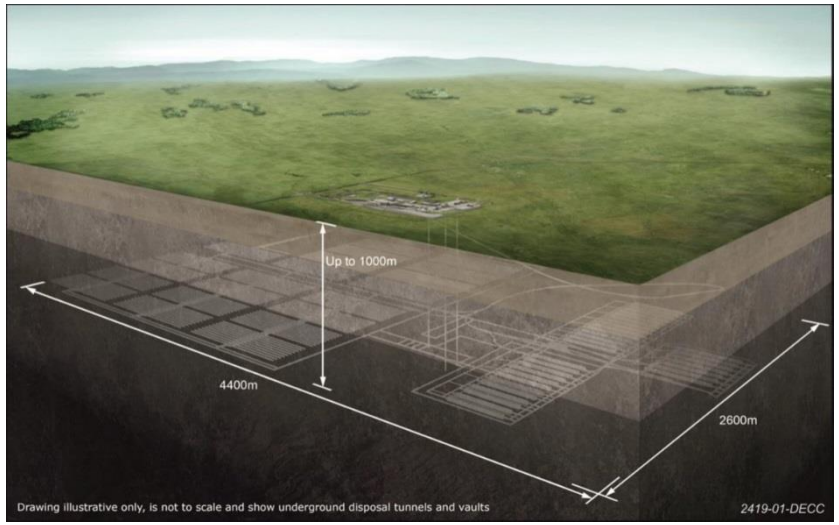

Artists impression of a GDF

Research Aims

- Production and characterisation of simulated unused and used MOX fuels to serve as baseline systems.

- Solution phase electrochemical corrosion and leaching behaviour studies of both of these MOX simulants, aiming to obtain fuel dissolution rates as a function of key variables such as pH, salinity, O2 availability and temperature.
  - Dissolution in these Circumstances can be considered a Corrosion Process.

- Facilitated by collaboration with NNL, to assess how closely the simulants represent the physico-chemical and materials properties of real spent fuel.

Pellet Production

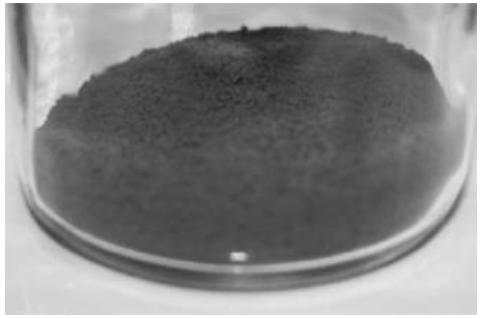


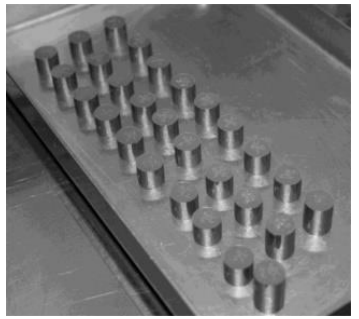
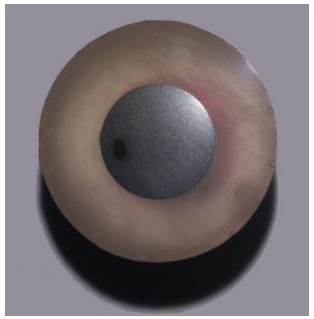

Various stages in SIMFuel Fabrication.

Pellet and SEM

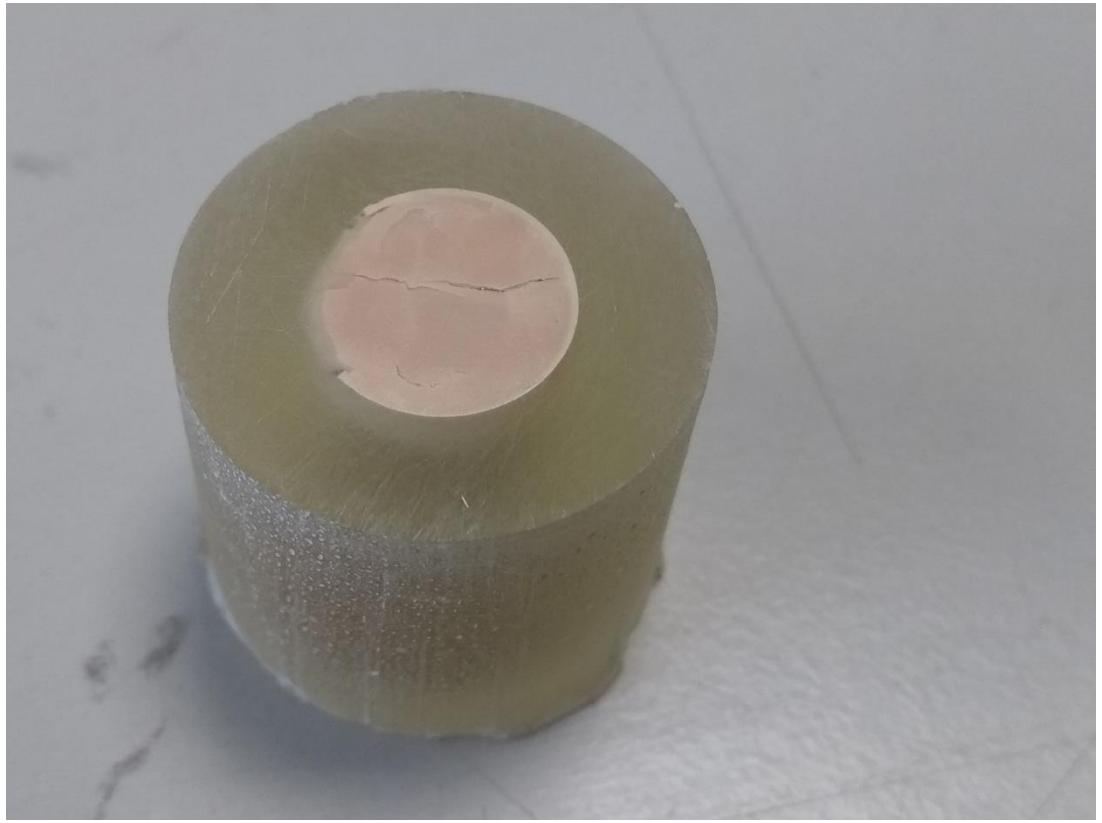

Sintered CeO_2 Pellet converted into an electrode.

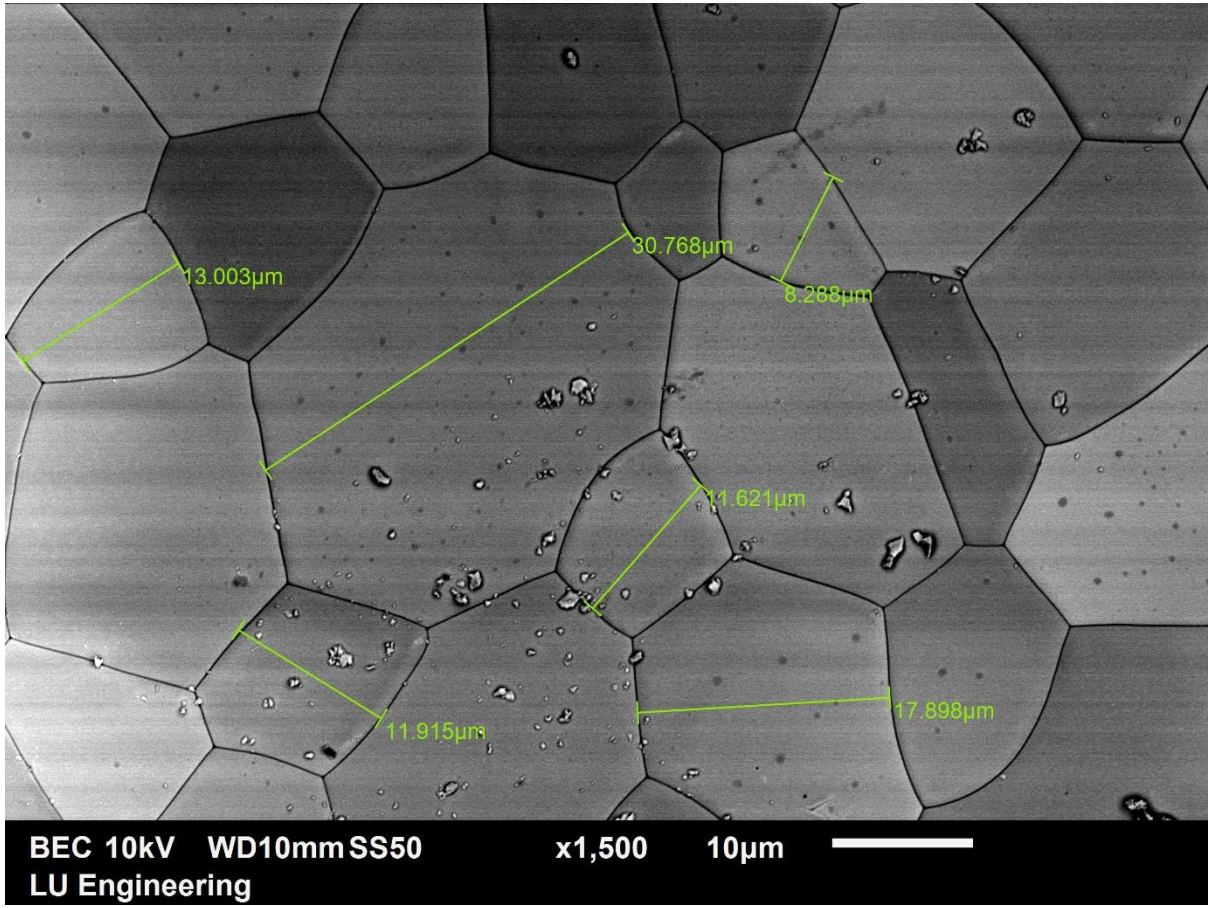

SEM of the Sintered CeO_2 Pellet Surface.

Pure CeO_2 Raman Spectrum

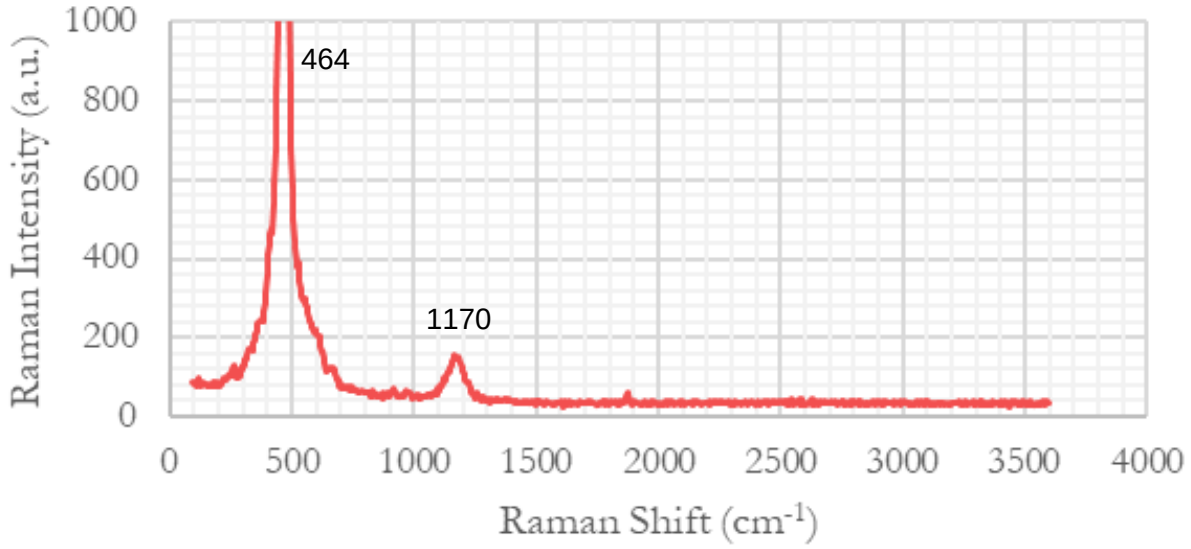

E-Chem Rig

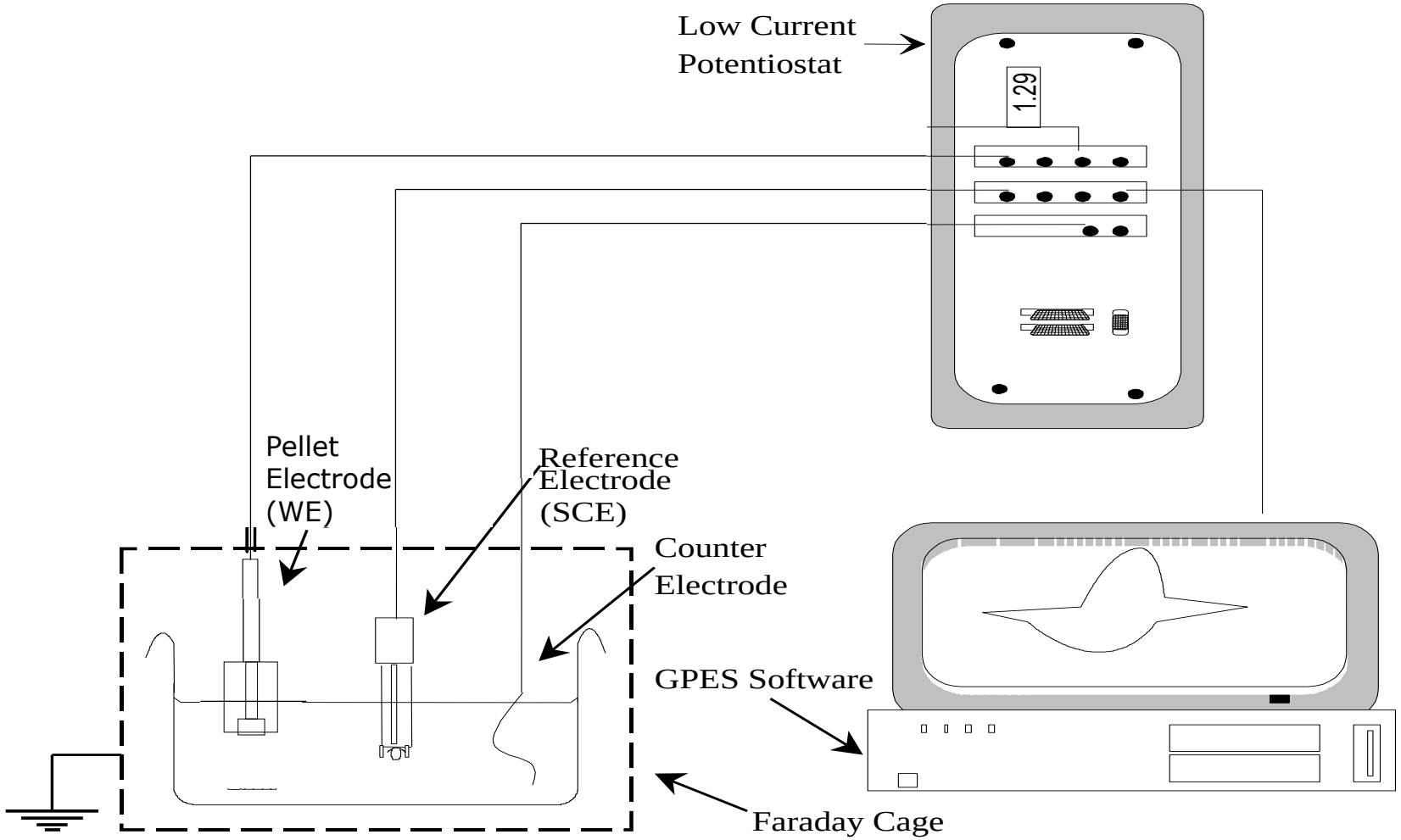
Low Current
Potentiostat
1.29
Pellet
Electrode
(WE)
Reference
Electrode
(SCE)
Counter
Electrode
GPES Software
Faraday Cage

Sintered CeO_2 CV

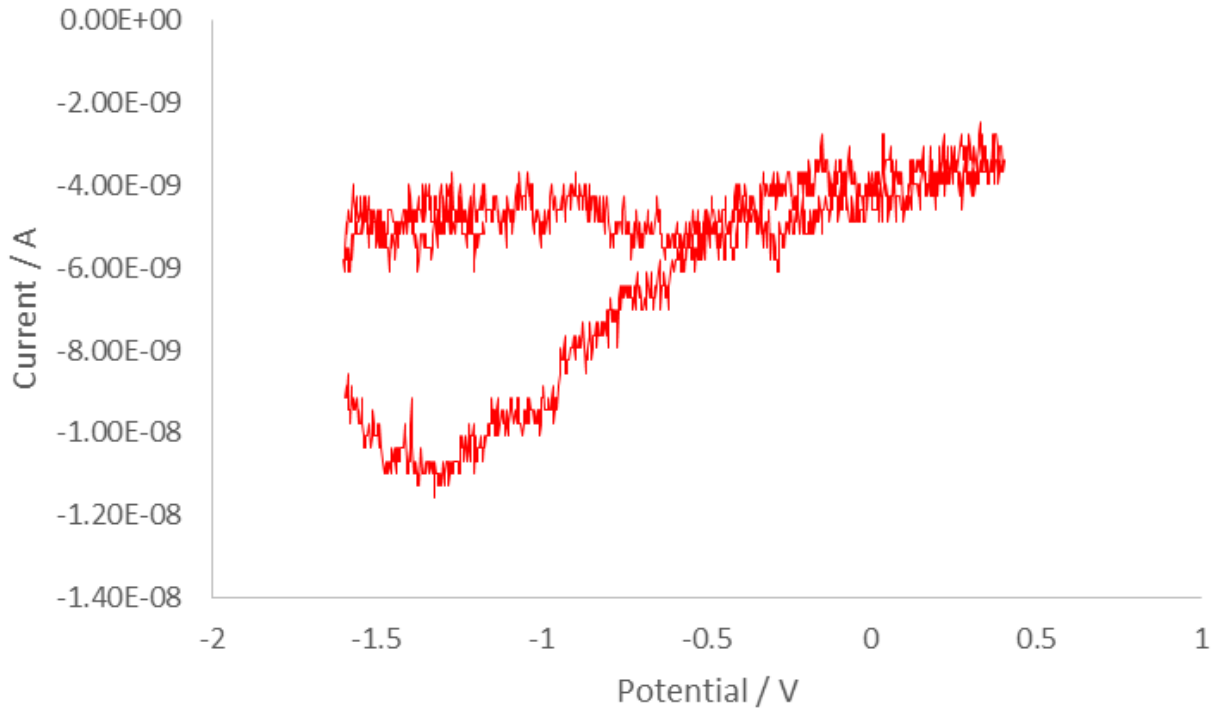

CV of CeO_2 pellet in 0.1 M NaCl pH 9.5 solution sparged with air for 1 hour. Scan Rate 0.01 V/s , IR Compensation 2.0 kΩ (Max)

1st Doped Pellet Raman Spectrum

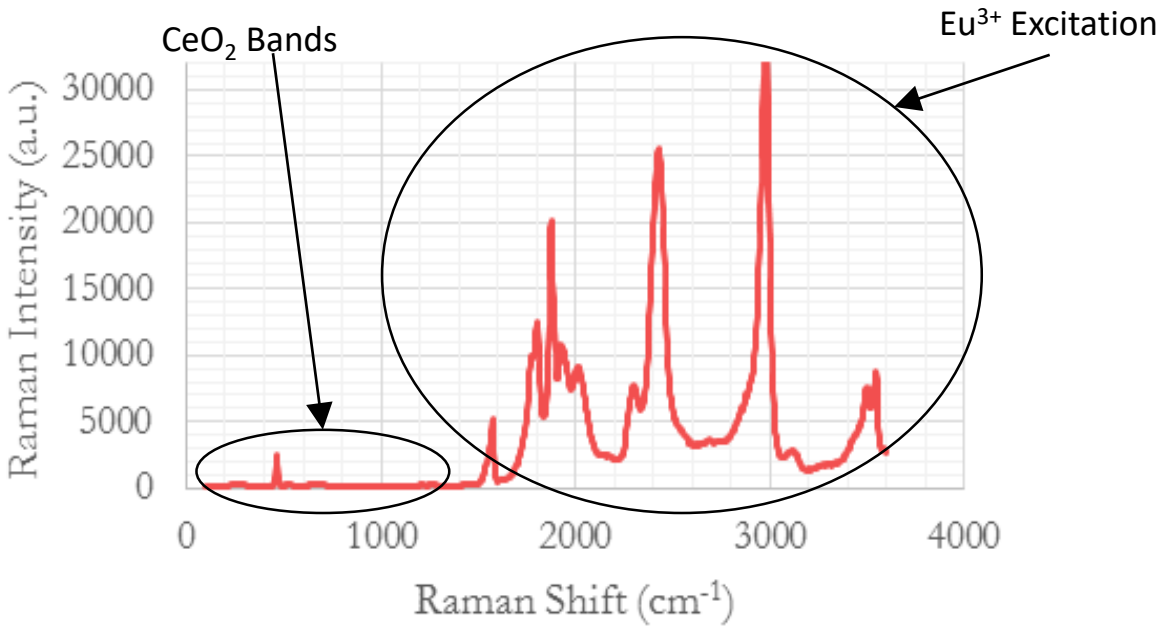

Raman Spectra of CeO_2 pellet doped with Eu_2O_3

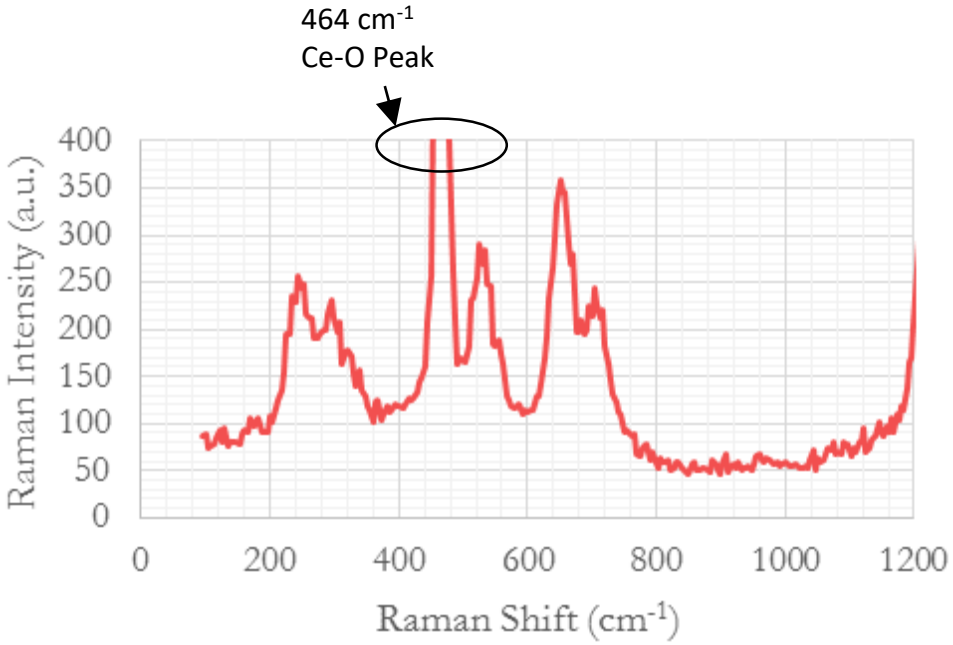

Eu_2O_3 doped CeO_2 pellet Raman Spectra for low intensity features.

Eu_2O_3 Doped CeO_2 Pellet CV

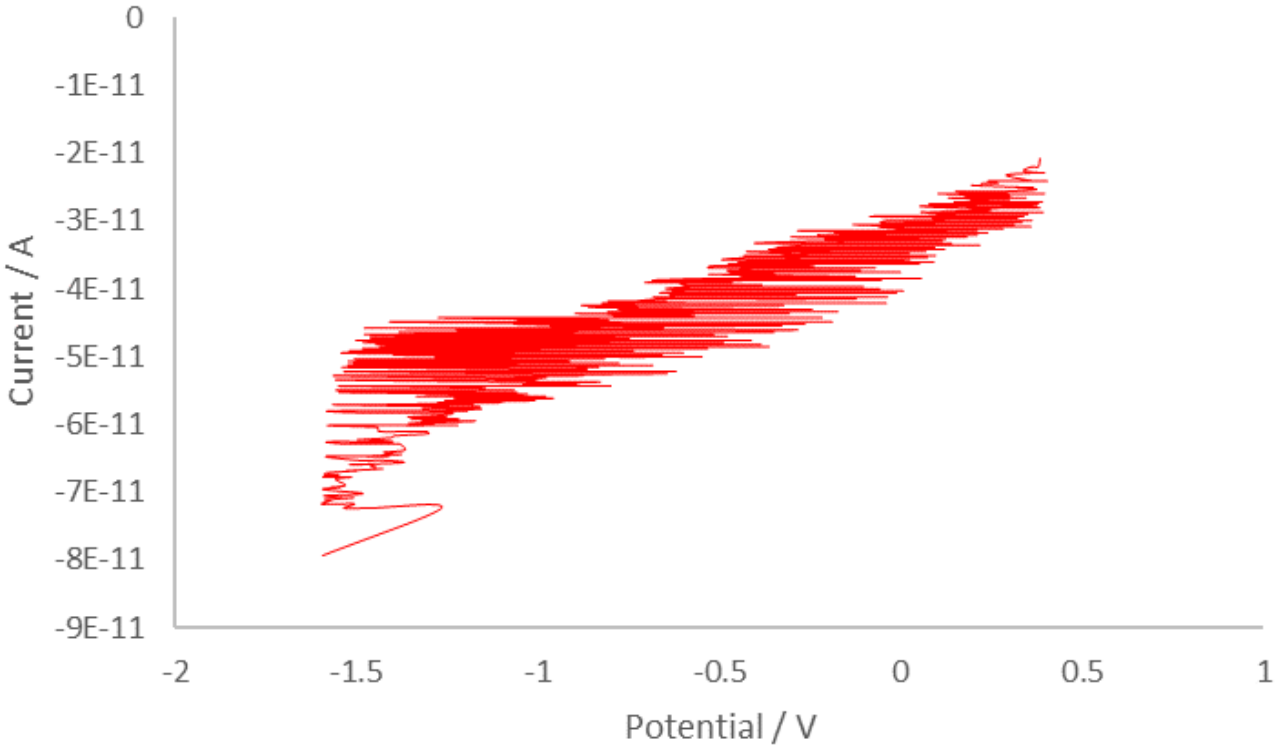

CV of Eu_2O_3 doped CeO_2 pellet in 0.1 M NaCl pH 9.5 solution sparged with air for 1 hour. Scan Rate 0.01 V/s , IR Compensation 2.0 kΩ (Max)

Oxalate Co-Precipitation Route

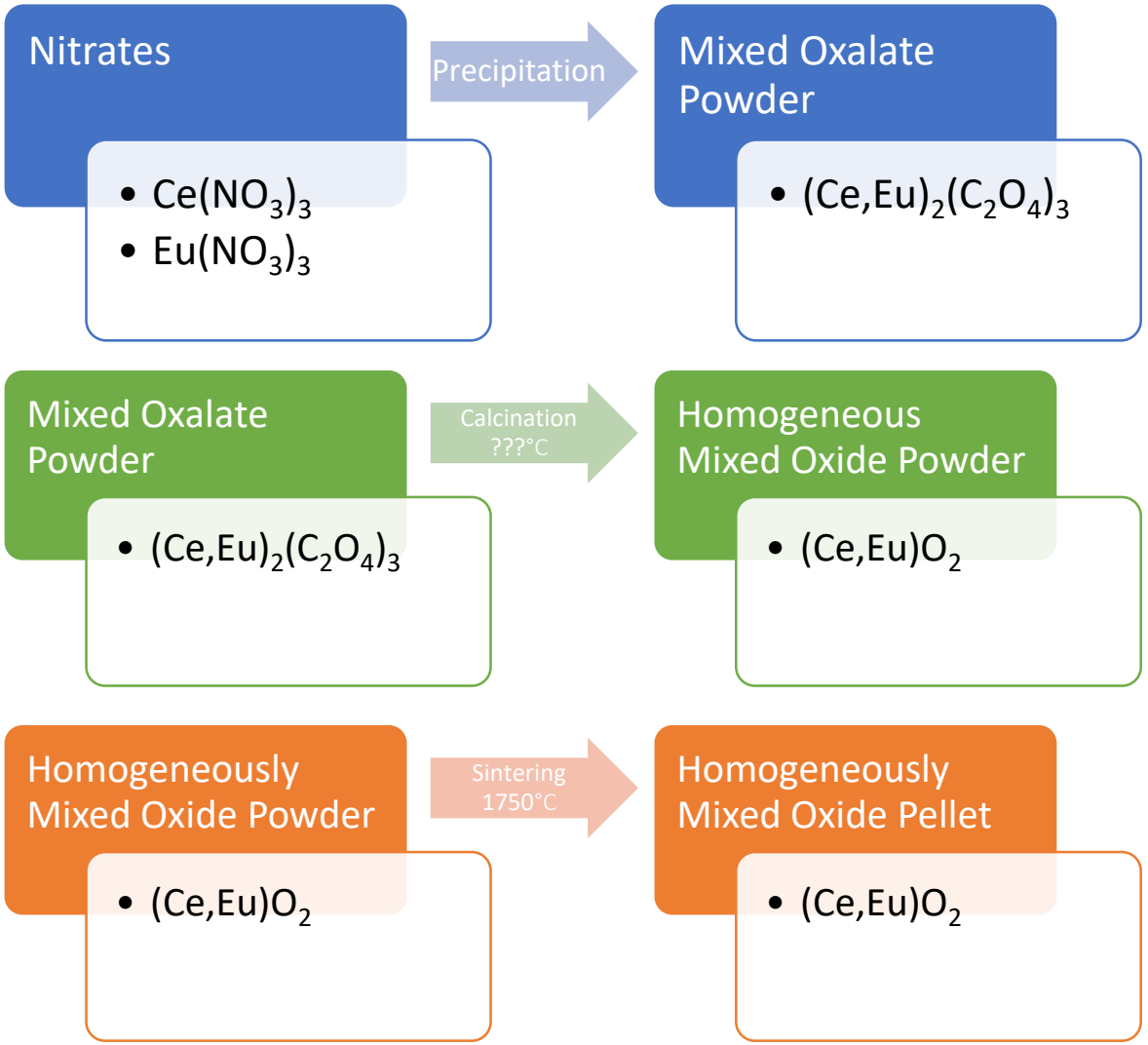

SEM of Mixed Oxalate

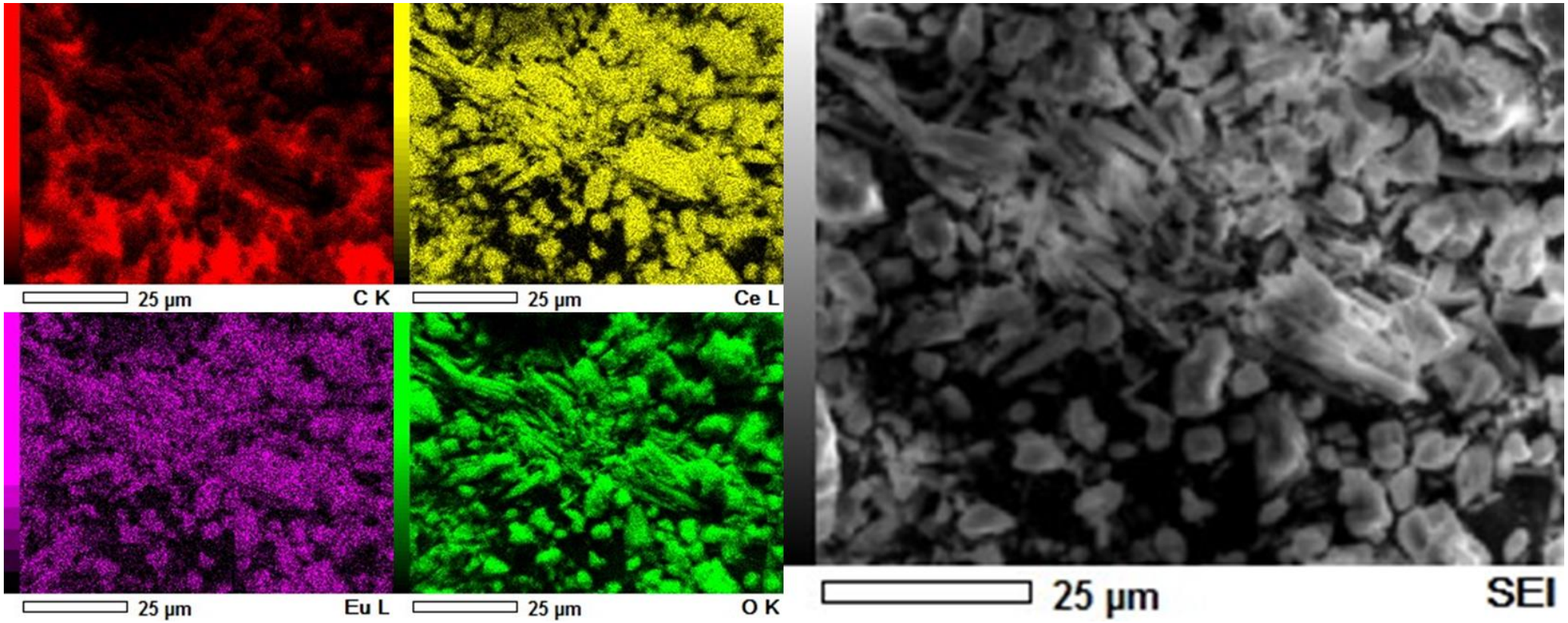

SEM EDS MAP of the Ce:Eu 99:1 Mixed Oxalate

- Homogeneous distribution of Europium in the Cerium Matrix.

Mixed Oxalate Comparison

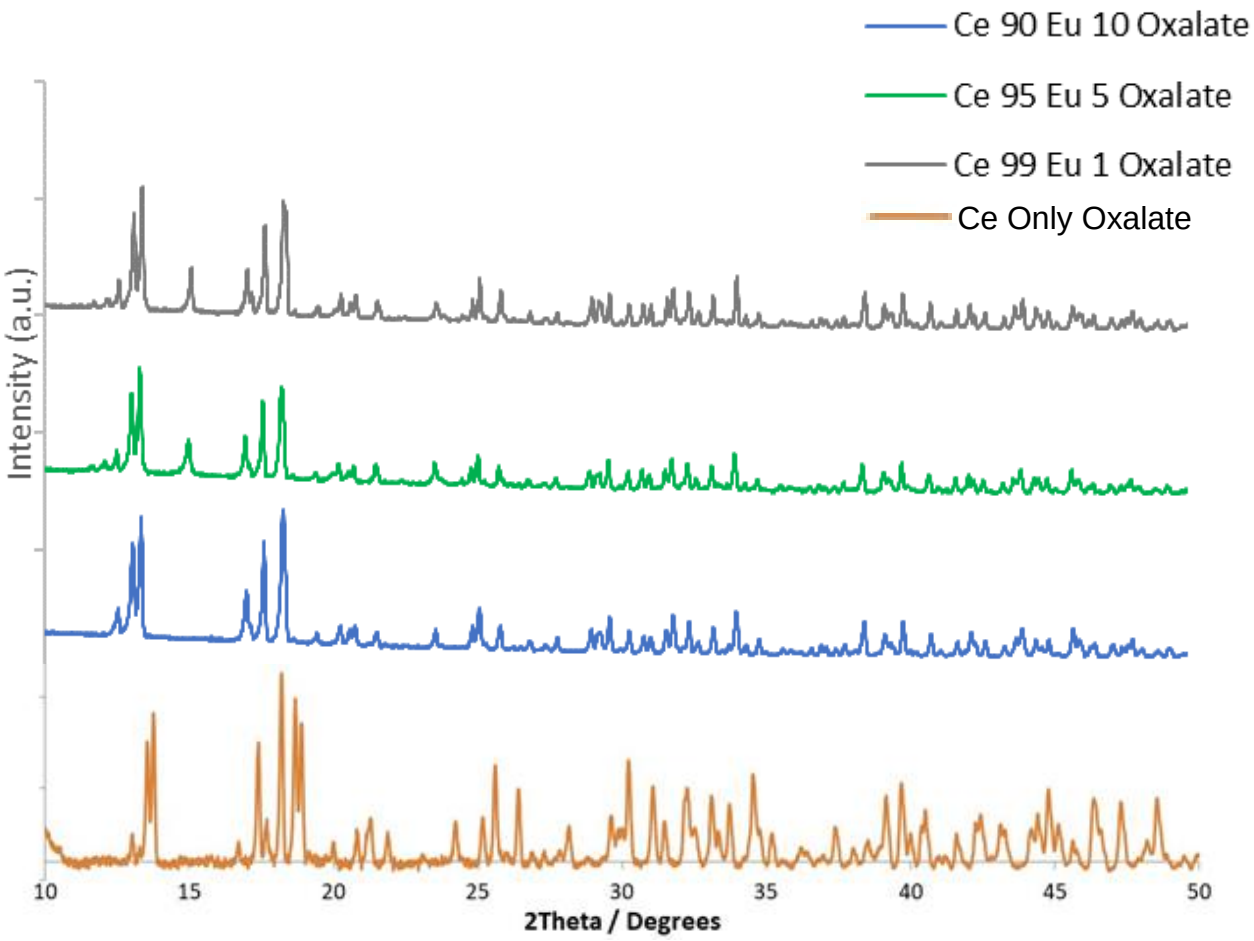

X-ray diffractogram of the Ce Eu mixed oxalate powders and of Ce only oxalate powder, $Ce_2(C_2O_4)_3(H_2O)_{10}$ (ICSD file no. 109637)

- The XRD presents no evidence of a separated Europium phase

Mixed Oxalate Raman

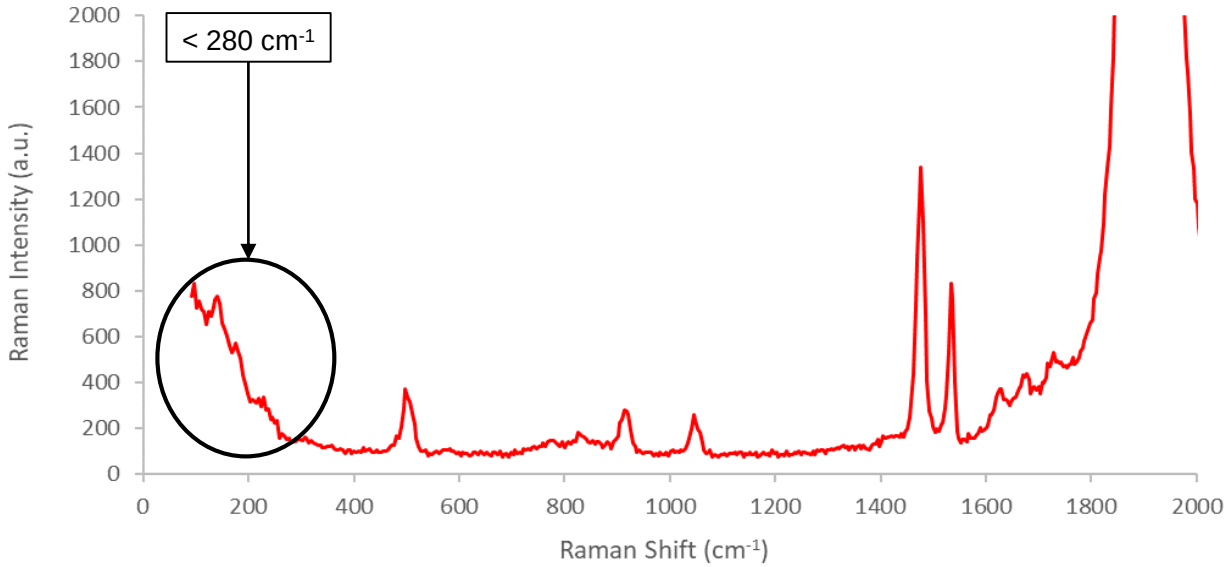

Raman Spectrum of Ce 99 Eu 1 Oxalate using a 532 nm laser

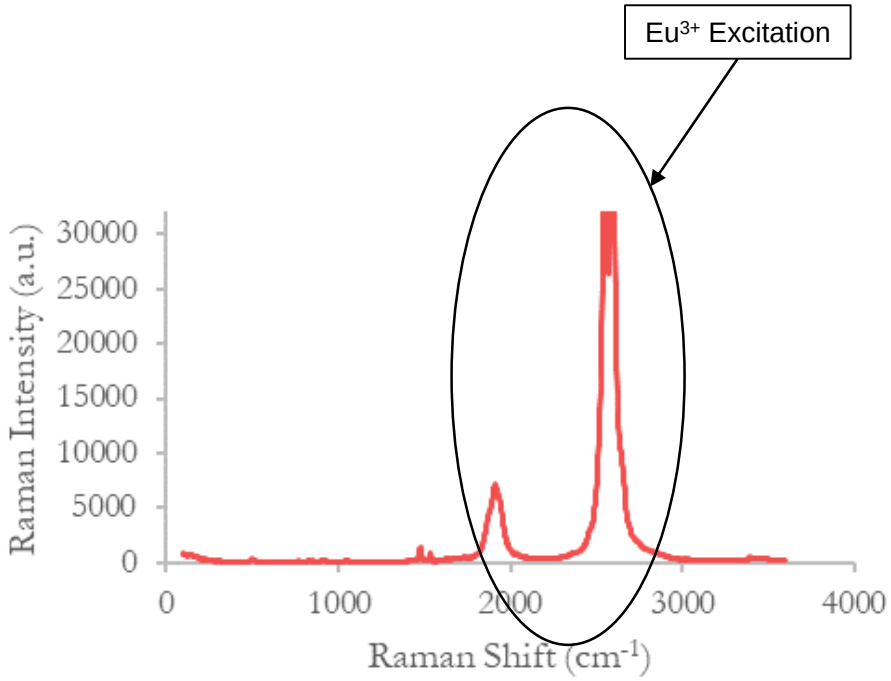

- The peaks below 280 cm^{-1} are assigned as the elongation and deformation of Ln (IV) and Ln (III) bands.
- Likely caused by Eu substituting Ce within the Ce Matrix.

Thermo-Gravimetric Analysis

TGA of Ce:Eu 99:1 Mixed Oxalate

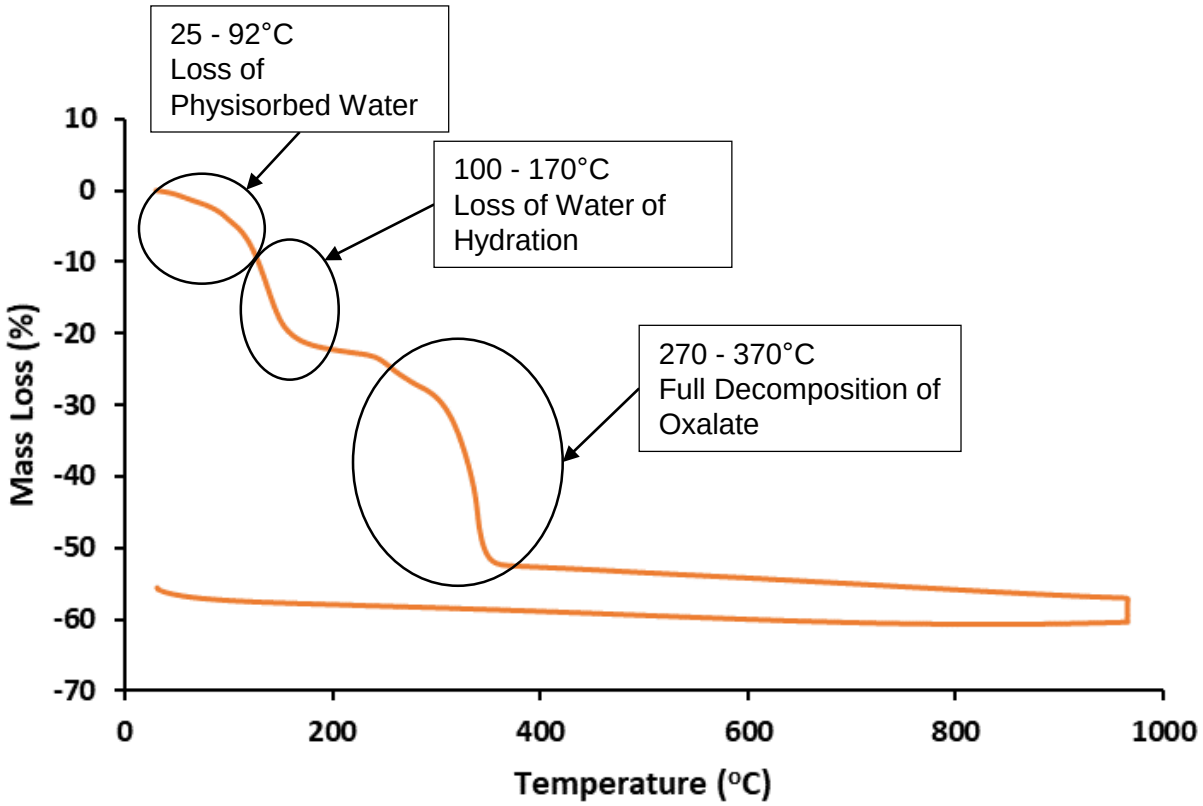

- Calcination can be reliably performed above 400°C.

Conclusion

- Pure Cerium Oxide and powder doped pellets are non-conductive
- Powder Doped pellet Raman suggested some Eu had made it into the CeO_2 Matrix
- SEM EDS of the Mixed Oxalate Powder revealed homogeneous distribution of the Eu amongst the Ce.
- Lack of Europium features in the XRD further evidences that the Europium is homogeneously mixed with the Cerium.
- Defect peaks in the Raman Spectrum further validate this
- TGA Analysis has informed that reliable calcination will occur above 400°C.

Future

- Characterisation of Mixed Oxide powders
  - XRD and SEM
- Fabrication and Sintering of pellets
- Electrochemistry of a sintered mixed oxide pellet electrode
- Production of two U:Ce mixed oxide pellets of the same composition
  - One by milling two oxide powders made from oxalates
  - One by the co-precipitation of a mixed oxalate
- Electrochemistry comparing the Corrosion Behaviour of the U:Ce mixed oxide pellets

Acknowledgements

- Colin Boxall[1] Supervisor (Lancaster University)
- Samuel Murphy[1] Supervisor (Lancaster University)
- David Hambley[2] (National Nuclear Laboratory)
- Rosie Hibberd[3] (Radioactive Waste Management ltd.)
- Melanie Brownridge[3] (Radioactive Waste Management ltd.)
- Richard Wilbraham[1] (Lancaster University)

- **Affiliations:** [1]Lancaster University, [2]National Nuclear Laboratory, [3]Radioactive Waste Management ltd.

UTGARD LABORATORY
Lancaster University
NATIONAL NUCLEAR LABORATORY
Radioactive Waste Management

TRANSCEND

Transformative Science and Engineering for Nuclear Decommissioning

TRANSCEND

Transformative Science and Engineering for Nuclear Decommissioning

An Investigation into Corrosion and Leaching of Carbide Fuels in a Geological Disposal Facility Setting

Dimitris Samaras, University of Bristol

MS Teams
18th May 2021

Energy
For a Low Carbon Future

Background

- UC: Exotic legacy fuel
- Highly susceptible to corrosion
  - Water: dissolves relatively fast
  - Oxygen: oxidation, potential pyrophoricity
- Disposal in GDF - > Groundwater (plus O_2 initially)

Hydrolysis and Oxidation

- Hydrolysis rate dependant on temperature
  - Vigorously at around and above 40 °C

    K.M. Taylor and C.H. McMurtry. Synthesis and Fabrication of Refractory Uranium Compounds, *U.S. Atomic Energy Commission,* 1960
- Formulas dependant on stoichiometry

  M.J Bradley and L.M. Ferris , Hydrolysis of Uranium Carbides between 25 and 100 °C : I and II (1962 & 1964)
  - UC -> CH_4
  - UC_2 & mixtures -> C_2H_6, C_3H_8, and heavier.
- Oxygen initially diluted in groundwater; eventually consumed
- Dry oxidation: linear rate law,

  K.A. Peakall and J.E. Antill, Oxidation of Uranium Monocarbide, *Journal of the Less-Common Materials,* 1962
- N.B.
  - Min temp: 230°C
  - Wet Oxidation

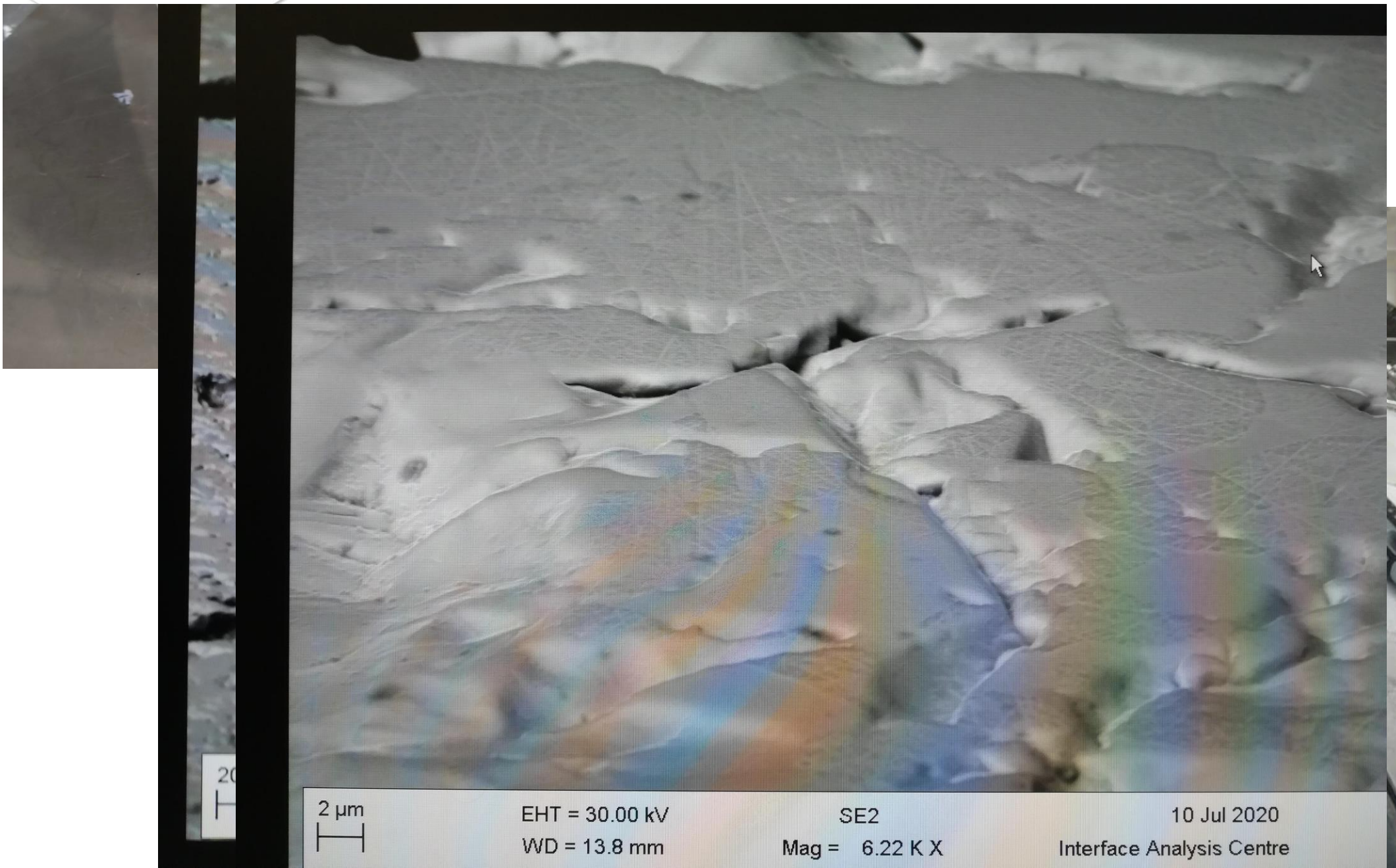
2 µm
EHT = 30.00 kV
WD = 13.8 mm
SE2
Mag = 6.22 K X
10 Jul 2020
Interface Analysis Centre

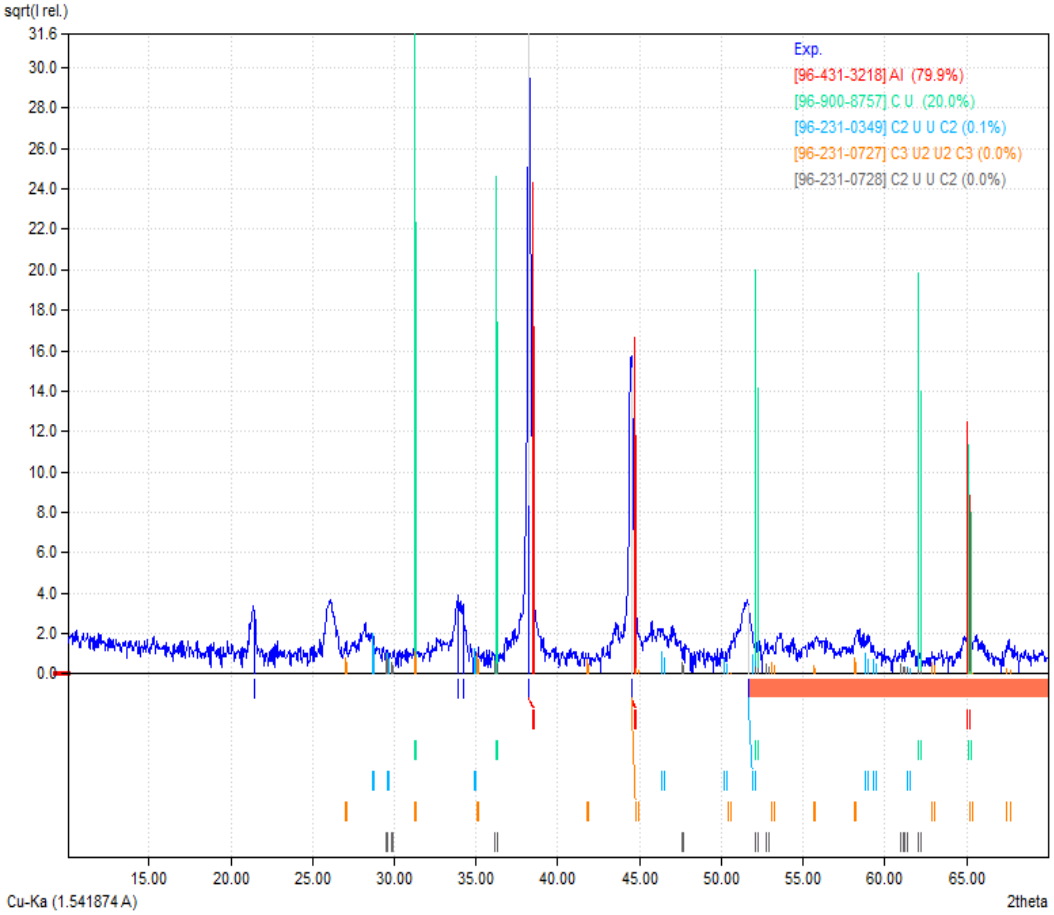
sqrt(I rel.)
Exp.
[96-431-3218] Al (79.9%)
[96-900-8757] C U (20.0%)
[96-231-0349] C2 U U C2 (0.1%)
[96-231-0727] C3 U2 U2 C3 (0.0%)
[96-231-0728] C2 U U C2 (0.0%)
Cu-Ka (1.541874 A)
2theta

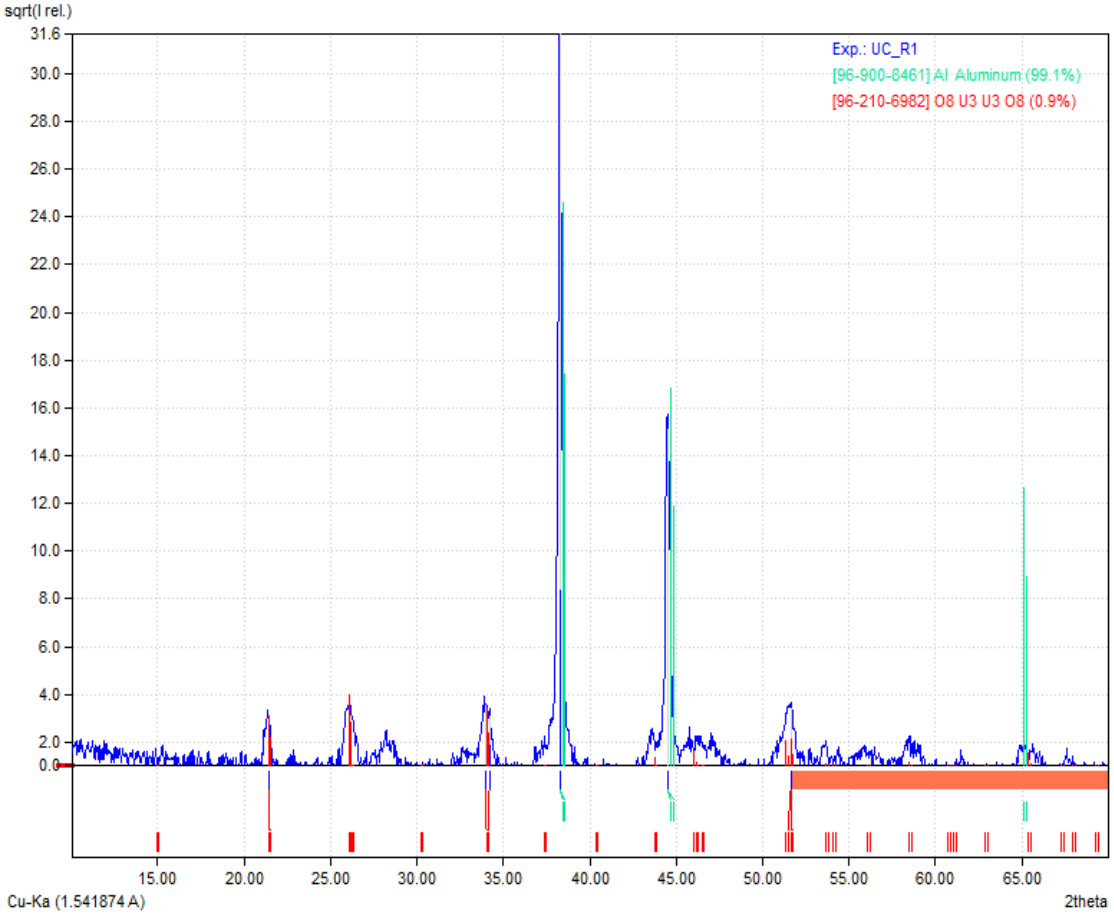
sqrt(I rel.)
Exp.: UC_R1
[96-900-8461] Al Aluminum (99.1%)
[96-210-6982] O8 U3 U3 O8 (0.9%)
Cu-Ka (1.541874 A)
2theta

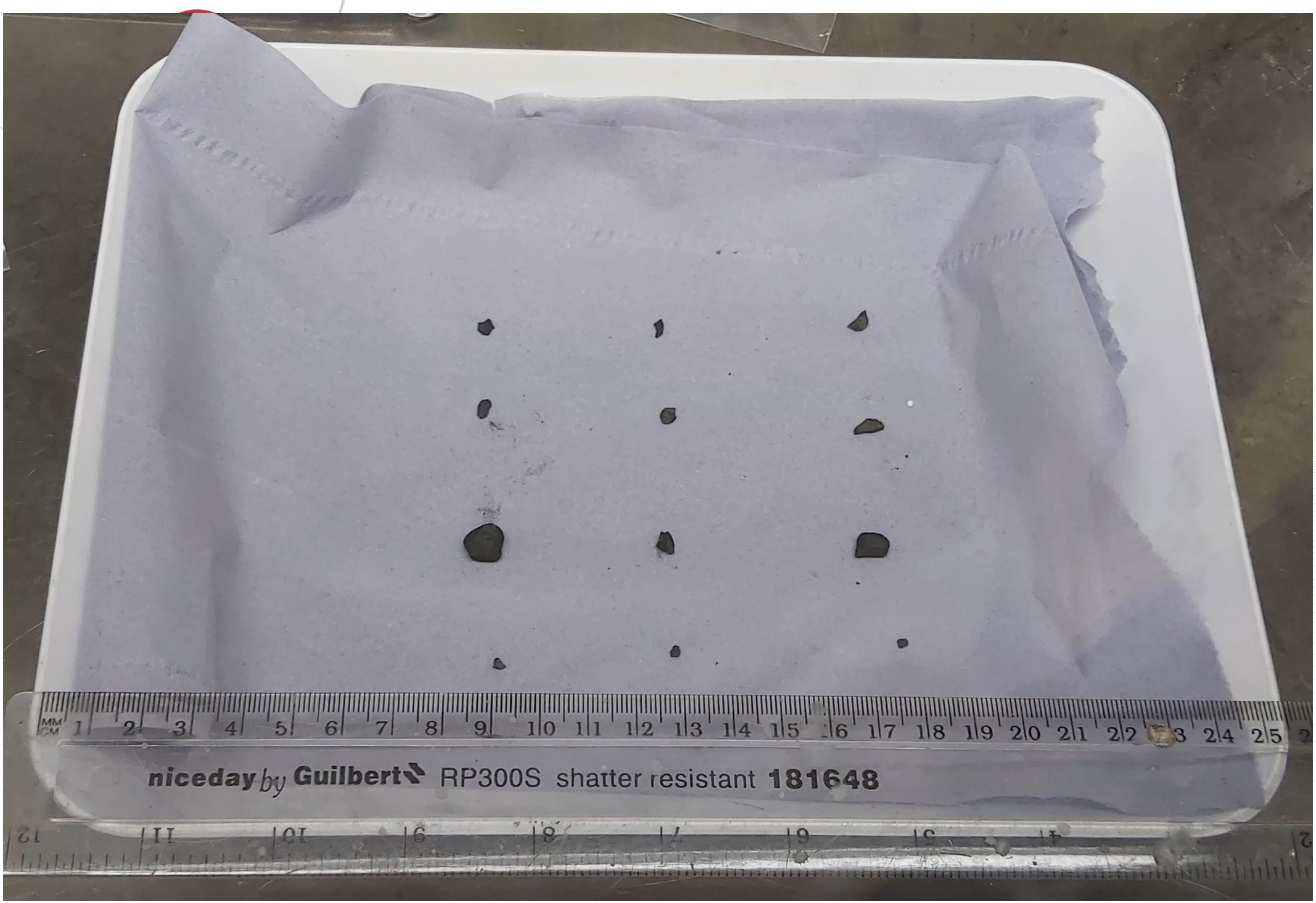
niceday by Guilbert RP300S shatter resistant 181648

TRANSCEND

Transformative Science and Engineering for Nuclear Decommissioning

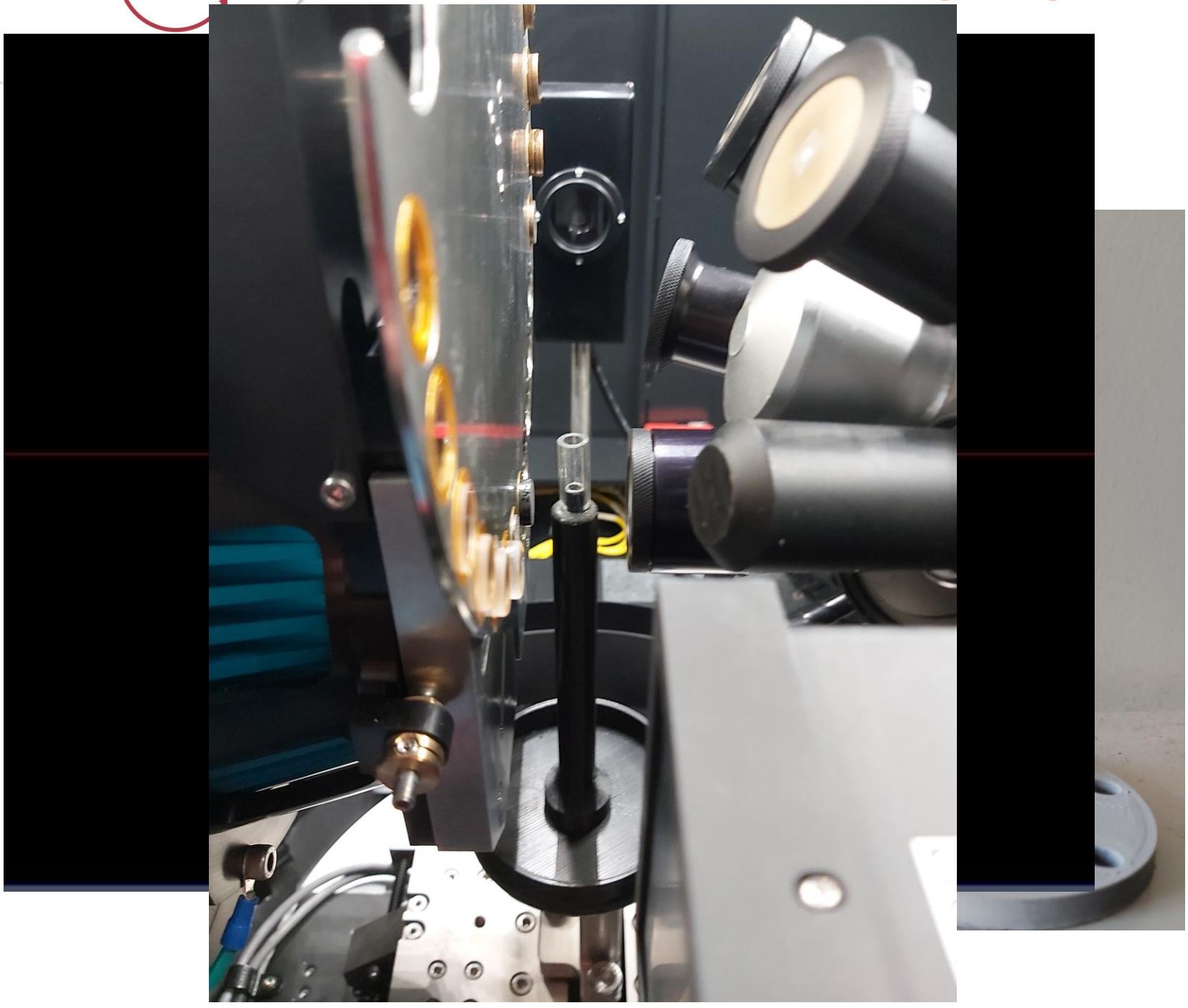

Tomography Procedure

- Load the cell in glovebox (for inert atmosphere)
  - Parafilm to seal
- Dry Scan
  - Capacity 0.4X, 4X, 10X, 20X, 40X
- Wet Scan
  - Solution -> Determined Optimal Magnification
  - Repeat several days later

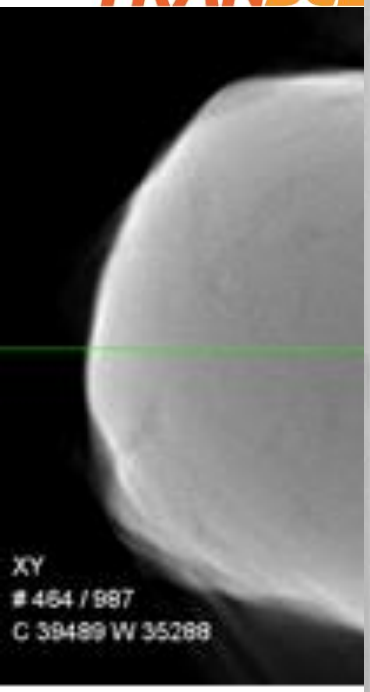
XY
464 / 987
C 39489 W 35288

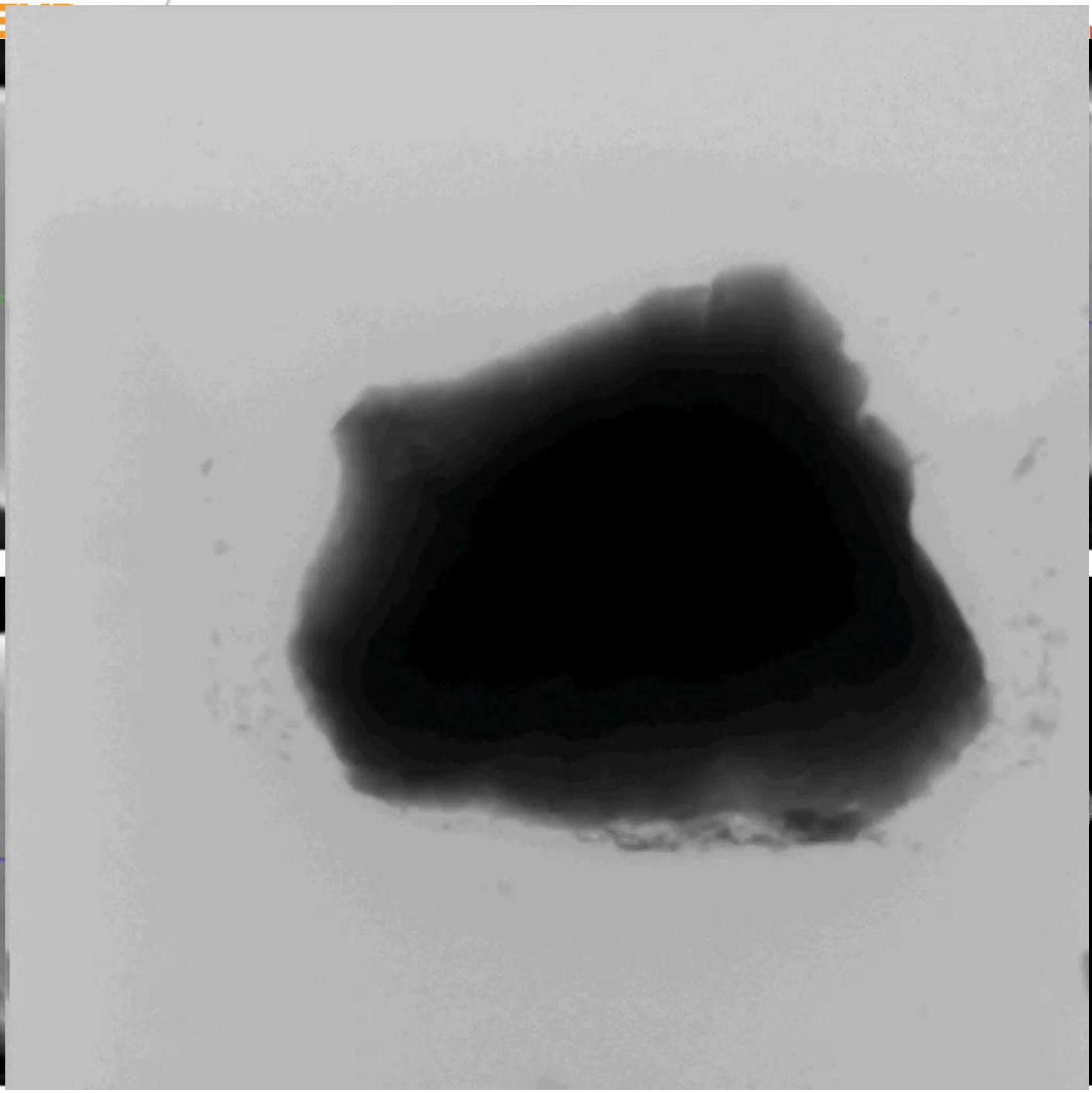

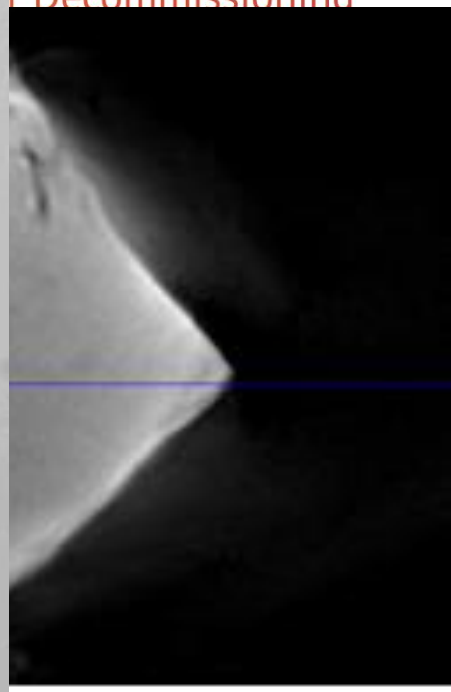

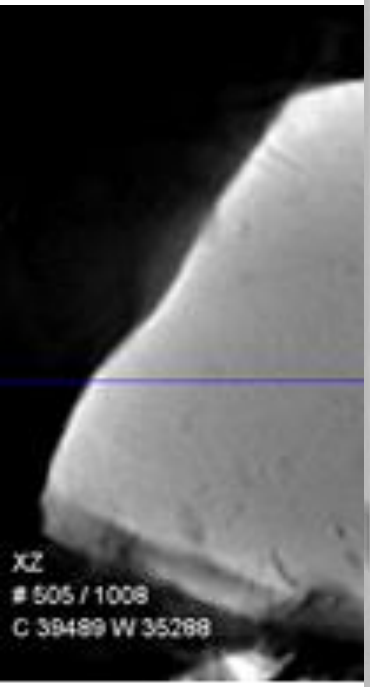
XZ
505 / 1008
C 39489 W 35288

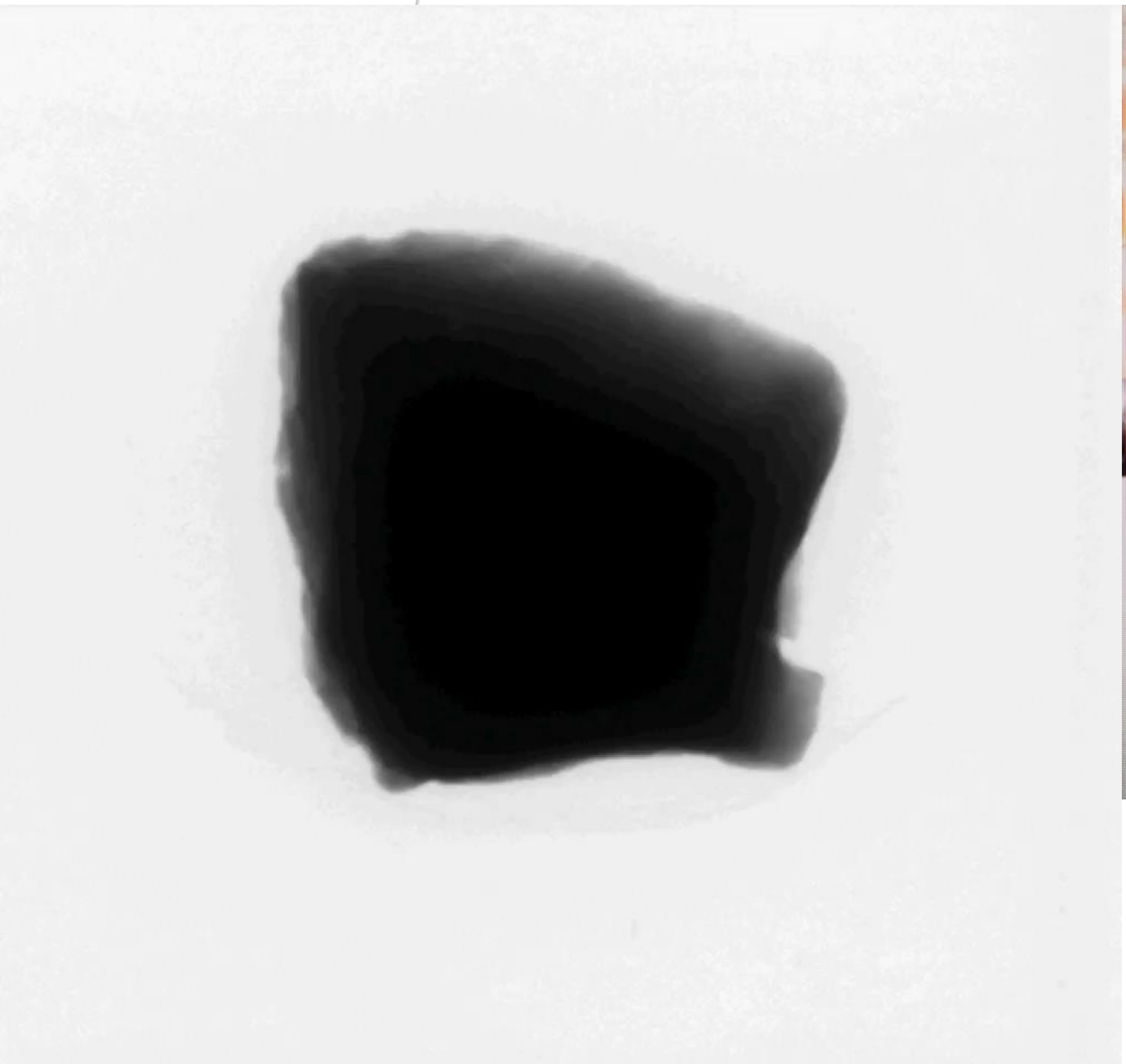

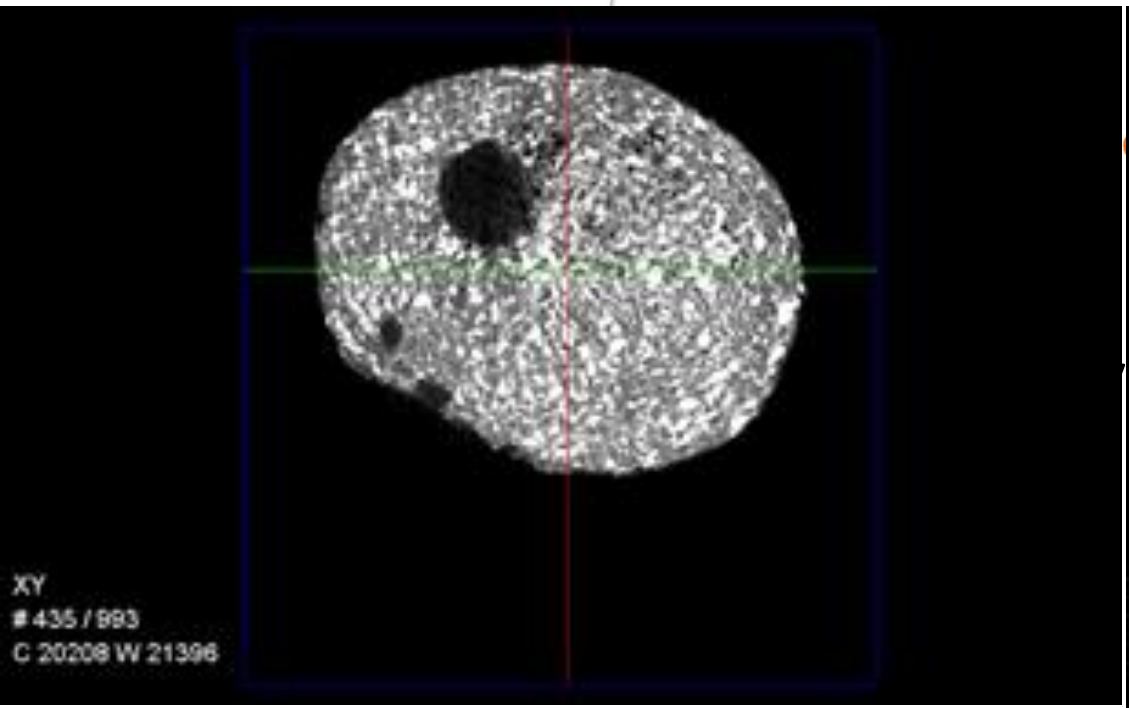
XY
435 / 993
C 20208 W 21396

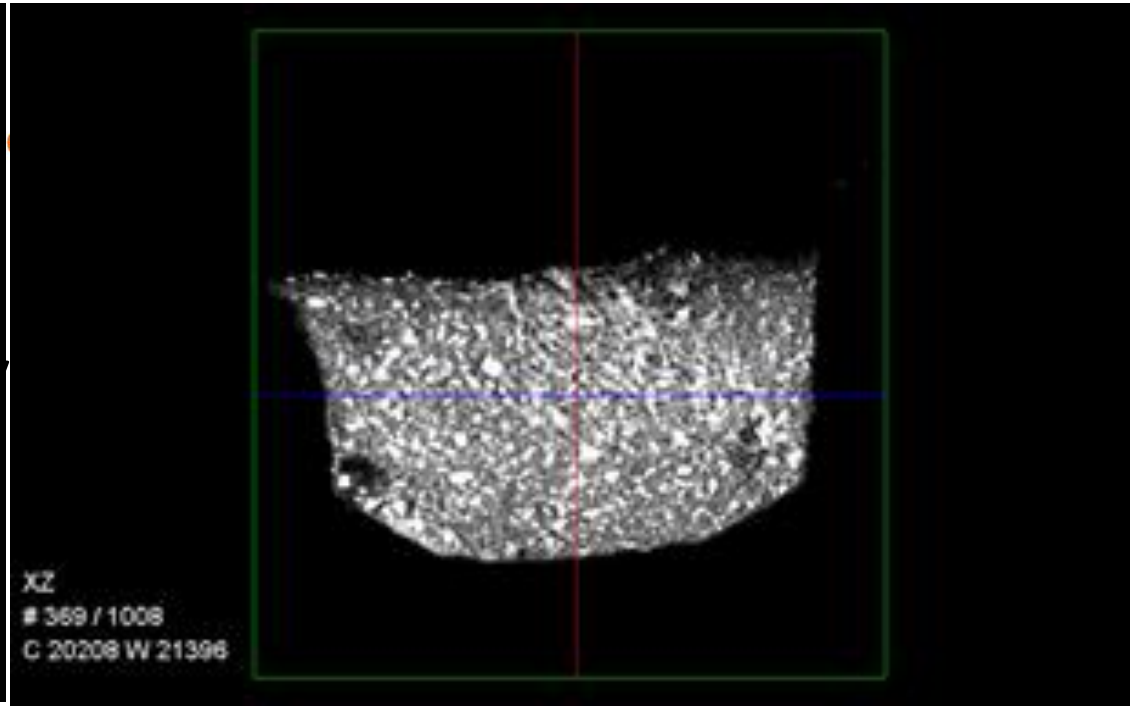
XZ
369 / 1008
C 20208 W 21396

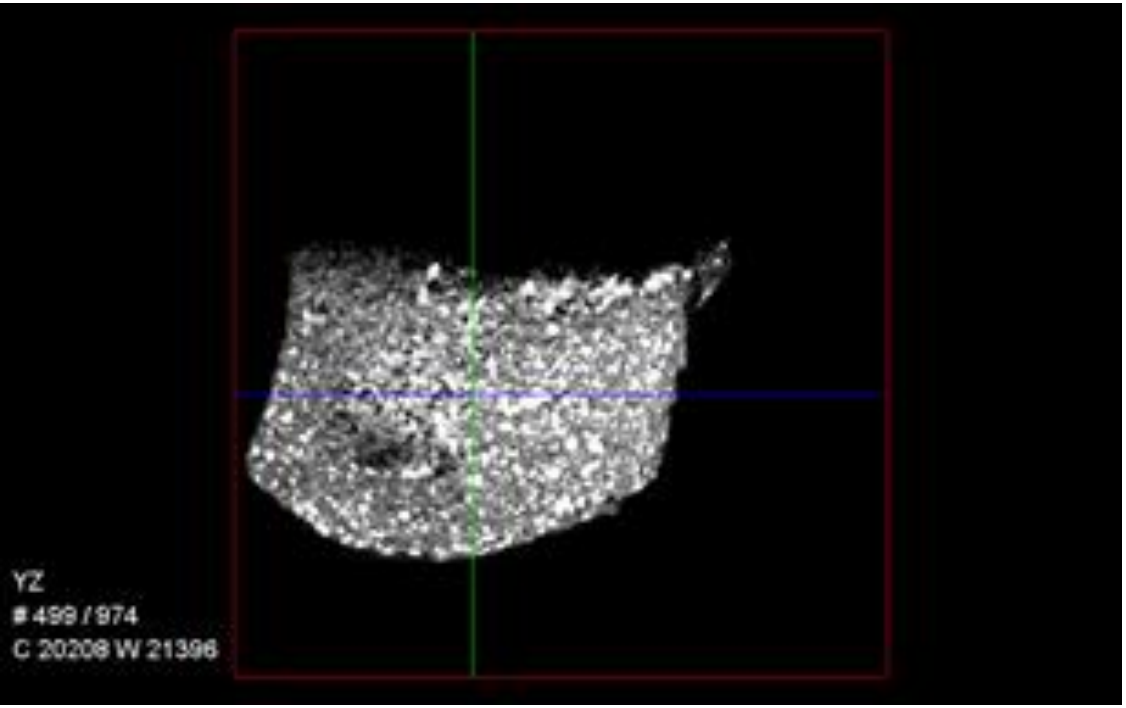
YZ
499 / 974
C 20208 W 21396

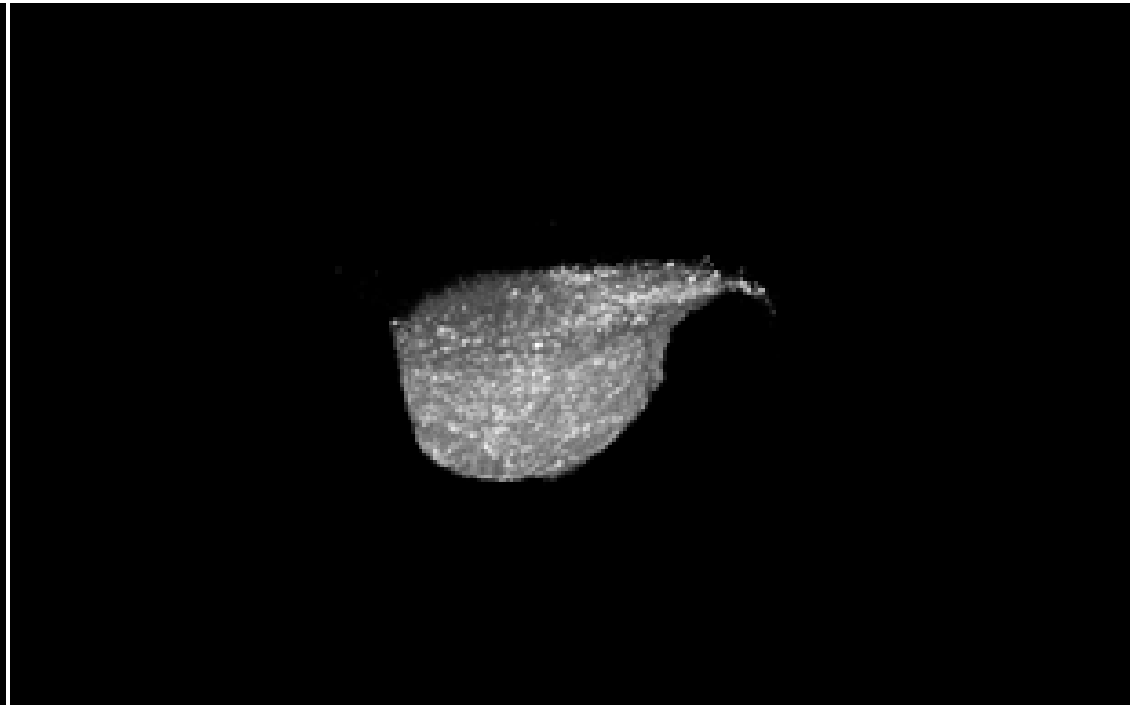

Potential for improvement

- Parafilm may slip in wet scans
  - Bleed valves
- Water chemistries
  - Milli-Q DI water not common 1000m underground
  - Chemistries representatives of GDF - High carbonate/pH
- Shape
  - Accommodate for RGA and pressure logging
  - Accessibility to residue#
  - More water
- N.B. Virgin vs Irradiated

- Bradley, M. J. and others. (1963). Hydrolysis of Neutron-Irradiated Uranium Monocarbide. *Inorganic Chemistry*, *3*(3), 454.
- Evered, S. and others. (1965). Hydrolysis of neutron-irradiated uranium and uranium-plutonium monocarbides. *Journal of Inorganic and Nuclear Chemistry*, *27*(8), 1867–1868.

Other Techniques

- XRD
  - Residue identification
- HSAFM
  - Surface morphology
  - Corrosion in situ
- SIMS
  - Elemental Identification
  - Corrosion layer thickness
  - Corrosion mechanism
- TRLFS
  - U and F.P. leaching
- ICP for solution analysis
  - MS
  - OES
- RGA
  - Gas identification

Conclusions so far

- X-Ray Tomography suitable for studying carbide corrosion
  - Tweaks required to optimise results
- Other techniques must be included
  - Residue composition
  - Solution alteration
  - Corrosion from additional points of view

TRANSCEND

Transformative Science and Engineering for Nuclear Decommissioning

Mail: dimitris.samaras@bristol.ac.uk

TRANSCEND

Transformative Science and Engineering for Nuclear Decommissioning

3D pFIB/EBSD Characterisation of the Susceptibility to Thermal Sensitisation of 304 Stainless Steel

Kuo Yuan, University of Bristol

Transcend Theme 3 Meeting

18th May 2021

Energy
For a Low Carbon Future

Introduction

- Spent AGR (advanced gas-cooled reactor) fuel cladding is stored in cooling ponds and stress corrosion cracking (SCC) may initiate because of irradiation-induced sensitisation.
- Thermally sensitised 304 stainless steel is used as the substitute material to develop a micromechanical testing method for SCC in this PhD research.
- A FE (finite element) model will also be developed to predict SCC based on the thermally sensitised specimens.
- Thermal sensitisation occurs when chromium carbide precipitates form near the boundary, depleting the chromium concentration around these precipitates, which reduce the corrosion resistance.
- The main factor affecting sensitisation and further SCC, is the grain boundary of an austenitic steel.

Background: Grain Boundary Misorientation

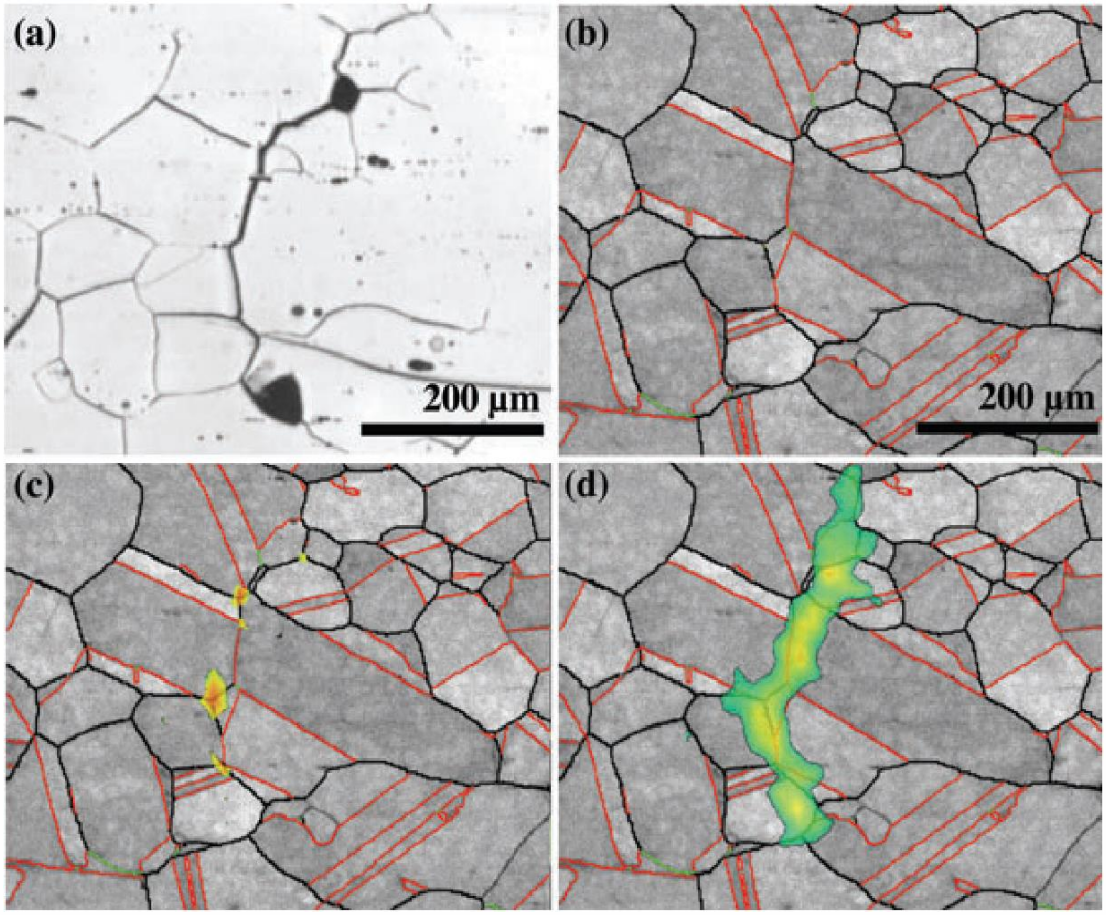

Fig. 1 Correlation between observations in the microstructure of 304 stainless steel:
(a) optical image of an intergranular crack,
(b) EBSD map of the same area of microstructure,
(c) strain map obtained after 16 h,
(d) strain map after 24 h.
In (b), (c) and (d), the Σ3 boundaries are represented in red lines, Σ9 and Σ27 boundaries are green lines, low-angle grain boundaries (Σ1) are white lines and random boundaries are black lines [1]

Boundary misorientation was believed to be the main factor of sensitisation [1]:

- LAGBs (low angle grain boundaries, <15°) are more resistant to sensitisation than HAGBs (high angle grain boundaries, >15°).
- However, among HAGBs, the boundaries with special CSL (coincidence site lattice) numbers are more resistant to sensitisation, including CSL=Σ3, Σ9, Σ27 or Σ≤29.
- Additionally, these special boundaries act as bridges when the crack propagates near them.

Background: Boundary Plane Misorientation

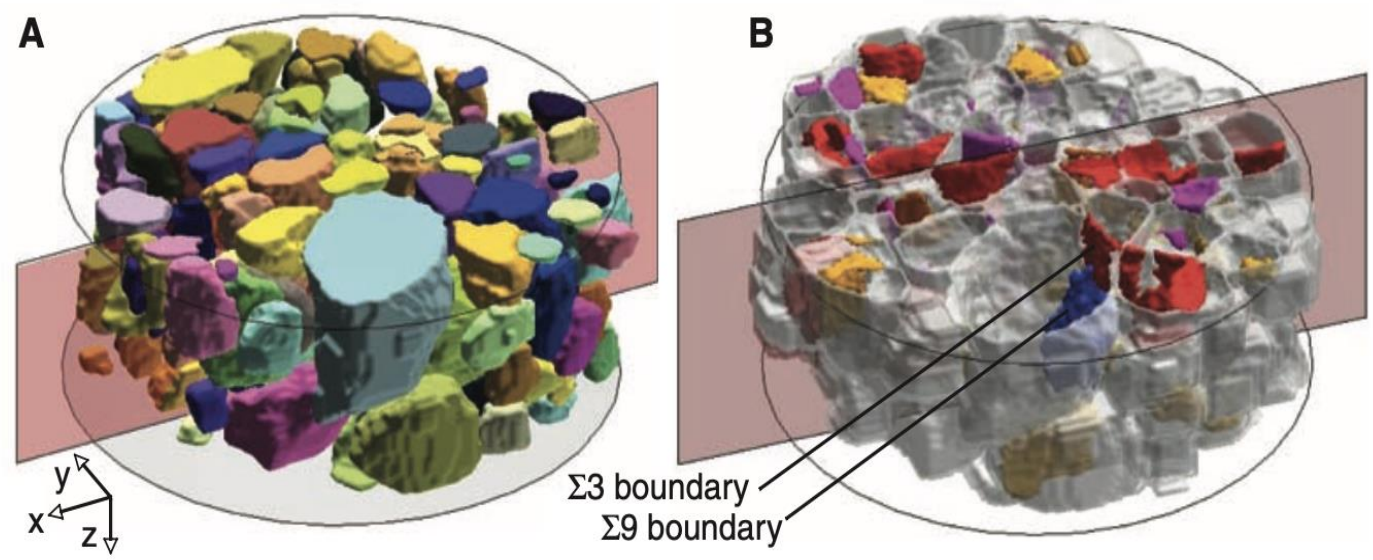

By scanning a stainless steel wire with DCT (diffraction contrast tomography) at a synchrotron x-ray source, King et al., [2] found that these special boundaries that were resistant to sensitisation are located near low {hkl} Miller index planes of both grains.

Fig. 2 3D DCT grain map of a section from a wire sample:
(A) crystallographic orientation of grains,
(B) low ∑ CSL grain boundaries are shown in colour: LAGBs, orange; ∑3, red; ∑9, blue; other boundaries ∑ ≤ 29, purple [2]

However, only a thin wire was scanned in this study. Based on this, a research topic was proposed: using FIB serial sectioning to find the boundary plane orientation of a large number of grains, to validate this theory.

Experimental Methods: Sample Preparation

- A small piece of 304 stainless steel was aged at 600 °C for 50 hours, as past work indicated that this method can make the steel thermally sensitised.
- The specimen was then cut into a cuboid shape with a length and width of 6 mm and 3 mm. It was then ground into a wedge shape (fig. 4) with a thickness of 200 µm at the edge for FIB milling.
- The specimen surface was finally polished to EBSD standard.

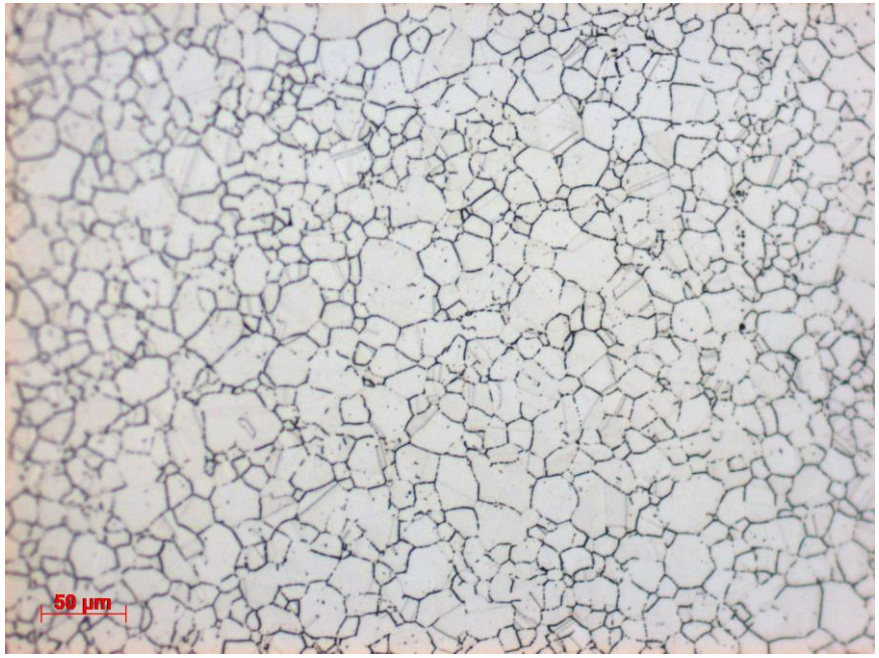

Fig. 3 Optical microscope image of etched 304 stainless steel aged at 600 °C for 50 hours

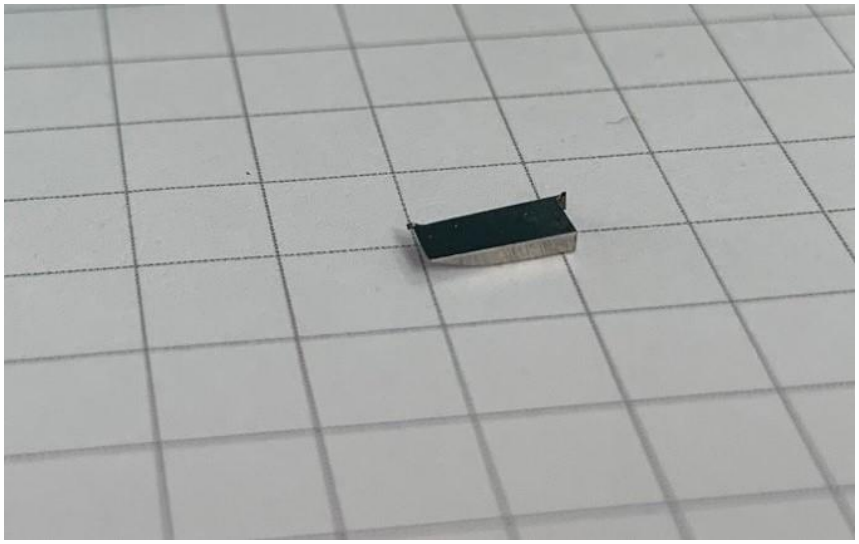

Fig. 4 Prepared specimen

Experimental Methods: Testing

- The specimen was then sent for serial sectioning (fig. 5) at the plasma FIB of the Henry Royce Institute at the University of Manchester to find the boundary plane orientation.
- A few special grain boundaries, which are supposed to have good resistance to sensitisation, but have a large amount of carbides, will be identified and scanned using a TEM to confirm that the chromium level is lower the threshold value of SCC initiation.
- The two theories then can be compared based on the severity of sensitisation.

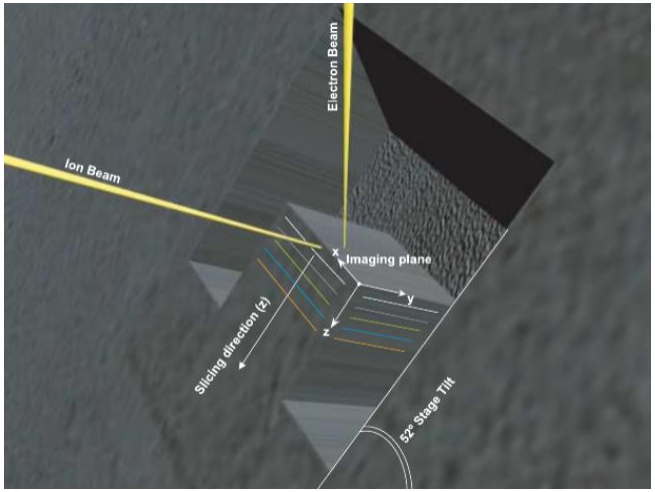

Fig. 5 Schematic of FIB serial sectioning [3]

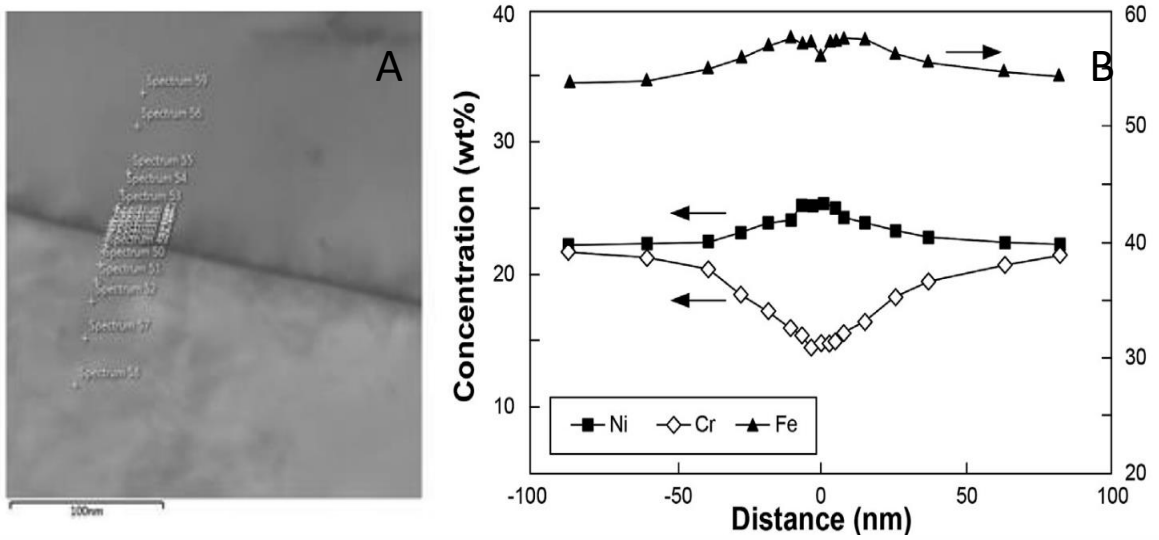

Fig. 6 TEM scanning on a thermally sensitised 20/25/Nb stainless steel sample: (A) location of the scans; (B) composition profile [4]

Results:
FIB Serial Sectioning

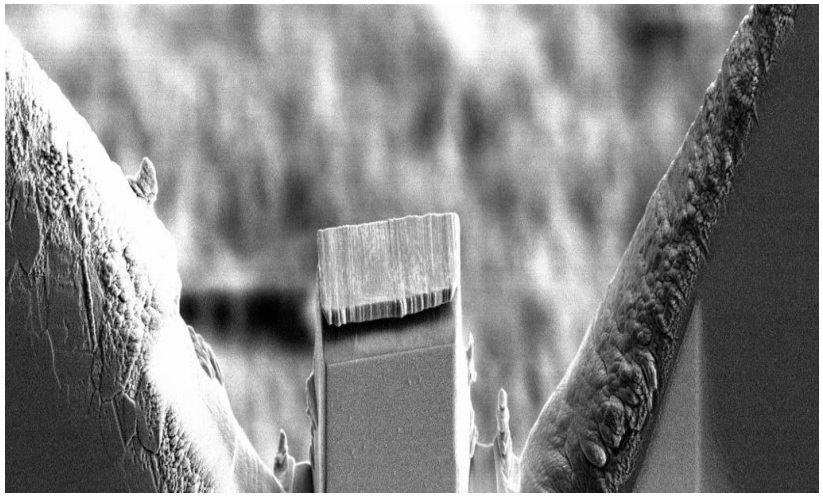

Fig. 7 Secondary electron image of the serial sectioning area

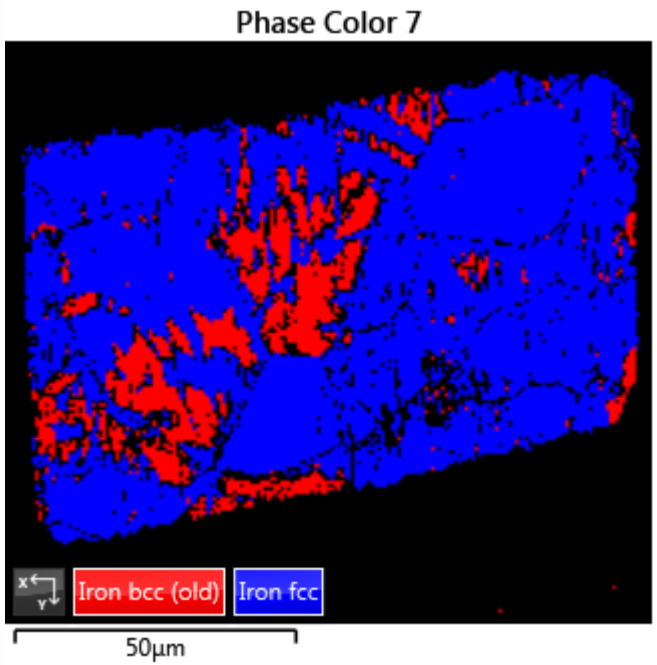

Fig. 8 Phase image of the serial sectioning area

Fig. 9 Band contrast image of the sectioning area

- Several locations were serial-sectioned to have the best results.
- Under the plasma FIB, austenite (fcc) tends to transform to delta (bcc) phase.

Results: FIB Serial Sectioning

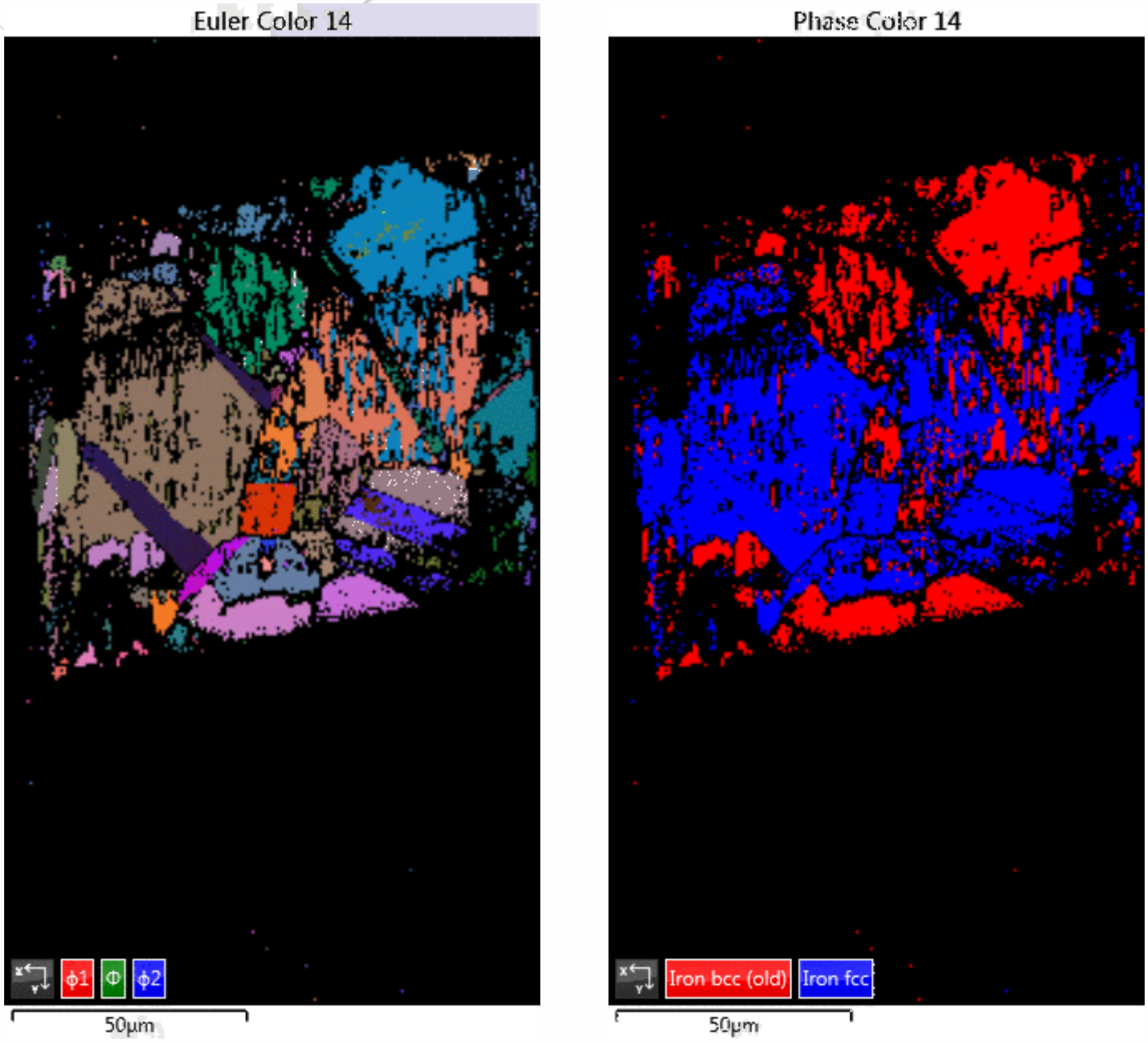

The grain boundaries change while the sectioned area is sliced down.

However, the effect of phase transition is also quite obvious in the animation on the right.

Fig. 10 animations of the sectioned areas, left: Euler coloured maps; right phase images

Results: Reconstruction

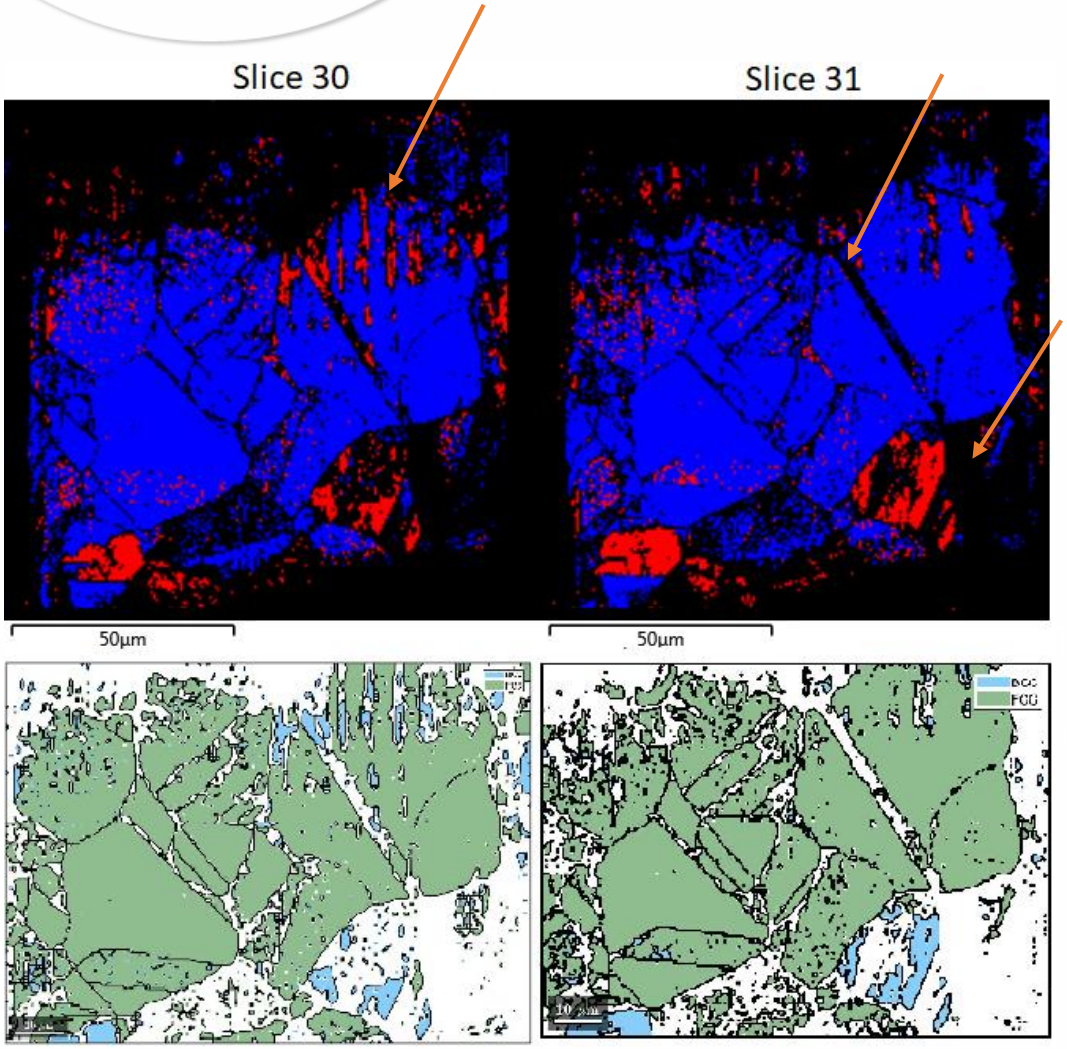

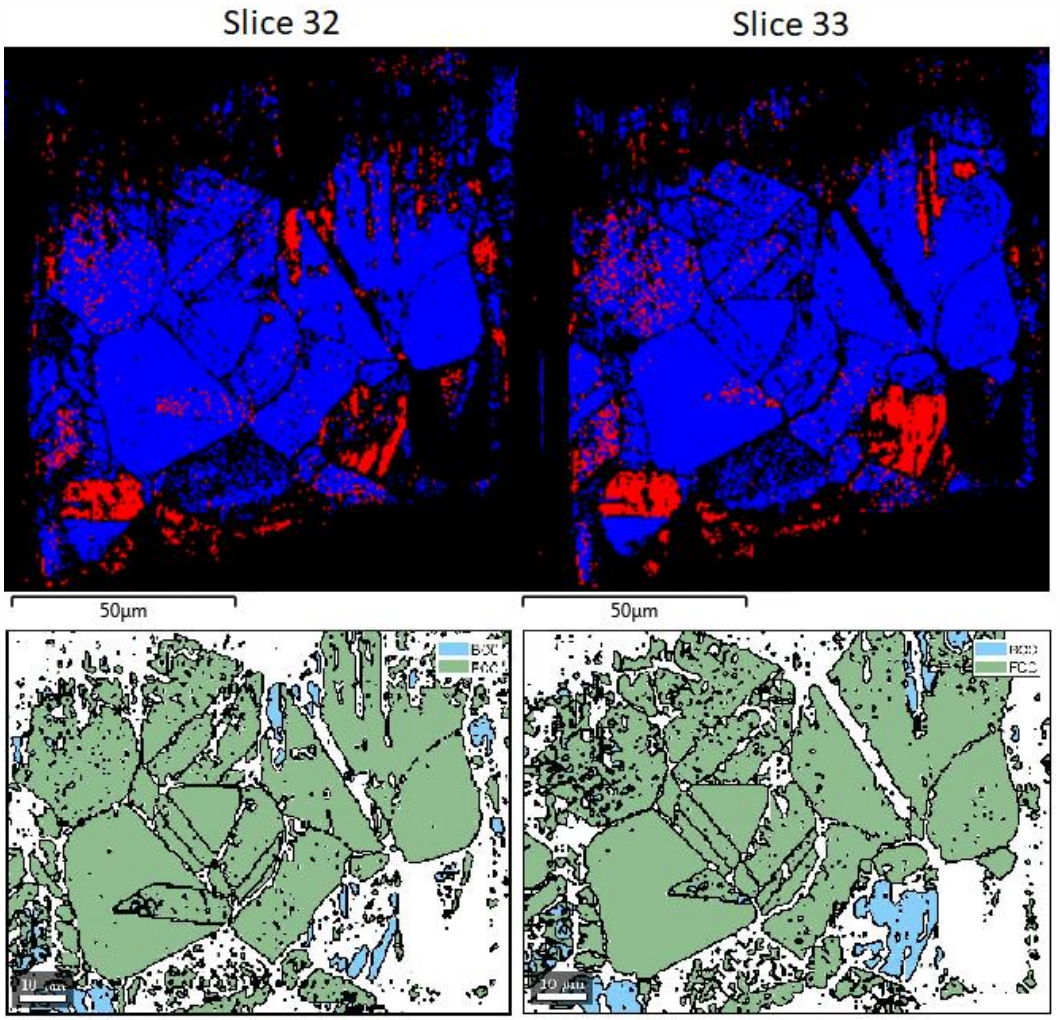

Fig. 12 Phase images (top row; FCC: blue, BCC: red) and boundary reconstruction (bottom row; FCC: green, BCC: blue) of slice 30-33

Conclusions and Plans

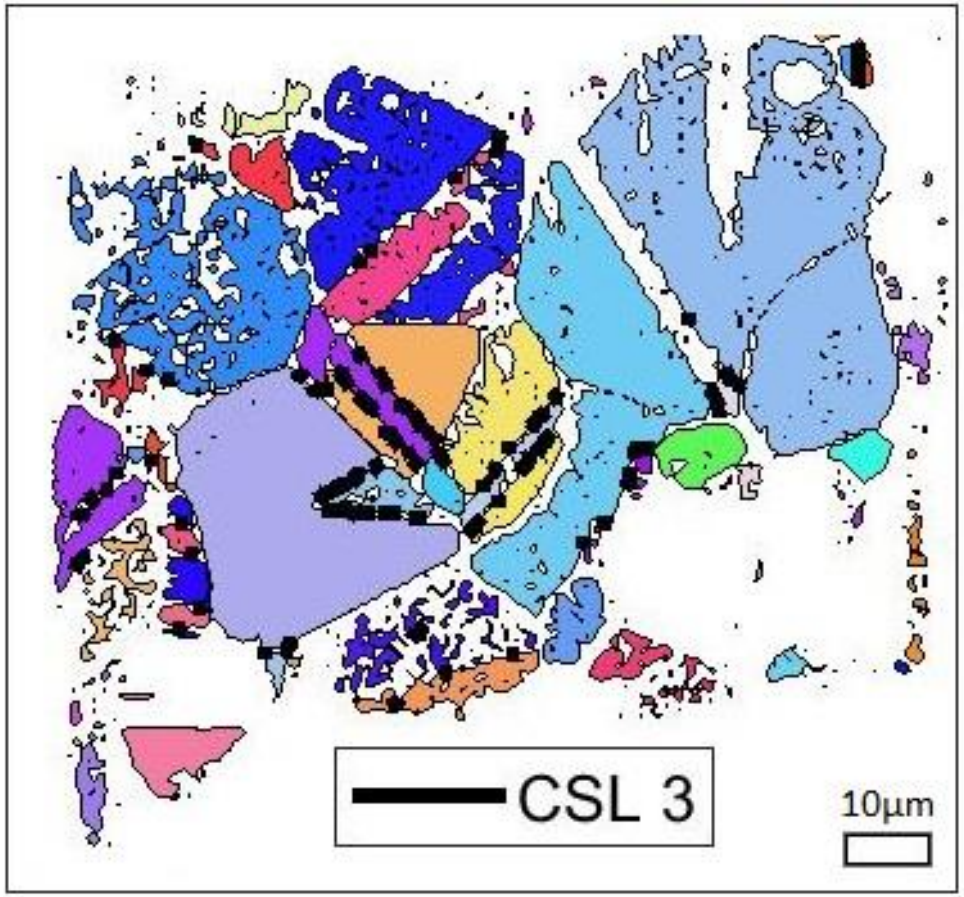

Fig. 13 CSL= 3 grain boundaries on the final slice (slice 33)

- Thermally sensitised 304 stainless steel specimens were serial sectioned with plasma FIB.
- Grain boundaries may vary significantly through the depth of the material.
- Austenitic stainless steel suffers from phase transition under the ion beam.
- Grain boundaries of the serial sectioned specimen have been reconstructed and the plane orientation of them can be found.

The specimen will be further EBSD scanned to identify the special grain boundaries:

- With special CSL number, but show carbide precipitation, or
- Without special CSL number, but show no carbide precipitation.

These boundaries will finally be scanned in TEM to find the exact chromium contents at the boundary.

TRANSCEND

Transformative Science and Engineering for Nuclear Decommissioning

Acknowledgements

Xiangli Zhong, Henry Royce Institute
Ronald Clark, National Nuclear Laboratory
Mahmoud Mostafavi, University of Bristol

References:

[1] S. Rahimi, D. L. Engelberg, J. A. Duff, and T. J. Marrow, "In situ observation of intergranular crack nucleation in a grain boundary controlled austenitic stainless steel," *J. Microsc.*, vol. 233, no. 3, pp. 423–431, 2009, doi: 10.1111/j.1365-2818.2009.03133.x.

[2] A. King, G. Johnson, D. Engelberg, W. Ludwig, and J. Marrow, "Observations of intergranular stress corrosion cracking in a grain-mapped polycrystal," 2008.

[3] L. HOLZER, F. INDUTNYI, P. H. GASSER, B. MÜNCH, and M. WEGMANN, "Three-dimensional analysis of porous BaTiO3 ceramics using FIB nanotomography," *J. Microsc.*, vol. 216, no. 1, pp. 84–95, Oct. 2004, doi: https://doi.org/10.1111/j.0022-2720.2004.01397.x.

[4] G. O. H. Whillock, B. J. Hands, T. P. Majchrowski, and D. I. Hambley, "Investigation of thermally sensitised stainless steels as analogues for spent AGR fuel cladding to test a corrosion inhibitor for intergranular stress corrosion cracking," *J. Nucl. Mater.*, 2018, doi: 10.1016/j.jnucmat.2017.10.017.

Thank you

k.yuan@bristol.ac.uk

University of BRISTOL

NATIONAL NUCLEAR LABORATORY

HENRY ROYCE INSTITUTE

TRANSCEND

Transformative Science and Engineering for Nuclear Decommissioning

Density Functional Theory simulation of UO2 Spent Nuclear Fuel alteration During Storage and Disposal

Joshua W. G. Bright, Victoria L. Frankland, Marco Sacchi and David Read

18 May 2021

Department of Chemistry, University of Surrey, Guildford, Surrey, GU2 7XH, United Kingdom

Energy
For a Low Carbon Future

PhD project focus, Year 2

- Computational modelling and experiment together to determine alteration mechanism of UO_2 fuels.
- Use of thin films and laser based techniques to study surface reactions in real time in tandem with surface alteration reaction simulations.
- Characterisation of reactants and products.

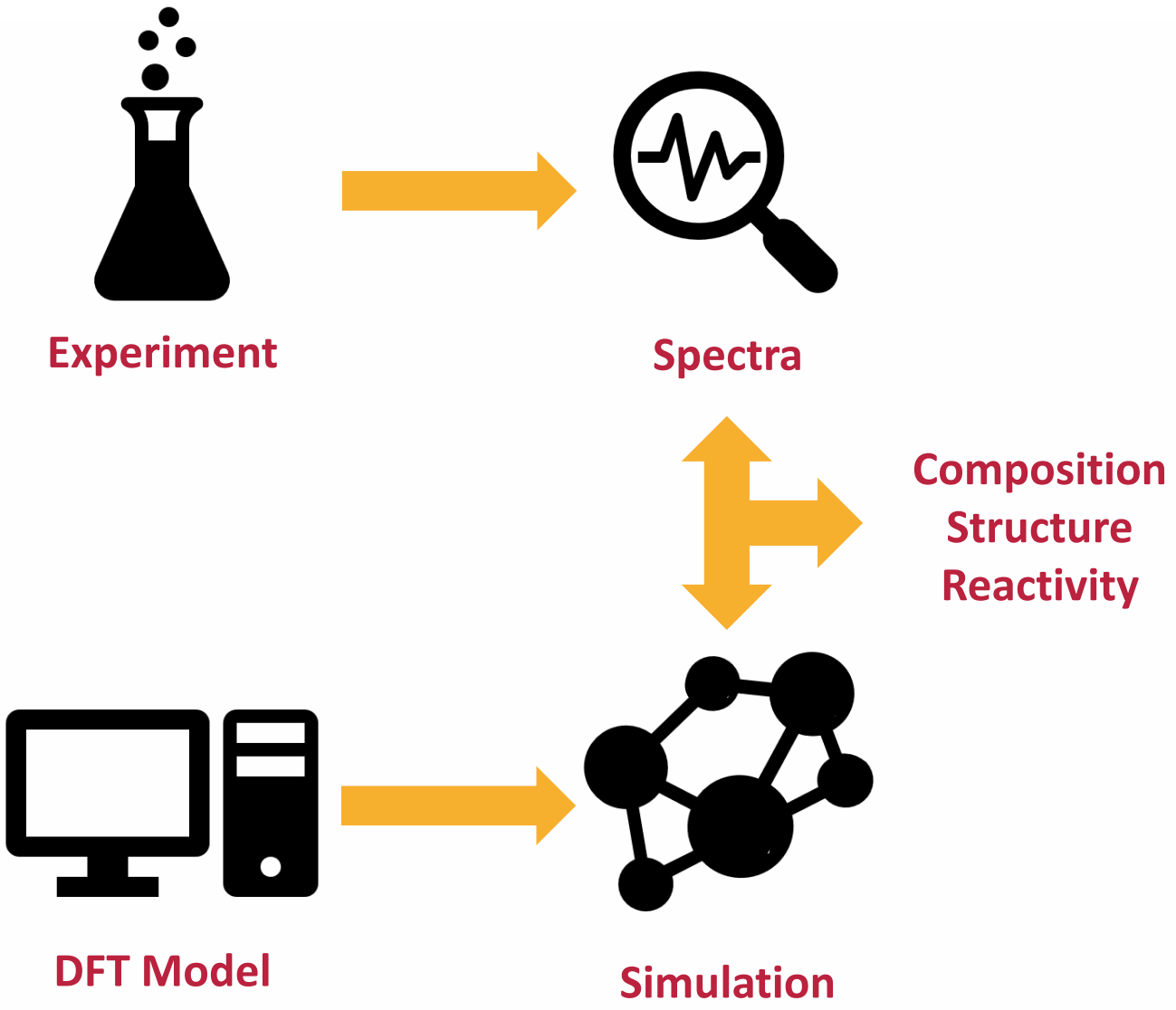

Predicting the Alteration of Spent Nuclear Fuels

- Alteration of uranium fuels is expected to lead to the formation of any of the 250+ naturally occurring uranium minerals.

Suggested mechanisms of alteration

Uranium Metal, U

↓

Uraninite, UO_2

↙ ↘

U_3O_7 / U_3O_9

↓

U_3O_8

↓

Uranium Trioxide, UO_3

McEachern and Taylor, 1998

Ianthinite, $U(UO_2)_5O_7 \cdot 10H_2O$

↓

Schoepite, $(UO_2)_8O_2(OH)_{12} \cdot 12H_2O$

Studtite, $(UO_2)\,O_2(H_2O) \cdot H_2O$

↓

Metal Uranyl Oxyhydroxides

↓

Metal Uranyl complexes i.e. phosphates, silicates

Baker, 2014

Preparation of UO_2 Surfaces for Simulation

- The UO_2 [001] and [110] surface orientations have been simulated in preparation for reaction modelling with DFT.

- For this work, CASTEP 19.11 and the Perdew-Burke-Ernzerhof (PBE) functional were used.

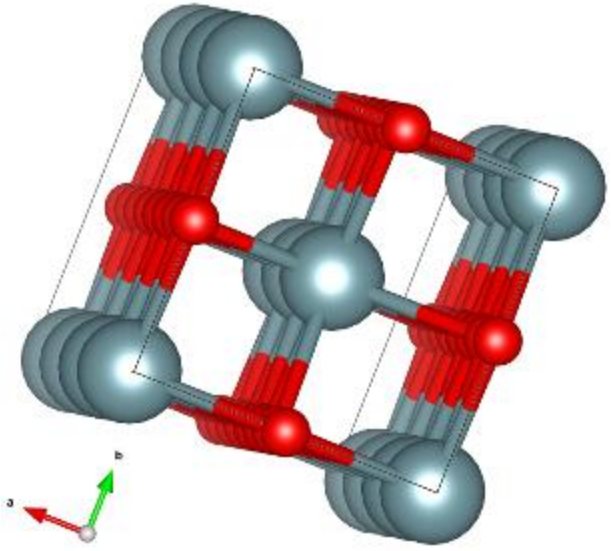

0 0 1

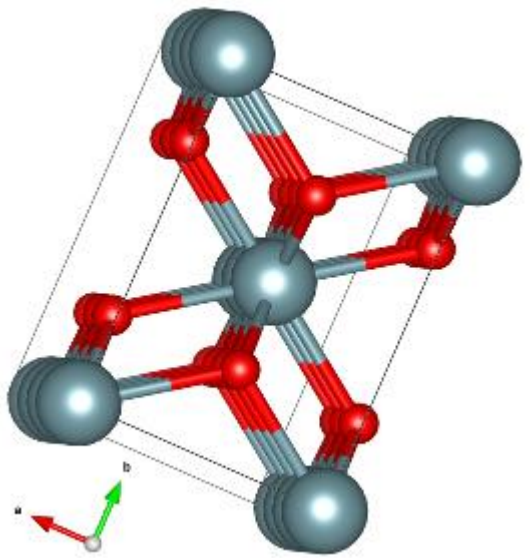

1 1 0

Clark et.al., ***Z. Kristall***., 2005, **220**, 567-570
Perdew et.al., ***Physical Review Letters***, 1996, **77**, 3865-3868

Preparation of UO_2 Surfaces for Simulation

0 0 1

1 1 0

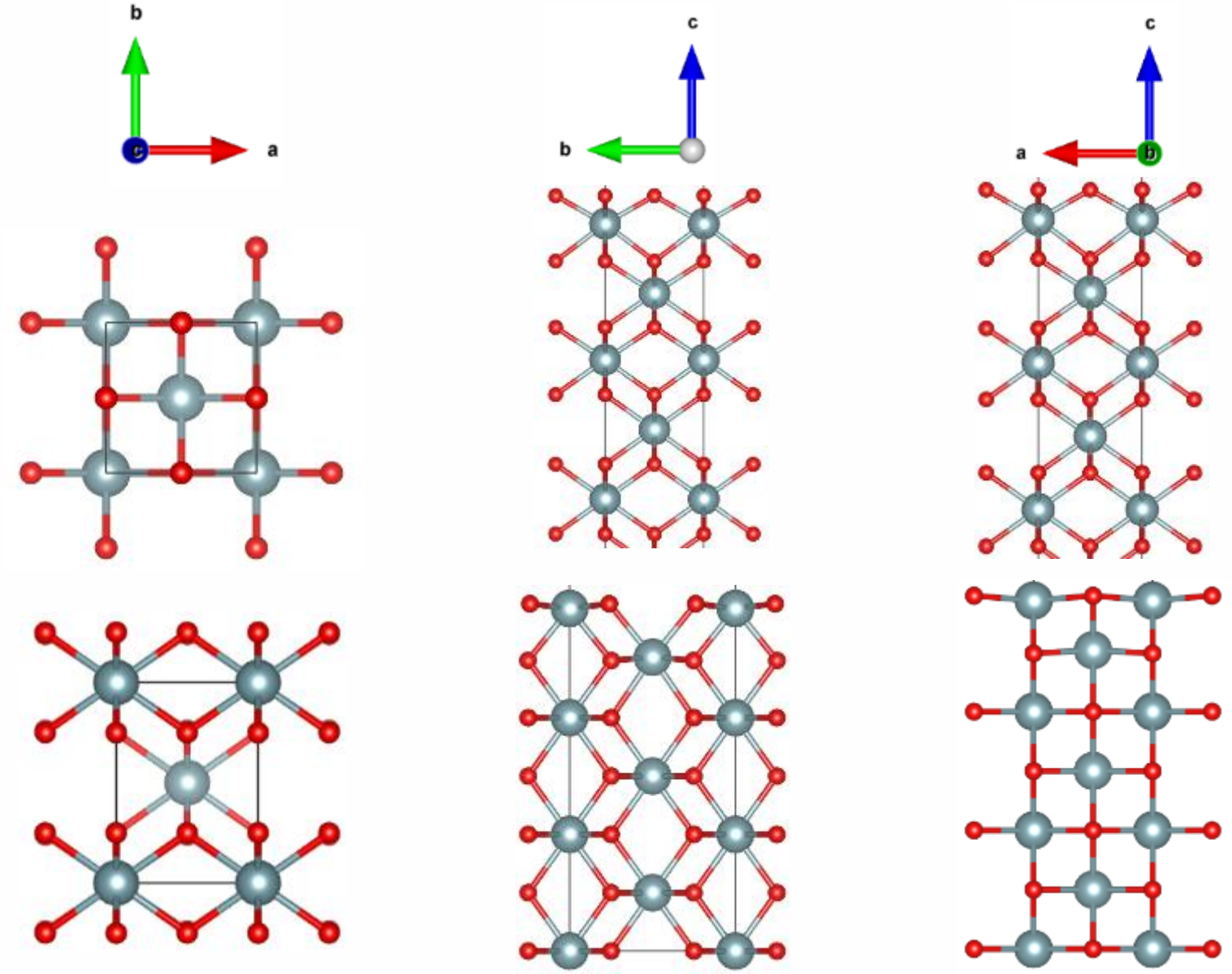

Future Computational Work:

Simulating thin film alteration

- Match surface reaction modelling to experimental reactions on epitaxial thin films, specifically with oxidising components produced by water radiolysis in pond water.

- Model Raman and IR spectra of reactants and alteration products. Allows for direct comparisons to experimentally obtained Raman and IR.

- Determination of the mechanism for UO_2 SNF alteration.

	Control	Simulated Pond Water			
UO_2 Surface	H_2O	H_2O_2	$OH^{\cdot}$	$HO_2^{\cdot}$	OH^-
0 0 1					
1 1 0					

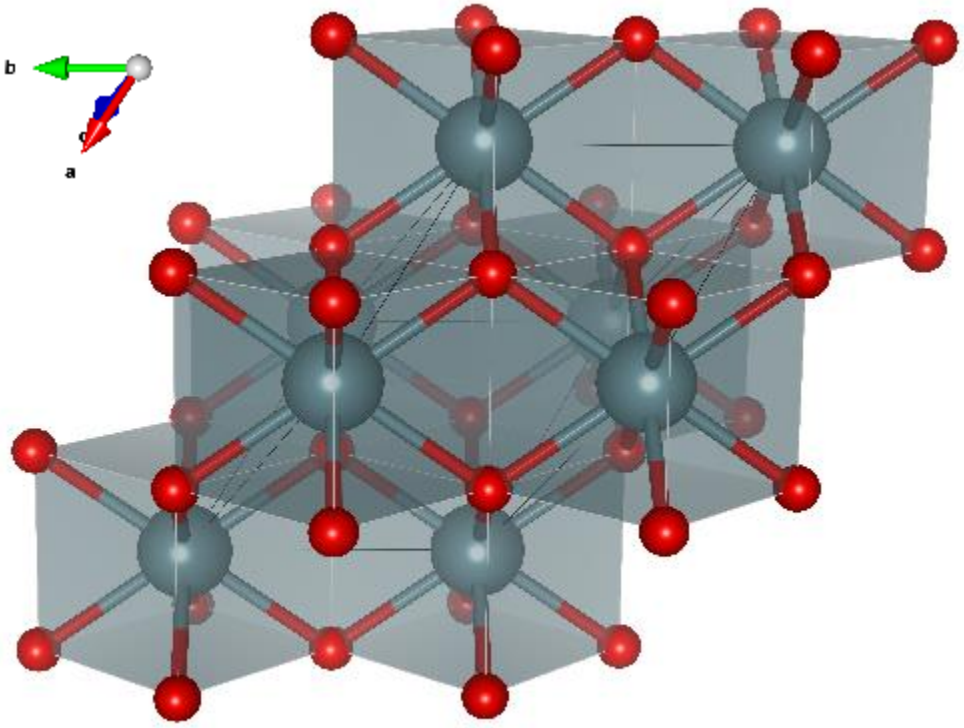

The Bridge Between Simulation and Experiment

- Combining techniques creates a more complete understanding of reactivity, composition and structure.
- Alteration of epitaxial UO_2 thin films in tandem with simulating these reactions on selected surface orientations.
- Simulations of reactant and product spectra.

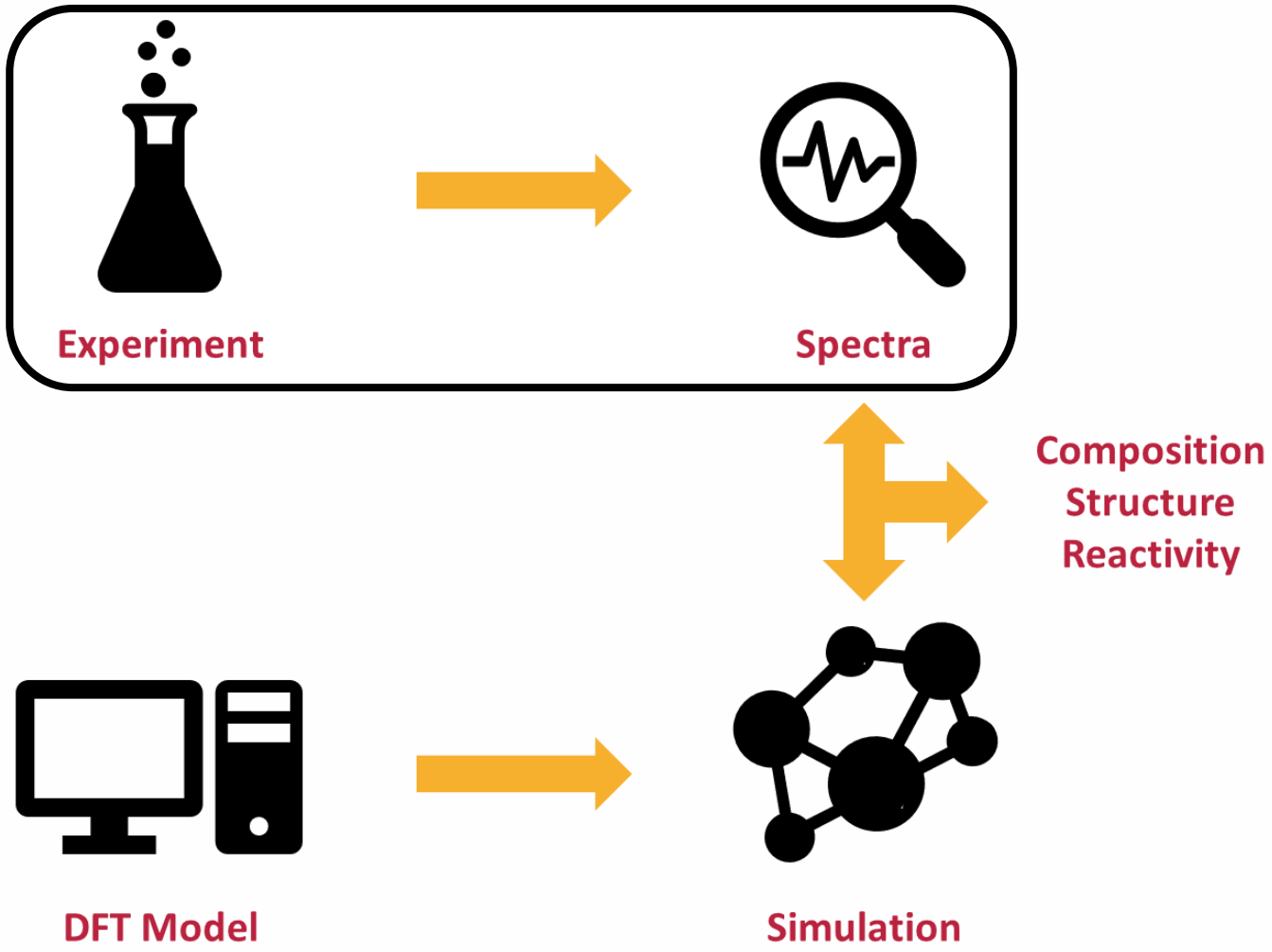

Characterisation of analogues: Fluorescence Spectrum from UO_2 Mineral Sample

- Natural "UO_2" mineral sample
- Evidence for surface alteration with U(VI) peak at 554.0 nm.

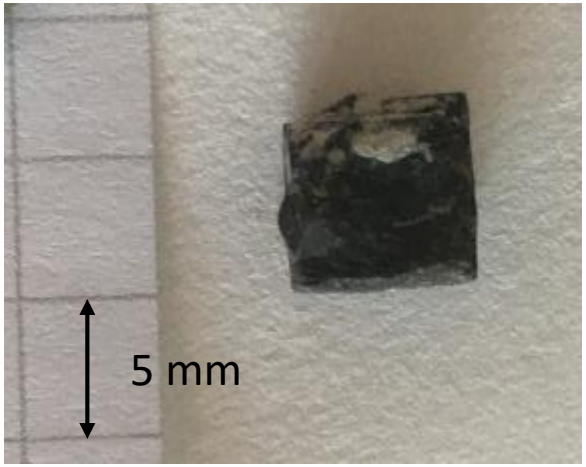

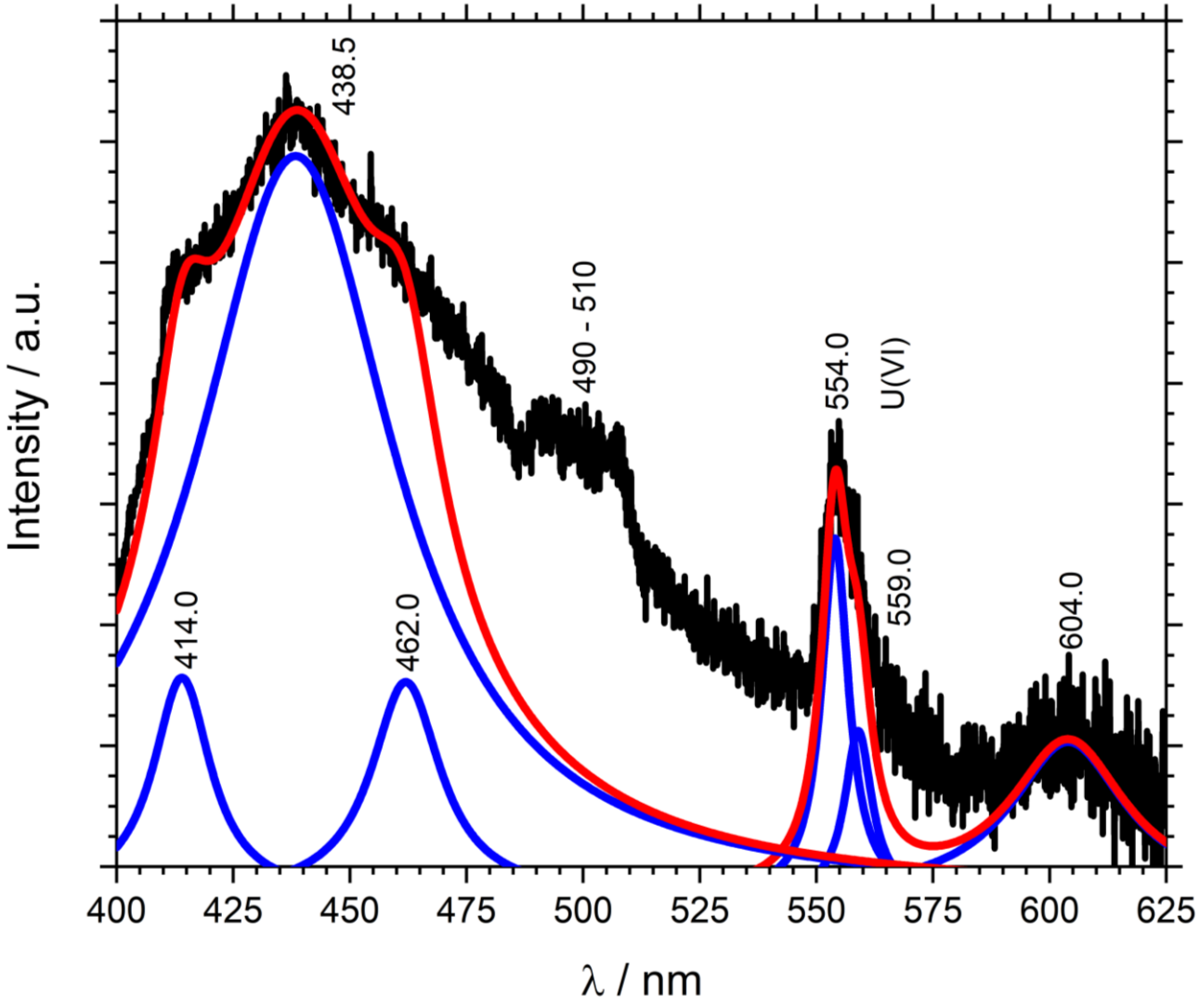

SEM-EDX spectroscopy from UO_2 Mineral Sample

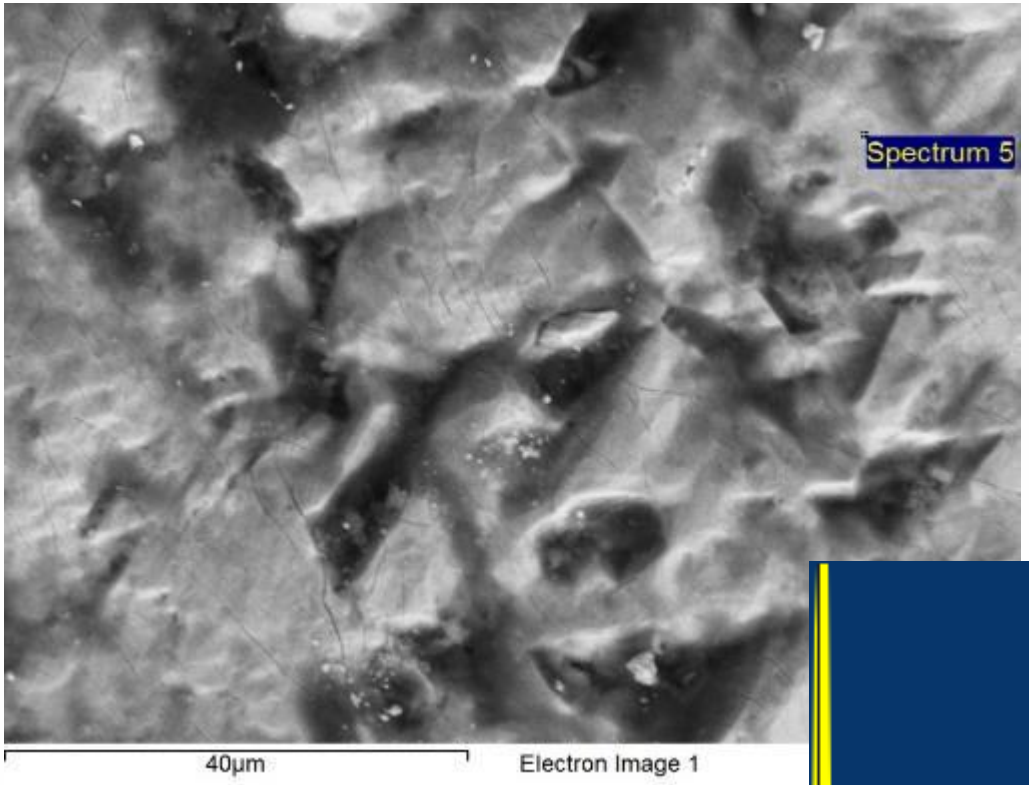

- Thorian Uraninite $(U,Th)O_2$
- Rich with Pb
- Accessory minerals including zircon and fluorite

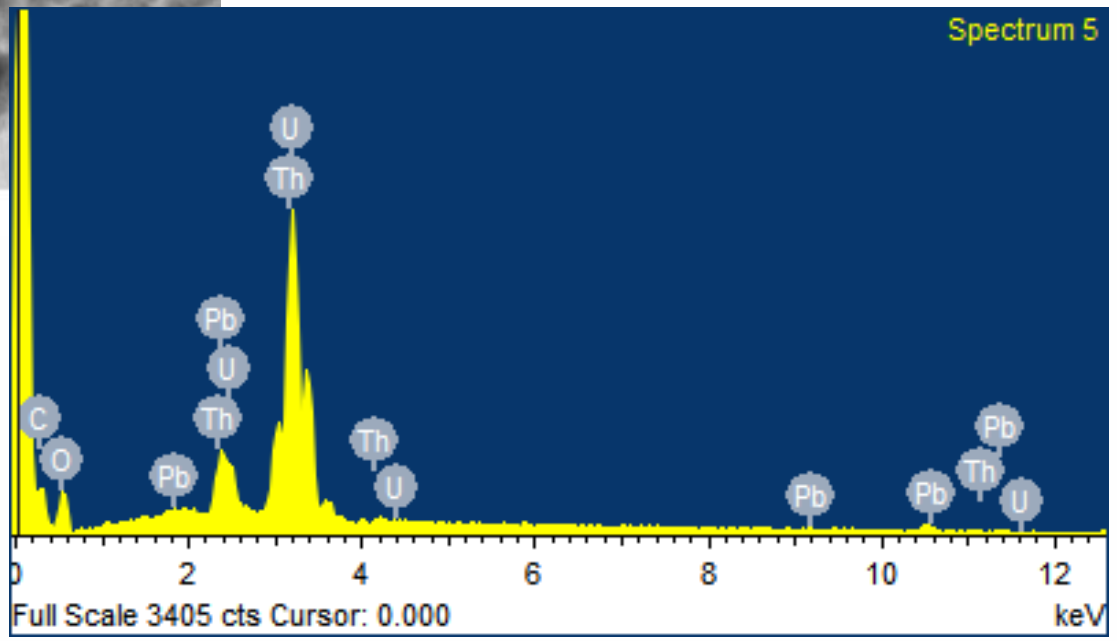

- U:Th ≈ 4:1
- Th:Pb ≈ 5:2

Future Experimental Work:

Thin Film Alteration

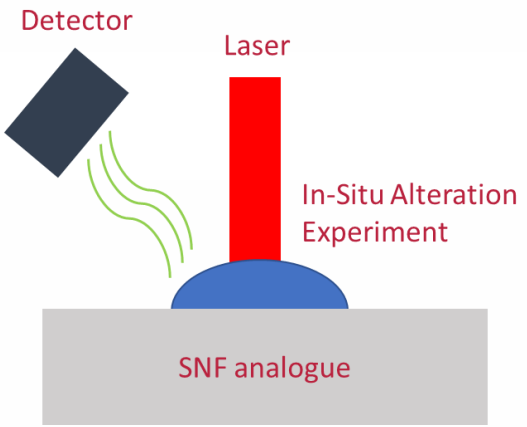

- Alteration of epitaxial UO_2 thin films with deionised water.
- Monitor real time alteration with Raman spectroscopy.
- Identify dissolved species with Fluorescence spectroscopy and ICP-MS of remaining solution.
- Elemental map of reactants and products with SEM-EDX, Raman and LA/LIBS-ICP-MS.
- Surface morphology with AFM.

Analogue	Deionised Water	Simulated storage pond water	Simulated deep groundwater
Epitaxial thin films			
Crystalline UO_2			
Sintered UO_2 pellets			
(AGR UO_2 Pellets)			

Experimental matrix

To Conclude

- Computational techniques selected and workflow designed to investigate alteration of selected surface orientations in simulated pond water environment.
- UO_2 surfaces prepared for computational simulations of surface reactions.
- Initial experiments on possible UO_2 analogue suggest mostly $U(IV)O_2$, therefore suitable for alteration experiments once prepared, however must account for additional Pb and Th.

TRANSCEND

Transformative Science and Engineering for Nuclear Decommissioning

Acknowledgements

SEM-EDX - David Jones

Thank you

Funding

TRANSCEND

Research Councils UK
Energy
For a Low Carbon Future

j.bright@surrey.ac.uk
linkedin.com/in/joshbri